MEASUREMENT AND DATA ANALYSIS TECHNIQUES FOR THE INVESTIGATION OF ADULT CEREBRAL HAEMODYNAMICS USING NEAR INFRARED SPECTROSCOPY

Clare Elizabeth Elwell, M.Phil

Thesis submitted for the degree of
Doctor of Philosophy (Ph.D)
of the University of London

August 1995

Department of Medical Physics and Bioengineering,
University College London.

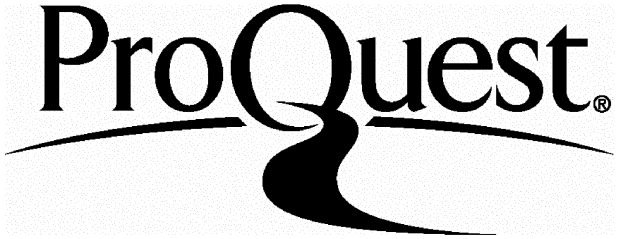

This work is dedicated to the memory of
my grandmother, Julia Britton.

ACKNOWLEDGEMENTS

During the preparation of this thesis I have been fortunate enough to be surrounded by many people who have made this an enjoyable rather than gruelling experience. My thanks must first go to my supervisor, Professor Dave Delpy, whose unfailing support and encouragement has seen me through. I have yet to find a question which he is unable to answer. I would also like to thank Dr. Mark Cope, whose own thesis has formed the basis of much of this work, for his important contribution to the technical content of this project.

I have benefitted enormously from the input of the NIRS clinical research team at University College Hospital. I am indebted to Dr. Huw Owen-Reece for the generous time spent in discussions and tutoring in adult neurophysiology and all things clinical, and for his infectious enthusiasm for clinical research. My thanks also go to Professor Os Reynolds, Dr. John Wyatt, Professor David Edwards and Dr. Judith Meek for their patient teaching and from whose collective wisdom I have learnt so much. I am grateful to my colleagues in Medical Physics who have tolerated various levels of discomfort as a result of my quest for "normal" volunteers - this work would not have been possible without them. I would especially like to thank Dr. Matthew Clemence for his welcome advice and skilful tutoring in the intricacies of C programming, and Dr. Chris Cooper and Dr. Jem Hebden for their continued encouragement and many useful discussions. The Medical Research Council has provided the funding for my post during the time taken to complete this work and Hamamatsu Photonics have generously provided equipment on many occasions.

My husband, Tim, has never failed to amaze me with his tolerance of this project and his faith in me to achieve this goal. His good humour and very active support over the last five years has made all the difference. I would like to thank my parents who have always inspired me to pursue my interests independently and who remain a constant source of support and encouragement. My thanks also go to my brothers, John and Simon, who have contributed far more than they realise.

ABSTRACT

The technique of near infrared spectroscopy (NIRS) has been widely used for several years as a monitor of tissue oxygenation in intact organs. The aim of the work described in this thesis was to investigate the applicability of the technique in performing quantitative measurements of cerebral haemodynamics in the adult.

The physiological background to the project is presented in the first chapter and describes the role of the cerebral circulation and the current methods employed for the measurement of cerebral blood flow (CBF) and cerebral blood volume (CBV) in adults. The physical principles behind the technique of NIRS are then described in the second chapter, with particular emphasis on the behaviour of light within a highly scattering media such as biological tissue. Chapter Three completes the technical background with details of the current instrumentation used for NIRS measurements.

Physiological measurements have been performed on healthy adult volunteers for the measurement of CBF, CBV and mean cerebral saturation ($SmcO_2$). These studies are described in the fourth and fifth chapters together with a detailed interpretation of the results. The relatively high blood flow of the adult brain imposes limits on the hardware and software requirements for the measurement of CBF and the resulting methodological problems and sources of error are also discussed. A description of the measurement of changes in cerebral haemodynamics during inspiration and expiration is given to demonstrate the use of the technique in monitoring rapid changes in cerebral oxygenation.

Chapter Six describes the development and testing of a novel analysis method for the calculation of CBF. It is hoped that this analytical method, which is based upon the measurement of cerebral vascular transit time, will improve the clinical usefulness of the technique.

TABLE OF CONTENTS

LIST OF FIGURES

LIST OF TABLES

GLOSSARY

ABP	Arterial blood pressure (mmHg)
B	Differential pathlength factor (DPF)
β	Differential pathlength (DP)
β_i	Beta coefficient of ith independent variable in stepwise regression analysis
CBF	Cerebral blood flow ($ml.100g^{-1}\ min^{-1}$)
CBV	Cerebral blood volume ($ml.100g^{-1}$)
CCD	Charge Coupled Device
CLVHR	Cerebral to large vessel haematocrit ratio
$CMRO_2$	Cerebral metabolic rate for oxygen
CPP	Cerebral perfusion pressure
CSF	Cerebrospinal fluid
CtOx	Oxidised cytochrome oxidase
CVP	Central venous pressure
CVR	Cerebrovascular resistance
DP	Differential pathlength
DPF	Differential pathlength factor
D_t	Cerebral tissue density ($g.ml^{-1}$)
$FiCO_2$	Inspired carbon dioxide fraction (%)
FiO_2	Inspired oxygen fraction (%)
Haematocrit	Fractional volume of blood occupied by red blood cells, sometimes quoted as a percentage
Hb	Deoxyhaemoglobin
HbCO	Carboxy-haemoglobin
HbO_2	Oxyhaemoglobin
HR	Heart rate (bpm)
ICP	Intracranial Pressure
IOS	Interoptode Spacing
LED	Light emitting diode
LCBV	Local cerebral blood volume
lg	Logarithm (base 10)
ln	Natural logarithm (base e)

λ	blood:tissue partition coefficient
μ_a	Absorption coefficent
μ_s	Scattering coefficient
molar	mol per litre
MW	Molecular weight
NIR	Near infrared
NIRS	Near infrared spectroscopy
NIRO 500	Commercial NIR spectrometer
NMR	Nuclear magnetic resonance
OD	Optical density
OER	Oxygen extraction ratio
P_{50}	Haemoglobin half saturation partial pressure (kPa)
$PaCO_2$	Arterial partial pressure of carbon dioxide (kPa)
PaO_2	Arterial partial pressure of oxygen (kPa)
PET	Positron emission tomography
PIN	Probability of F-to-enter stastitic in stepwise regression analysis
POUT	Probability of F-to-remove statistic in stepwise regression analysis
PMT	Photomultiplier tube
SaO_2	Arterial oxygen haemoglobin saturation (%)
$SmcO_2$	Mean cerebral oxygen saturation (%)
SO_2	Haemoglobin oxygen saturation
SPECT	Single photon emission computed tomography
SvO_2	Venous oxygen haemoglobin saturation (%)
τ_{bp}	First transit break point
tcHb	Total cerebral haemoglobin concentration
tHb	Total haemoglobin concentration in large blood vessels (g/dl)
TPSF	Temporal point spread function
T_t	Cerebral vascular transit time
rCBF	Regional cerebral blood flow
$TcPCO_2$	Transcutaneous carbon dioxide tension (kPa)
^{133}Xe	^{133} Xenon

PREFACE

The ultimate goals of diagnostic medical science are based around the development of techniques for imaging the human body and viewing deep non superficial organs to assess their structure and function. A common problem encountered in many types of physiological measurement is that the actual act of making a measurement can directly or indirectly influence natural physiological behaviour and hence change the variable under observation. Uninterrupted cerebral function is essential for the control and coordination of bodily processes and for this good reason the brain is an extremely well protected organ. Disturbance of its function may obviously have very serious effects, thus requiring that any methods of interrogating cerebral anatomy and function must be safe, minimally invasive at least and ideally completely non invasive.

This thesis will describe a new technique for the measurement of absolute cerebral haemodynamics in adults. Near Infrared Spectroscopy (NIRS) is a non invasive, portable, inexpensive technique which allows repeated measurements of, among other parameters, cerebral blood flow (CBF) and cerebral blood volume (CBV). Since it was first described by Jobsis in 1977[1], the technique has been used to monitor blood and tissue oxygenation in a variety of intact organs. The non invasive and portable nature of the technique combined with the relative transparency of the neonatal head led to its first clinical applications in monitoring the cerebral oxygenation status of preterm infants[2-5]. In these studies, the NIRS data was not quantified and only provided an indication of trends in increased or decreased oxygenation. Subsequently, with the development of methods for measuring optical pathlength in tissue, the changes in oxygenation became quantifiable[5]. This technological advancement, combined with the novel application of basic physiological principles led to the development of methods for quantifying CBF[6] and CBV[7] in the neonate. More recently observations have also been made of human fetal cerebral haemodynamics during labour and childbirth[8-10]. A few studies of qualitative changes in cerebral oxygenation in adults have been reported[11-15], but no quantitative measurements have yet been cited.

The aim of this project was to investigate whether NIRS can be used to make quantitative measurements of cerebral haemodynamics in the adult. As with many physiological measurements, an understanding of both the physical principles and appropriate clinical application is required if the technique is to be further developed. For this reason the introductory chapters of this thesis contain information about the field of cerebral

haemodynamic monitoring as well as the technology currently available for spectroscopy measurements in tissue.

The physiological measurements are described as self contained projects with interpretation of results and discussion included within the relevant sections. References are listed at the end of each chapter rather than being collated at the end of the document.

CHAPTER 1

PHYSIOLOGY OF THE CEREBRAL CIRCULATION

1.1 INTRODUCTION

When contemplating any new physiological measurement, an understanding of the system to be monitored is essential. This chapter will provide an overview of the cerebral circulation and pay particular attention to those aspects which will effect its measurement, e.g. the regulation of cerebral blood flow (CBF) and its sensitivity to changes in systemic parameters. A brief outline of the anatomy of the cerebral circulation is given followed by a description of current measurement techniques. The theoretical background to some of these methods is given in detail to establish the basic principles already employed. Although cerebral blood flow and cerebral blood volume (CBV) are intrinsically linked, they are treated as separate measurements for the purpose of this chapter.

1.2 CEREBRAL BLOOD FLOW

The importance of the stable maintenance of cerebral circulation and oxygenation is clearly demonstrated by considering that although the brain comprises only 2% of body weight, its circulation accounts for 15% of the total cardiac output and its metabolism 20% of total oxygen used by the whole body[16]. The storage capacity of the brain for supplies of glucose and oxygen are negligible and as such the organ depends almost entirely upon blood borne energy supply. The fact that the brain is particularly sensitive to changes in its blood supply coupled with the vulnerability of the cerebrovascular system to different pathogenic factors means that changes in brain function can often be related to systemic circulatory

disorders. CBF is usually quoted in units of ml of blood per 100g of brain tissue per minute and is known to have a mean value of 50 $ml.100g^{-1}.min^{-1}$ in the healthy adult[17, 18]. A decrease in CBF to 40 $ml.100g^{-1}.min^{-1}$ causes protein synthesis in the brain to cease[19], spontaneous electrical activity stops at levels below 20 $ml.100g^{-1}.min^{-1}$ and evoked responses of the brain to various stimuli falls off when a value of 15 $ml.100g^{-1}.min^{-1}$ is reached[20]. Ultimately cerebral nerve cell death in certain regions of the brain occurs after only 4-5 minutes of complete ischemia (i.e. cessation of blood flow to the brain) a phenomenon which has never been observed in any other organ in the body[21].

The delivery of blood to and from the brain controls the transport of:

i) Oxygen (O_2) necessary for oxidative metabolism. The high cerebral metabolic rate makes constant O_2 supply to the brain particularly important.

ii) The nutritive substances such as glucose, carbohydrates, amino acids and fats used for synthesis of high energy compounds and to maintain brain tissue structure.

iii) The end products of cerebral metabolism such as carbon dioxide (CO_2) and ammonia, whose presence in cerebral tissue disturb normal function.

iv) Hormones and vitamins.

Because of its low metabolic reserves the brain is unable to employ anaerobic metabolism as efficiently as other organs, thus indicating its need for priority blood supply. The delivery of these nutrients must therefore be a carefully controlled mechanism capable of responding quickly to changes in demand.

It can be misleading to consider the brain as a constant, homogeneous consumer of oxygen and nutrients. Within the brain there is a continuous readjustment of local blood flow distribution depending upon the metabolic requirements of a particular region. Many investigations have demonstrated that specific motor or cognitive tasks produce local changes in CBF and oxygen uptake in regions associated with those particular functions[22, 23]. This adjustment in CBF is therefore under active control which acts not only to respond quickly to local changes in metabolic demand but also to maintain cerebral blood flow, volume and pressure constant during systemic changes in the circulation.

1.2.1 The Control of the Cerebral Circulation

Early investigators[24] described the Monroe-Kellie doctrine which postulated that since cerebral tissue, cerebrospinal fluid and cerebral blood are incompressible the amount of blood and therefore CBF should remain constant under any physiological or pathological condition. Understanding of the control of the cerebral circulation has come a long way since then and it has now been shown that both arterial blood pressure (ABP) and cerebrovascular resistance (CVR) (due to major cerebral arteries and small pial arteries) play an important role.

The term *autoregulation* is often used in the description of CBF control. It must be remembered that this term applies purely to changes in cerebrovascular resistance which maintain CBF constant. Several other factors affect CBF (some of which are outlined in later sections), but the control of the circulation is achieved by regulation of pressure effects. Cerebral autoregulation is a homeostatic mechanism which maintains the constancy of cerebral capillary pressure and assures the steady supply of the essential metabolites such as oxygen and glucose.

The perfusion pressure of the blood supplying the brain, as for any other organ, is the difference between the arterial blood pressure and the venous blood pressure, i.e. the arterio-venous pressure difference. The cerebral perfusion pressure (CPP) is sometimes defined as the difference between the arterial pressure and the intracranial pressure (ICP), since the latter is approximately equal to the systemic venous pressure. Under normal physiological conditions ABP may vary due to changes in cardiac output or total vascular resistance, but these changes are usually very small. However certain pathological conditions can cause ABP to increase or decrease significantly. Central venous pressure (CVP) is also near constant at a level close to atmospheric pressure under normal conditions. Pathological conditions are far less likely to affect CVP, and when they do, CVP can only rise slightly. It is clear then that changes in arterial blood pressure have a much greater effect on CPP than changes in venous pressure (as much as 15 times greater). Changes in APB are therefore more important when considering autoregulation effects.

It has been shown that in unanaesthetised adults ABP can be varied over a wide range (between 50 -150 mmHg) while CBF remains constant[25, 26]. This effect is due to constriction of cerebral arterioles (thus increases in CVR) during increases in ABP. Conversely, dilation of cerebral arterioles (and a decrease in CVR) is induced at low levels of ABP. Thus CBF regulation depends directly upon active changes in the resistance to flow in the cerebral

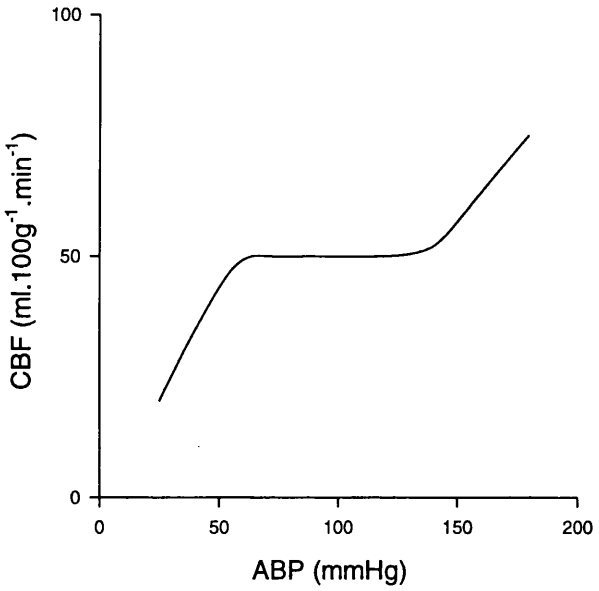

Figure 1.1 *The response of the cerebral circulation to changes in arterial blood pressure indicating the limits beyond which CBF is not maintained constant.*

vasculature.

There are designated limits however beyond which the cerebral circulation is not protected from the affects of abnormally high or low systemic blood pressure. Beyond the upper limits of autoregulation high ABP causes increased fluid leakage across the blood brain barrier leading to cerebral oedema. At low levels of ABP decreased cerebral perfusion causes cerebral hypoxia. Figure 1.1 shows this effect schematically[27]. The limits of autoregulation can vary considerably between healthy individuals and are also readily disturbed under pathological conditions, such as hypertension[28].

1.2.2 The Relationship Between $PaCO_2$ and CBF

Cerebral blood flow is exquisitely sensitive to changes in arterial blood carbon dioxide tension ($PaCO_2$). An increase in $PaCO_2$ above normal levels causes a significant increase in CBF due to intense cerebral vasodilatation. Around the normal range an increase in $PaCO_2$ of 1 kPa produces a 30% rise in CBF[29]. Hypocapnia causes a reduction in cerebrovascular tone, with decreases in $PaCO_2$ below 3.5kPa producing a decrease in CBF of 35%[30]. The relationship between CBF and $PaCO_2$ is only linear in the range of normal $PaCO_2$ values,

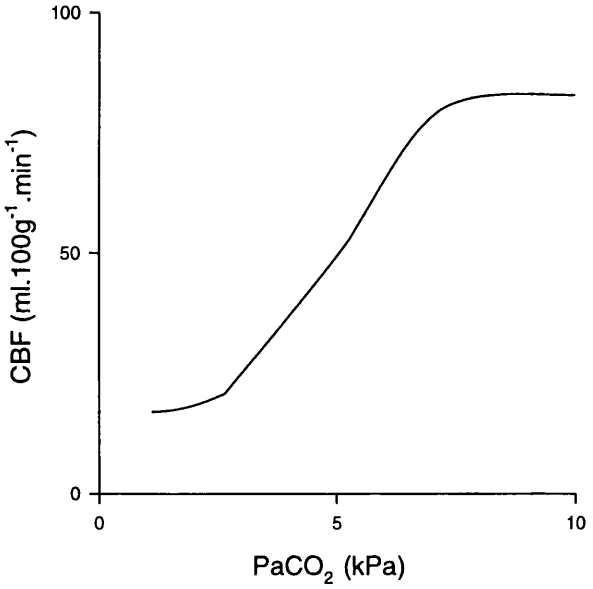

Figure 1.2 *The response of cerebral blood flow to changes in arterial carbon dioxide tension.*

otherwise the plot has a sigmoid shape. Figure 1.2 shows an example of this responsivity curve in the rhesus monkey[31]. The lower limit of the hypocapnic response has been measured to be 2.7 kPa, beyond which there is no significant further reduction in CBF[31]. This effect is thought to be in response to the induced brain hypoxia at this level of CBF.

The time response of the changes in CBF to changes in $PaCO_2$ should also be considered. In hypercapnia, although the increase in CBF starts almost immediately it probably takes 5 to 15 minutes to reach a stable plateau value[32, 33]. The response to hypocapnia is probably more rapid, as demonstrated by Severinghaus and Lassen[34], who measured a time constant of 0.3 seconds for a steep decline in $PaCO_2$ to 3.3kPa. In addition, according to the work of Raichle[35], this decrease in CBF is unlikely to be maintained for more than a few hours. These differences need to be remembered when the CO_2 reactivity of the cerebral circulation is to be measured.

1.2.3 The Relationship Between PaO_2 and CBF.

The effects on CBF due to changes in arterial oxygen tension (PaO_2) are far less pronounced than those due to changes in $PaCO_2$. In conditions of moderate hypoxia and hyperoxia CBF does not change measurably, and as such tissue PO_2 is not a controlled factor.

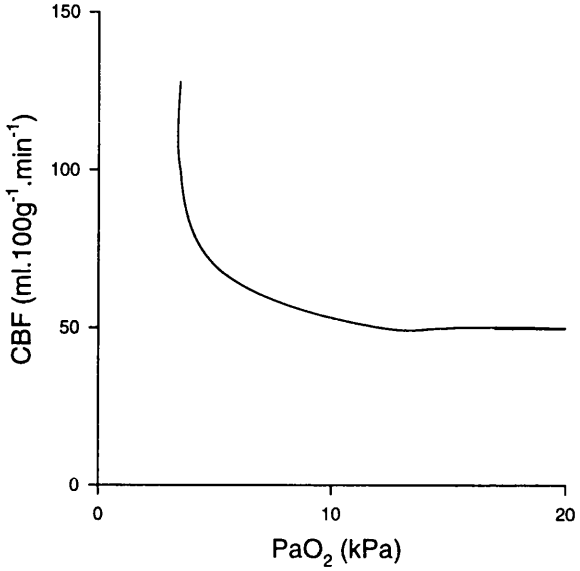

Figure 1.3 *The response of cerebral blood flow to changes in arterial oxygen tension.*

It is not until PaO_2 falls to 6.7kPa (at a constant $PaCO_2$) that CBF rises markedly[36] and from here doubles at a PaO_2 of 4kPa [37, 38]. This effect is shown schematically in Figure 1.3[27].

There are fewer studies on the effects of hyperoxia although it has been shown that when PaO_2 is increased above 14kPa CBF is reduced[39]. Contra-intuitively, hypoxia does not change cerebral oxygen consumption. Cerebral metabolic rate of oxygen remains unchanged during alterations in PaO_2 even during the severe physiological challenges described by Lassen[25].

McDowall's work[36] also shows that at constant $PaCO_2$, CBF progressively falls as PaO_2 rises beyond a defined point. This is evidence that high oxygen tension has a constrictor effect on cerebral blood vessels that is independent of changes in $PaCO_2$. These effects indicate that PaO_2 affects CBF by a direct influence on cerebral blood vessel diameter rather than a change in cerebral tissue metabolism. It is likely that there is a dual mechanism involving the simultaneous and coincidentally directed responses of the major arteries and the pial arteries[40]. However it is true to say that the exact mechanisms of cerebral circulatory response to hypo- and hyperoxia are not yet well understood.

1.3 THE ANATOMY OF THE CEREBRAL CIRCULATION IN ADULTS

To fully understand the approaches and techniques which have been developed for the measurement of CBF, some appreciation of the anatomy of the cerebral circulation is required.

1.3.1 The Cerebral Arterial Supply

A map of the distribution of the cerebral vascular bed is shown in Figure 1.4[40]. The brain is different from other organs in the body in that four major arteries are responsible for its blood supply. These vessels are the two internal carotid arteries and the two vertebral arteries which join to form the basilar artery. The junction of these primary arteries is known as the Circle of Willis, an equalising distributor, which is designed to provide exquisite protection of the cerebral perfusion should any of the supplying arteries become occluded or obstructed. Under normal conditions blood is not mixed in the Circle of Willis but rather redistributed to the respective blood vessels on the ipsilateral side of the brain. The vertebral arteries supply the posterior fossa, i.e. the brain stem and cerebellum, while the internal carotid arteries supply the cerebral hemispheres. This ipsilateral distribution can be explained

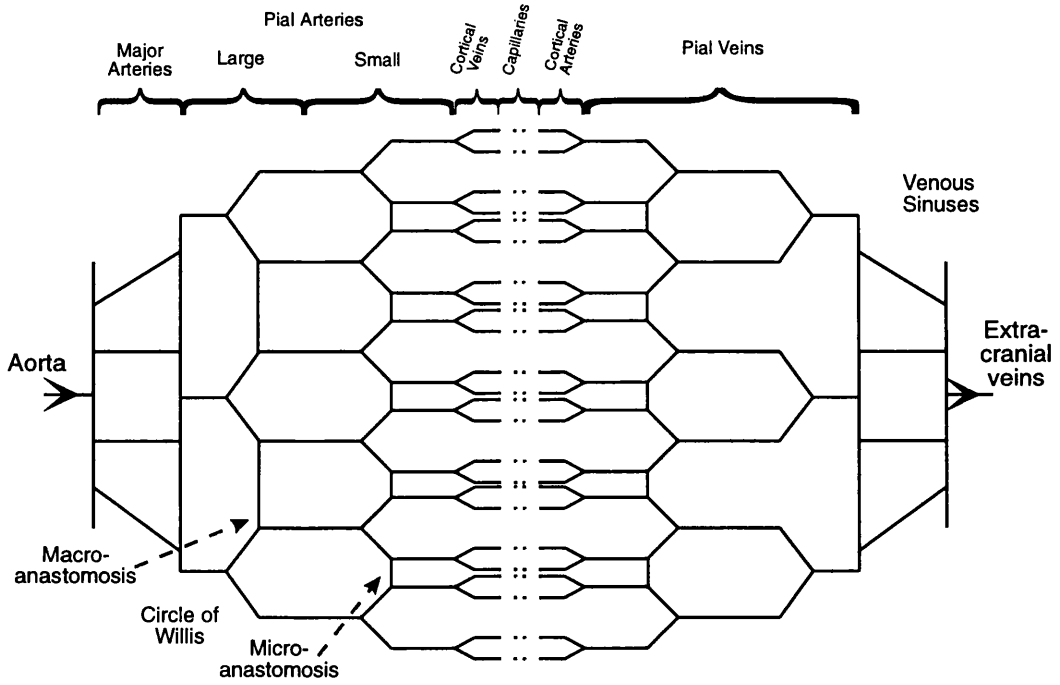

Figure 1.4 *Schematic of the subdivisions of the cerebral arterial, capillary and venous beds.*

by the absence of blood flow in the anastomoses of the Circle of Willis under normal conditions due to there being no pressure gradient at the terminal end of the major cerebral arteries. It is only if there is an occlusion in one of the major arteries that blood flows through the anastomoses. This results in a collateral blood supply to the region of cerebral tissue under threat of interrupted perfusion.

From the Circle of Willis the internal carotid arteries branch to form three pairs of blood vessels, the anterior, middle and posterior cerebral arteries. These arteries further anastomose on the surface of the cerebral hemisphere and form the complex pial arterial bed. The boundary between the large anterior, middle and posterior cerebral arteries and the pial system is called the pial macroanastomoses. The numerous interarterial anastomoses in the pial artery system are responsible for maintaining collateral blood supply when either the anterior, posterior or middle cerebral arteries or their branches become occluded.

The third interconnection in this arterial supply system are the pial microanastomoses which connect the terminal branches on the surface to the small radial arteries which dip into the brain substance and continue to branch from there. The role of these microanastomoses is to maintain blood supply to the smallest areas of the cerebral cortex. Finally these branches produce an uninterrupted microvascular network of capillaries within the cerebral tissue. These cerebral capillaries are a direct continuation of the smallest arterioles that represent terminal branches of the radial arteries. They may penetrate the brain tissue over a small area within the cortex or for a longer distance towards white matter and deeper brain structures. No interarterial anastomoses have been found inside the cerebral cortex[41]. So, although the capillary system of the brain forms a continuous network it cannot compensate and provide normal microcirculation in capillaries deprived of blood supply from the respective arterioles.

1.3.2 Cerebral Venous Drainage

Blood is drained back to the central circulation from the cerebral capillaries via two groups of cerebral veins, the superficial veins and the deep veins. The superficial veins collect blood from the cerebral hemispheres and are comparable to the pial vessels on the arterial side. The deep veins are equivalent to the arteries supplying the basal ganglia and collect blood into the great cerebral vein of Galen. The venous blood from both these groups drains into cerebral sinuses, extracranial veins and finally the jugular veins in the neck.

Considerable intermingling of venous blood takes place in the cerebral venous drainage

system. In the internal jugular vein it is estimated that 70% of the blood has drained from the ipsilateral intracerebral region, 3% from the extracerebral tissue and the remainder from the contralateral hemisphere. It must be remembered however that the level of extracerebral contamination of jugular venous blood is significantly elevated in many animals which may be used as models for the study of human cerebral circulation.

1.3.3 The Extra-Cerebral Blood Supply

The internal carotid artery is itself a product of the bification of the larger common carotid artery. The external carotid artery (a product of the same bification) is responsible for the blood supply to the scalp, face and extracranial tissues which are also supplied by the occipital artery.

1.3.4 Vascular Distribution in the Brain

Although the blood volume of each of the arterial, capillary and venous compartments is changeable, the mean blood volume in each can be estimated with a certain degree of

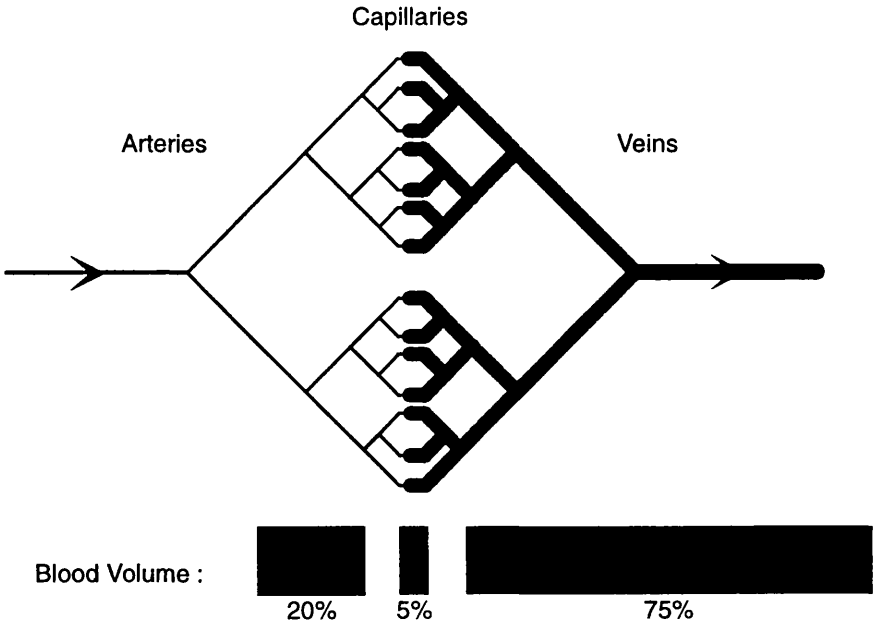

Figure 1.5 *Relative blood volumes in the arterial, capillary and venous beds of the peripheral cerebral circulation.*

accuracy by considering the distribution of blood in the peripheral circulation[40, 42]. Figure 1.5 demonstrates this distribution[40]. It can be seen that three quarters of the blood volume is stored in the venous system. This is due to the comparatively wide lumina of veins compared to those of arteries and capillaries. It should be remembered however that the total cross-sectional area of the capillary bed is significantly greater than the veins or arteries since the mean length of the capillaries is comparatively small. The density of the capillary network throughout the adult brain is by no means homogeneous and is certainly related to the function and metabolic rate of the tissue supplied. There is for example a very dense capillary network in the grey matter which is comprised almost entirely of cellular elements, whilst the white matter which is formed from myelinated nerve fibres, is more sparsely populated. The measured ratio of the volume of the capillary bed of grey matter to that of white matter was found by Lierse et al.[43] to be approximately 4:1.

Under normal conditions only 30-40% of the oxygen supplied to the brain is extracted by tissues for metabolism. So for a normal arterial haemoglobin oxygen saturation (SaO_2) of 98-100% the cerebral venous haemoglobin saturation (SvO_2) is between 60-70%. It is difficult to estimate the haemoglobin oxygen saturation in the capillary bed, but it is thought to closely resemble the cerebral mixed venous saturation of 67%[44].

1.4 Cerebral Blood Flow Measurement Techniques

1.4.1 The Clinical Importance of Cerebral Blood Flow Measurements

The importance of CBF measurements in the clinical management of patients can be demonstrated in many situations. When patients undergo intensive care, for what ever reason, the effects of the intensive therapy regimes such as elevated $PaCO_2$ and disturbed ABP, on the cerebral circulation must be assessed. At some stage it may be appropriate to assess cerebral function and viability, particularly when clinical intervention has little or no effect. In specific conditions such as stroke or head injury it is important to localise the effects of any damage and therefore target treatment more effectively. It is clear from the lack of data available in the literature that little is yet known about the effects on the cerebral circulation of general anaesthesia. A variety of anaesthetic drugs are used in different types of surgery

and their specific effects are not well defined. Certain surgical procedures directly disturb or interrupt blood flow to the brain, e.g. cardiovascular surgery, carotid repair and neurosurgery and in these circumstances knowledge of cerebral oxygenation is essential. The case for accurate, reproducible measurements of cerebral haemodynamics is quite clearly a strong one not just in the clinical arena but also in animal studies where the mechanisms controlling the cerebral circulation can be more thoroughly investigated.

1.4.2 Methods Using Inert Diffusible Tracers

Before 1945 there were no recognised methods for obtaining either qualitative or quantitative values for CBF in humans. With their publication in the American Journal of Physiology in that year describing the nitrous oxide uptake technique[45], Kety and Schmidt revolutionised the science of clinical CBF measurements. The majority of clinical methods used in the present day can be attributed to the principles described in that paper. The authors themselves based their work on a principle first described by Fick in 1870 outlining the basis of material conservation.

1.4.2.1 *Fick Principle*

The Fick principle states that the amount of substance taken up by an organ per unit time (Q_t) is equivalent to the difference between the rate of the arrival of the substance and the rate of the departure of the substance from the organ. The rate of the arrival of the substance is the product of the blood flow through the organ (F_t) and the arterial concentration of the substance (C_a) and applying the same logic, the rate of departure of the substance is the product of F_t and the venous concentration of the substance (C_v). Hence:

$$dQ_t = F_t \cdot (C_a - C_v) \qquad \textbf{(1-1)}$$

If the quantity of tracer varies over time t, then by integration the equation becomes:

$$F_t = \frac{Q_t}{\int_0^t (C_a - C_v) \cdot dt} \qquad \textbf{(1-2)}$$

Kety and Schmidt recognised that Q_t was not readily measurable directly. However Q_t is simply the product of the concentration of tracer in the tissue (C_T) and the unit weight of tissue (W). In other words tissue perfusion could be measured in units of ml of blood per 100g of brain tissue per minute rather than the total blood flow to the whole organ in ml per minute,

$$\frac{F_t}{W}\ (ml.100g^{-1}.\min^{-1}) = \frac{C_T}{\int_0^t (C_a - C_v) \cdot dt} \qquad \textbf{(1-3)}$$

Obviously C_T may be just as difficult to measure as Q_t but an assumption was made that if equilibrium has been reached C_T is proportional to C_v. The constant of proportionality in this relationship is λ, the blood : tissue partition coefficient which describes the relative chemical affinity of blood and tissue for the tracer substance. Hence equation 1.3 becomes:

$$\frac{F_t}{W} = \frac{C_v \cdot \lambda}{\int_0^t (C_a - C_v) \cdot dt} \qquad \textbf{(1-4)}$$

1.4.2.2 *Nitrous Oxide Technique*

The first application of the above technique described the use of nitrous oxide (N_2O) as the inert gaseous tracer substance. The subjects in Kety and Schmidt's initial study breathed a mixture of 15% N_2O and 85% O_2 for ten minutes[18]. During this time simultaneous arterial and venous blood sampling was performed from the femoral artery and the right internal jugular vein respectively at 2, 4, 6 and 10 minutes following the onset of inhalation. The

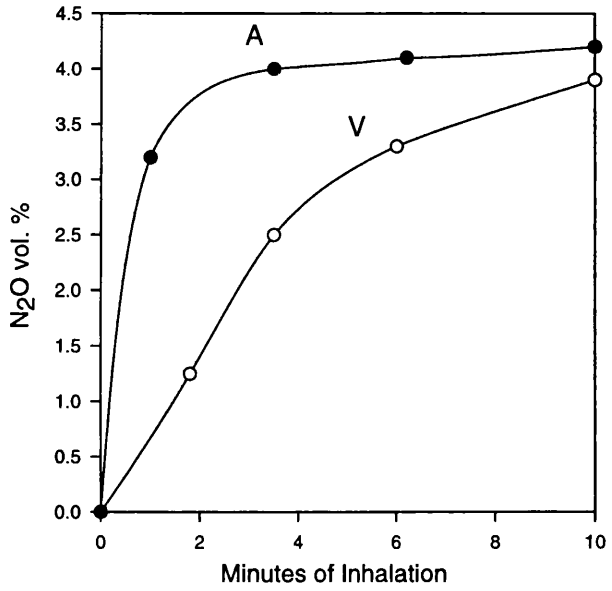

Figure 1.6 *Arterial (A) and cerebral venous (V) curves of N_2O concentration during inhalation of 15% N_2O during the course of a CBF measurement.*

blood samples were analysed using manometric methods after the absorption of O_2 and CO_2 and denitrogenation. A continuous plot of arterial (A) and cerebral venous (V) curves of N_2O concentration during the inhalation could be made (as shown in Figure 1.6[46]), until a state of equilibrium had been reached and $C_a = C_v$. At this point $\int(C_a - C_v)$ is the area between the A and V curves. With knowledge of λ, the flow of blood per unit mass of brain can be easily computed in $ml.100g^{-1}.min^{-1}$.

Although the principles of this technique were well accepted, the technical limitations of using N_2O as a tracer were also recognised. At that time the chemical analysis of N_2O was a laborious, time consuming and inefficient task and the small number of samples compromised the accuracy of the results. Accurate placement of the venous sampling catheter is also a consideration to ensure that cerebral venous blood is being sampled with minimal contamination from extracerebral tissue. The technique allows only global measurements of CBF to be made and since it is only perfused areas of tissue which are accounted for, regions of total ischemia will not be represented.

However despite these limitations N_2O is still used clinically today and has several advantages over more modern tracer techniques. In seriously ill patients with arterial and venous sampling lines in situ (particularly those with trauma or head injury) it may be the

preferred method because measurements can be made easily at the bedside and in theatre with a minimal amount of inexpensive specialized equipment[47, 48]. In addition the cerebral metabolic rates for oxygen ($CMRO_2$), glucose (CMRG) and lactate can be measured from the product of the arteriovenous differences of the substances and CBF[49].

It was clear that when first described, the potential of this new technique was enormous and approximately 20 years after the introduction of N_2O as a tracer the use of radioactive tracers was demonstrated. With this the theoretical possibility of performing local rather than global CBF measurements *in vivo* became a reality.

1.4.2.3 *Radioactive Gas Washout Technique*

The use of an inert radioactive gas to measure CBF was first described by Lassen et al.[50] who used the β emitting gas ^{85}Kr dissolved in fluid. The solution was injected into the common carotid artery and its washout from the brain was measured using a Geiger-Muller tube placed directly over the exposed cortex. Due to the limited penetration of β particles only a superficial 1mm of cortex could be interrogated.

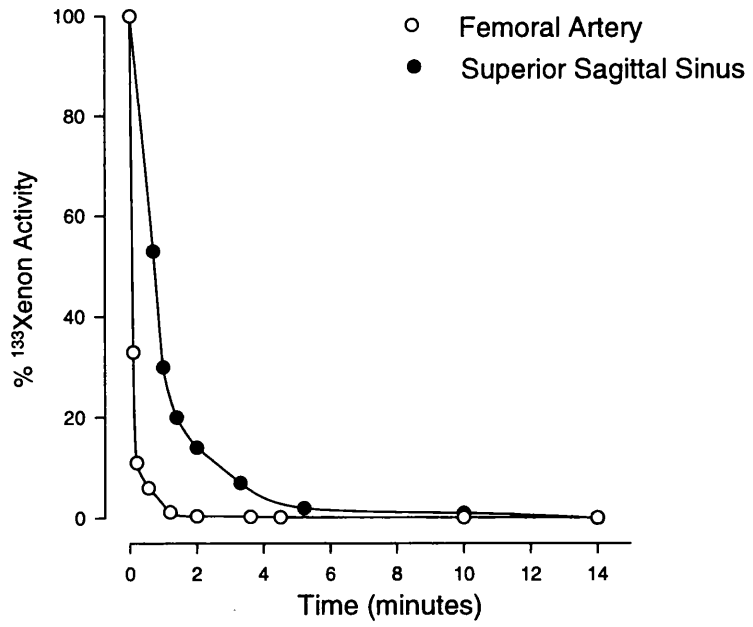

Figure 1.7 *Typical curves for desaturation of ^{133}Xe during the measurement of CBF in the rat. ^{133}Xe activities in the femoral artery and superior sagittal sinus as a percentage of venous activity.*

Of more importance was the subsequent use of ^{133}Xenon (^{133}Xe), a γ emitter, which could be inhaled directly in small concentrations[51] or dissolved in saline for intra-arterial administration directly into the internal carotid artery through a catheter inserted during cerebral angiography[52]. Intravenous injection of ^{133}Xe is now also being used[53].

When ^{133}Xe is injected into the body, either by inhalation or via the vascular system, it diffuses rapidly into the brain and very quickly an equilibrium state is reached between its concentration in the blood and brain tissue. At the same time ^{133}Xe is cleared after a single passage through the lungs with minimal whole body redistribution. Therefore when the injection is stopped, fresh blood containing none of the tracer enters the brain and immediately causes the deposited tracer to be washed out of the brain tissue. The rate of clearance of the ^{133}Xe is dependent upon the flow of blood through the brain and is hence the basis of CBF measurement using this technique.

Scintillation cameras which are capable of detecting the γ emissions from the ^{133}Xe in the tissue are placed over the intact skull. Using an array of multiple detectors it is possible to measure the regional washout of tracer and hence the localised CBF. Clearance curves for ^{133}Xe can then be plotted as shown in Figure 1.7[46]. It can been seen that the concentration of tracer in the tissue (C_T) decreases exponentially with time from the initial or peak concentration at the time of the injection.

The theoretical basis of the method depends upon an extension of the Kety-Schmidt computation described in section 1.4.2.1. It is assumed that after time zero, i.e. directly after the injection, C_a falls to zero. When $C_a = 0$ equation 1.3 becomes

$$\frac{F_t}{W} \cdot C_v = \frac{-dC_T}{dt} \qquad \textbf{(1-5)}$$

If λ_x is the blood:brain partition coefficient for ^{133}Xe then $C_T = \lambda_x.C_v$ and therefore

$$\frac{F_t}{W\lambda_x} \cdot C_T = \frac{-dCT}{dt} \qquad \textbf{(1-6)}$$

Equation 1.6 is a differential equation whose solution yields the following expression for the concentration of ^{133}Xe in the tissue at time t after injection:

$$C_T(t) = C_{T(0)} \cdot \exp -\frac{F_t \cdot t}{W \cdot \lambda} \qquad \textbf{(1-7)}$$

This expression describes the clearance curve shown in Figure 1.7.

There are three well recognised analysis methods by which CBF can be derived from these curves: stochastic, compartmental and initial slope index. It is worth considering the details of these analysis techniques briefly now.

(i) *Stochastic analysis* derives mean CBF over the whole washout period. Since it does not take into account the differences in CBF between the white and grey matter in a specific region of the tissue, a mean value for λ_x, which is tissue specific, is required. Average CBF can be obtained by dividing the height of the clearance curve by the total number of counts recorded:

$$\frac{F}{W} = \frac{(H_{max} - H_{10})}{A} \cdot \lambda \qquad \textbf{(1-8)}$$

where H_{max} = maximum height of the curve

H_{10} = height of the curve 10 minutes after the injection

A = the area under the curve.

This is a straight forward computational task and provides a simple easy calculation of mean CBF.

(ii) *Compartmental analysis* involves resolving the clearance curve into two components; a fast component measuring grey matter CBF and a slow component measuring white matter CBF. The relative weighting of each tissue can also be determined[52]. For 7-9 minutes after the injection two monoexponential curves can be fitted to the data, from which the high and low flow compartments can be derived. The flow for each compartment can then be calculated directly from the half-life ($t_{½}$) of each single clearance curve.

Equation 1.7 can be rearranged to:

$$\frac{F_t}{W} = \ln\frac{C_T(t_0)}{C_T(t)} \cdot \frac{\lambda_x}{t} \qquad \textbf{(1-9)}$$

At $t = (t_{½})$, $C_T = ½ \cdot C_T(t_0)$ therefore:

$$\frac{Ft}{W} = \frac{0.693}{t_{½}} \cdot \lambda_x \qquad \textbf{(1-10)}$$

From this expression the specific flow for each compartment can be calculated with knowledge of λ_x for white and grey matter.

(iii) *Initial slope index* is a value derived from the first 30 - 60 seconds of the clearance curve. A straight line is drawn through the curve over this time and the half-life calculation described above is applied and a mean value for λ_x is used. This is a mean flow measurement but is weighted towards grey matter with a linear correlation to the value calculated by the stochastic method over the first 10 minutes of clearance.

The ^{133}Xe clearance technique has gained much credibility as a reliable method of CBF measurement and has itself led to more sophisticated methods employing radioactive tracers. One of the main limitations of the technique is in the accurate determination of λ_x. The solubility of ^{133}Xe between lipid and water can differ by as much as an order of magnitude thus making the differences between white and grey matter estimates very important. The ^{133}Xe technique favours surface detection and is, like the N_2O tracer technique, vulnerable to inaccuracies due to extracerebral tissue contribution if tissue labelling is non-specific. The theoretical basis of the analysis also relies upon an accurate definition of the point where arterial tracer concentration is zero.

The inhalation method using a stationary scintillation detector, although clinically useful and relatively inexpensive, has limited spatial resolution due to the possibility of gross cross-talk from one hemisphere to the other and the errors induced by Compton scatter effects. Direct injection into the carotid artery yields far more convincing results since all the isotope reaches only one hemisphere. The rapid elimination of ^{133}Xe from the lungs allows fairly high doses to be injected without radiation hazard and provides a very high count rate in the region of interest. In these studies the initial slope index calculation is used to estimate CBF over

only one minute or less in the high flow cortical region. The intracarotid ^{133}Xe method was used to investigate the functional activation of CBF, as well as a variety of cerebral disorders including focal hyperaemia (the luxury perfusion phenomenon) and focal cortical epilepsy. However the trauma involved in the intra-arterial injection means that this method is in practice only used in conjunction with diagnostic carotid angiography.

Although the technique depends upon the introduction of a radioactive tracer it is widely used clinically, even by some groups studying neonatal cerebral haemodynamics[54-56].

1.4.2.4 *Hydrogen Clearance*

Hydrogen can also be used as an inert gas tracer which freely diffuses into brain tissue but its methods of detection limit its use to exposed brain. The hydrogen sensing electrodes are placed directly into the cortical brain tissue and hydrogen is administered in a gas mixture (2-5% typically) until saturation of the cerebral tissue is achieved[57-59]. Once the hydrogen inhalation is stopped, clearance curves for the gas are obtained and the principles of calculation are as described in section 1.4.2.2. Localised and serial CBF measurements are possible but some tissue damage occurs around the electrode site[60, 61]. Hydrogen clearance has been the preferred method for many animal studies because of its capacity for repeated regional CBF measurements in the same animal and the avoidance of radioactive tracer materials. The technique therefore lends itself particularly to studies of sequential CBF and $CMRO_2$ studies[62].

1.4.2.5 *Autoradiography*

The development of autoradiography stemmed from the desire to obtain highly focal measurements of CBF which could be used to relate the haemodynamics of the brain to other variables such as histopathology and glucose uptake. The technique is purely an experimental tool to be used in animal experiments[63] but has led to the development of the clinical technique of positron emission tomography (PET) (section 1.4.2.7).

A diffusible indicator is injected intravenously and is then distributed throughout the brain tissue in a flow dependent fashion. The animal is then killed and the brain is immediately removed, frozen and cut into slices of uniform and known thickness calibrated for known radioactive concentrations. The concentration of tracer in the tissue is determined

by exposing radiographic films in contact with each brain slice. The optical density of various brain slices is read by a densitometer and with appropriate calibration, this can be converted into the radioactive concentration of the tissue. The arterial tracer function is calculated from blood samples taken during tracer injection. The theoretical basis for these calculations is again derived from the Kety-Schmidt modification of the Fick principle.

Rearranging equation 1.3 :

$$\frac{-dC_T}{dt} = \frac{F_t}{W} \cdot (C_a - C_v) \qquad \textbf{(1-11)}$$

If the assumption still holds that $C_T = \lambda.C_v$ then:

$$\frac{-dC_T}{dt} = \frac{F_t}{W} \cdot (C_a - \frac{C_T}{\lambda}) \qquad \textbf{(1-12)}$$

It is then assumed that (F_t/W) and λ can be incorporated into a single constant (k) such that:

$$\frac{-dC_T}{dt} = k \cdot (C_a\lambda - C_T) \qquad \textbf{(1-13)}$$

This simple differential equation can be integrated between time zero (the start of the injection) and time t_1 (the duration of the study):

$$C_T(t_1) = \frac{F_t}{W} \cdot \int_0^{t_1} C_a \cdot \exp -k\,(t_1 - t)\,dt \qquad \textbf{(1-14)}$$

where C_T (t_1) is the concentration of the tracer in the tissue at the end of the study measured by the densitometer, and C_a is the value of the radioactivity in the arterial blood during the study. In this way CBF can be calculated in a large number of discrete portions of brain tissue. Although CBF can be extremely well localised, since the technique involves brain removal no serial flow measurements can be obtained.

The technique requires a tracer which is non-volatile and does not suffer from significant diffusion limitations. It appears that the search for a suitable compound has been

a difficult one. The first tracer used was the radioactive gas ^{131}I-trifluoroiodomethane[64], although it soon became apparent that this was not ideal. In 1969 the use of the first non gaseous tracer, antipyrine-14, was described[65], but again there were reservations about its use in quantitative measurements of CBF. The preferred choice in most recent studies is iodo-[^{14}C]-antipyrine[66] although the search for a more suitable tracer continues[67].

1.4.2.6 *Single Photon Emission Computed Tomography*

The principle of tomography has been defined for many years, i.e. that a two or three dimensional object can be reconstructed from an infinite set of all its projections. Single photon emission computed tomography (SPECT) uses this principle to yield a three dimensional image of the brain in the form of a stack of cross-sectional images similar to those used in CT scanning. In fact, SPECT was first developed into a useful clinical tool in 1963 by Kuhl and Edwards[68] some years before the invention of X-ray CT imaging. Their first studies used a rotating scintillation detector to scan around the head and form a cross-sectional image of the brain. The rectilinear scanner has now been replaced by a rotating γ camera. In 1978 a rapidly rotating and very sensitive four camera system was developed for tomographic CBF measurements using inhaled ^{133}Xe [69, 70]. The ^{133}Xe gas is inhaled for one minute and a series of four tomographs are made from three slices simultaneously, each lasting one minute. The spatial resolution of the technique is 1.7 - 2.0 mm in the three dimensions. Calculation of CBF is based upon the clearance principle and the bolus distribution principle described by Kety.

The clinical utility of SPECT has been enhanced by the development of new tracers. One such tracer is ^{99m}Tc-D-L-hexamethylene propyleneamine (^{99m}Tc-HMPAO), which is chemically trapped in the central nervous system over the first few minutes after intravenous injection. Imaging can be carried out up to six hours after the injection so that the tracer can be injected during a short lived spontaneous event such as a seizure, and the imaging of that same event can be performed hours later perhaps even in a different hospital. The quantitation of SPECT data is difficult due to many sources of error; attenuation, scatter, the partial volume effect where sampling is not contained completely in a transverse slice, and the sampling effect where the observed concentration of the activity appears to be a function of the size of the region in which it is concentrated. However SPECT does provide excellent maps of relative CBF distribution and the delay in imaging time offers important flexibility

in a clinical setting[71, 72]. SPECT has also improved understanding of the pathophysiology of cerebrovascular disorders such as classic migraine[73] and stroke[74] and has been shown to provide more useful images than corresponding CT scans[75].

1.4.2.7 *Positron Emission Tomography*

Technological advances over the last two decades have allowed the further development of tomographic emission techniques in the form of positron emission tomography (PET).

The measurement of regional cerebral blood flow (rCBF) using PET and ^{15}O-labelled water has been described using a number of different implementations including the steady state technique[76], the integrated projection technique[77] and the autoradiographic or dynamic clearance technique[78, 79]. The following theoretical and practical considerations apply to all PET measurements, but the details of the most commonly used methods will be dealt with in turn.

There are a number of positron emitting isotopes (O^{15}, C^{11}, N^{13} and F^{18}) which can be incorporated into biologically active molecules such $H_2{}^{15}O$ and ^{18}F deoxyglucose. Most have short half lives and therefore need to be prepared in a cyclotron on or close to the site of measurement. When such a radionuclide is injected into the body either intravenously or by inhalation, the emitted positrons travel only a few millimetres before colliding with an electron - this is an annihilation event. The products of this collision are two high energy photons which are emitted simultaneously and travel at almost 180° to each other. The photons are of unique and equal energy of 511 keV. External detection and localisation of the positron emitter takes advantage of their unique energy and coincidence. The detection of two coincident annihilation photons by detectors on opposite sides of the head places the position of the original annihilation event on a line between the two detectors. A series of polygonal or circular rings of detectors around the head maximises the detection efficiency of the three dimensional isotope distribution.

It is obviously very important that the head remains completely still during this procedure and for this purpose specifically designed head moulds are used to position the subject. The tracer is administered to the subject using either a face mask or via the intravenous route. Arterial blood is sampled from a catheter inserted into the radial artery and the samples obtained can also be used to monitor arterial blood gases (PaO_2 and $PaCO_2$) and

pH.

(i) *^{15}Oxygen steady state method.* The steady state method requires the subject to breathe a constant concentration of radioactivity which is supplied by the inhalation of $C^{15}O_2$. The ^{15}O rapidly generates $H_2{}^{15}O$ in the pulmonary circulation aided by the catalysis of carbonic anhydrase. The resulting radioactivity is then due to circulating $H_2{}^{15}O$ which is being constantly generated in the lungs. The distribution of this labelled water in the brain is obviously flow dependent. The surface area of the cerebral capillary network and its permeability mean that water is completely extracted across the capillary wall from blood to tissue. However the partitioning of water between blood and tissue differs for white and grey matter with the partition coefficient of white matter being higher than grey (1.04 and 0.88 respectively). The values of these coefficients in diseased tissue must be considered when pathological states of the brain are investigated, although Lammertsma[80] has shown that the assumption that blood:brain tissue partitioning can be considered to equal unity is a valid one.

After 8 minutes the $H_2{}^{15}O$ reaches an equilibrium and a steady cerebral $H_2{}^{15}O$ tissue concentration results. The tissue concentration of $H_2{}^{15}O$ depends upon the arterial supply of the radiolabel and its loss due to radioactive decay and cerebral venous washout. From these assumptions rCBF can be calculated from knowledge of C_T measured by the PET camera and C_a measured from the arterial blood samples by a calibrated well counter.

The PET camera itself produces a cross-sectional image of the brain showing regional uptake of radioactivity. With reference to anatomical atlases or other computerised tomographic (CT) or magnetic resonance imaging (MRI) scans of the subject, regions of interest (ROI) are drawn around structures under investigation. An absolute value of the number of counts in that region can be obtained and from this an absolute value of rCBF derived. It is obvious that the calculation of rCBF relies upon the tissue activity measured by the tomograph being related to C_a (measured by the well counter) by a simple calibration factor so that C_T and C_a can be measured in the same units. The positron tomograph must also have a linear response to radioisotope concentration. It is known that this model is more sensitive at low rather than high values of rCBF since at high flow rates water is not completely extracted by the tissue[81]. This flow limited permeability leads to an underestimation of rCBF[82].

The continuous inhalation method has the advantage that a steady-state equilibrium tissue concentration is maintained allowing time for sufficient data to be collected for accurate

statistical analysis. The obvious disadvantage is poor temporal resolution.

(ii) *Dynamic Clearance Techniques.* The use of an intravenous bolus injection of $H_2{}^{15}O$ for the measurement of CBF was first described by Herscovitch and Raichle in 1983[78, 79]. Their method was based upon the tissue autoradiographic technique described in section 1.4.2.5 and depends upon the use of a tomographic system capable of acquiring large sets of data over relatively short periods of time. The autoradiographic method assumes a monotonically increasing input function to provide a single measurement of C_T and a unique solution for CBF. The dynamic PET method effectively integrates the instantaneous radioactive tracer concentration in the tissue C_T over the time of the scan (usually 40 seconds). Following the intravenous injection the local counts per unit weight of tissue are recorded by the tomograph from a region of brain. Arterial blood samples are collected at the same time from an indwelling arterial catheter.

The dynamic method has produced results which appear to be scan time dependent[79]. This is probably due to the delay and dispersion of the measured arterial blood curve relative to the recorded tissue data[83]. It is also important that the duration of the study must not exceed one minute since CBF is then underestimated, although the mechanism behind this phenomenon is not fully understood[79].

It should be stressed that when only regional comparisons of CBF in the same brain are required, sampling of arterial blood may be unnecessary since the tissue concentration of the tracer in the brain is related to rCBF in an almost linear manner. In this case the PET *image* of the tracer distribution will provide an accurate representation of local tissue blood flow distribution[78].

It is known that once emitted from the isotope the positron travels at least a few millimetres in the tissue before collision with an electron occurs. The exact distance which the positron travels is dependent upon the isotope used but is, for example, 4 - 5mm in the case of $^{15}O_2$. The range of this positron therefore limits the spatial resolution of the technique since it is the position of the isotope nuclei which is required for imaging the CBF distribution rather than the position of the annihilation event. Another inherent error is introduced by the fact that the electron with which the positron collides is actually moving. This movement alters the angle between the two emitted photons, typically by 0.2° producing a further spatial uncertainty of 1 - 2 mm. Despite these inherent limitations PET is still considered the gold

standard method of CBF measurement against which most other techniques are compared.

1.4.3 Microspheres

This technique relies upon the flow dependent entrapment of radioactive carbonised microspheres in end-organ capillaries. The γ emitting particles are injected into the left side of the heart and are then trapped in the cerebral capillaries. The animal is killed, the brain removed and a liquid scintillation counter is used to detect the energy peaks of the trapped microspheres. In this way the microspheres act as a single pass tracer from which blood flow can be calculated in discrete regions of the brain. There are a number of different isotopes suitable for labelling the microspheres including ^{153}Gd, ^{57}Co, ^{141}Ce, ^{51}Cr, ^{113}Sn, ^{103}Ru, ^{46}Sc, ^{85}Sr and ^{95}Nb. Usually four to six isotopes can be used in one animal and in addition different size microspheres can also be injected[84]. In order to quantify CBF absolutely blood is withdrawn from a reference organ during the microsphere injection. The microspheres in this blood are counted and the known flow:microsphere ratio is used to calibrate the counts obtained from the brain tissue.

There are obviously certain requirements which must be met if the microsphere count is to accurately reflect CBF;
(i) thorough mixing must take place at the injection site, (ii) the distribution of the microspheres in the blood must be assumed to be proportional to blood flow and clumping of microspheres near the centre of the blood vessel should be avoided, (iii) all the microspheres are completely trapped on the first passage of the circulation, (iv) the injection of the microspheres does not itself affect or disturb circulatory parameters and (v) the microspheres should remain lodged and radioactive until they are counted.

A considerable amount of technical expertise is therefore required for accurate results and the technique is obviously only applicable in animal experiments. At flow rates below 120 $ml.100g^{-1}.min^{-1}$ the microspheres technique correlates well with ^{133}Xe clearance as measured in a group of baboons[85] and dogs[86]. Above 120 $ml.100g^{-1}.min^{-1}$ the microspheres measurements were consistently less than the those measured using ^{133}Xe, however this discrepancy may be due in part to the inadequacies of the Xenon method at high flow rates.

1.4.4 Thermal Clearance

Thermal diffusion systems rely upon the thermal conductivity of cortical tissue. Two gold plate sensors are placed directly on the exposed cortex of the brain, one is heated the other is neutral. The temperature difference between the two sensors is continuously monitored as ΔT. At zero flow ΔT is dependent only upon the fixed conductivity constant of the tissue between the sensors. As flow increases the heated plate loses heat by convection and ΔT decreases in proportion to the cortical blood flow. ΔT can then be converted into changes in blood flow $ml.100g^{-1}.min^{-1}$.

The probe housing the sensors can be placed directly on the exposed brain during neurosurgery or through burr holes, although care must be taken since the measured thermal gradient will be contaminated by blood, cerebrospinal fluid or air between the sensors. Continuous monitoring of cortical blood flow in epilepsy patients is also possible with implantation of subdural electrodes[87]. The technique has the advantage of very good temporal resolution although the region interrogated is restricted to the cortical tissue directly beneath the sensors. The changes in cortical blood flow measured in this way have been compared with those using hydrogen clearance[88], but Schroder and Muizelaar[89] demonstrated no correlation with the stable Xenon-CT method and have doubted its use as a routine clinical monitor. However since it is a continuous monitor with good temporal resolution it may still be useful in assessing pathophysiological mechanisms such as CO_2 reactivity.

1.4.5 Electromagnetic Flowmeters

For a direct measurement of the inflow of blood into the brain, flowmeters, usually electromagnetic, can be placed around the carotid and/or vertebral arteries[90, 91]. The technique is generally thought to be of limited use due to the inevitable, and largely unavoidable, contamination of the signals due to intra and extracranial anastomoses. Extensive, intricate surgery is required for implantation and in certain species it can be almost impossible to identify vessels which solely supply the cerebral circulation. Unfortunately ligating the vessels responsible for the contamination can actually worsen the situation. The absolute measurement of CBF is also vulnerable to variations in haematocrit[92].

Measurements of venous outflow have also been attempted and have had limited success in the sagittal sinus of the dog and rabbit[93]. Concerns about whether blood is draining

solely from the brain with no mixing from extracerebral tissues is still an issue. For these reasons direct vessel measurement is not a generally recommended technique.

1.4.6 Doppler Techniques

1.4.6.1 *Doppler Ultrasound*

This technique also involves the direct measurement of blood flow within a specified vessel. The Doppler frequency shift of ultrasound reflected from moving particles can be applied to the measurement of red cell flow velocity and, with knowledge of the vessel diameter, CBF can be derived[94]. The carotid and vertebral arteries as well as the terminal branches of the ophthalmic arteries can be used for measurement. Transcranial ultrasound probes can be used to measure the blood flow velocity in the middle cerebral artery[95], and this technique has been adopted as a routine clinical measurement in many intensive care units. More importantly perhaps, the Doppler ultrasound technique has also found favour with paediatricians who have applied it to non invasive measurements of CBF in neonates[96]. The accuracy of absolute measurements is still in doubt, but Doppler ultrasound does provide reliable data on the dynamics of the cerebral circulation.

1.4.6.2 *Laser Doppler*

This technique, which uses a coherent light source, was first demonstrated in whole tissue by Stern in 1975[97]. The Doppler shift in the backscattered light (originally from a Helium-Neon laser) due to its interaction with the moving red blood cells is measured and red blood cell flux is derived. Since the spatial resolution of the technique is about 1mm it can be used to make direct measurements on exposed cortex in animals and intraoperatively in humans[98, 99]. Comparisons have been made between laser Doppler and both ^{133}Xe and radiolabelled microspheres[100, 101] and good agreement has been found.

1.4.7 Nuclear Magnetic Resonance

The role of nuclear magnetic resonance (NMR) for imaging of cerebral anatomy is well established. Developments in collection sequences including echo planar imaging (EPI) have pointed the way towards the rapidly growing field of functional imaging using NMR. Various contrast agents have been used to make high resolution qualitative measurements of CBF[102]. Since deoxyhaemoglobin is more paramagnetic than oxyhaemoglobin it can be used as an endogenous contrast agent and provides the perfect tracer for measurements of tissue perfusion. Over the last decade many groups have attempted to measure distribution in defined regions during audio, sensory or visual stimuli[103]. The debate rages as to the exact clinical usefulness of NMR as a true imager of function and structure and there are still many (particularly in the field of PET imaging) who have yet to be convinced that it will fulfil the potential which has so often been quoted.

1.5 Cerebral Blood Volume

1.5.1 The Control of Cerebral Blood Volume

The distribution of CBV between the different vascular compartments in the brain has already been described in section 1.3.4 and Figure 1.5. When looking at the brain as a rigid fluid filled container a fundamental physical principle can be applied. The rigid skull contains three incompressible constituents; the blood inside the cerebral vasculature, the brain tissue (which is composed of 80% water) and the cerebrospinal fluid (CSF) in the brain ventricles and subarachnoid spaces. These constituents determine their own volumetric equilibrium inside their rigid housing and as such none can change in mass without an equal and opposite change in another. Thus arterial blood inflow and venous blood outflow should be maintained in equilibrium. This equation, initially postulated in the Monroe-Kellie doctrine in the 19th century is in principle correct. However, as discussed in section 1.2.1, the natural conclusion of the doctrine concerning the constancy of CBF is erroneous. Evidence has come to light which challenges the absolute conclusions of the doctrine; the relative compliance of the non-

bony cerebral and spinal cavity walls, the possibility of displacement of CSF inside the cavity, alterations in vessel diameter and volume which are sufficient to change the cerebrovascular resistance and rCBF, and finally the dissipation of the volume changes of pial arteries over the whole intracranial cavity. However, excessive accumulation of blood in the skull must cause displacement of other components in its interior. This will lead to an increase in intracranial pressure, a decrease in CSF volume and compression of cerebral tissue. These effects in turn promote excessive water filtration from the blood into the brain tissue and in pathological conditions such as trauma or hypoxia an increase in CBV can seriously augment the development of cerebral edema. For this reason there is a special control mechanism to protect against such potentially damaging effects.

Increases in CBV are caused by either of the following reasons. First, surplus inflow of arterial blood from the central arterial system may occur while the cerebral venous outflow is unable to maintain intracranial blood volume constant. Secondly, accumulation of blood in the cerebral vessels may be caused by the obstruction or restriction of blood outflow into the extracranial veins from inside the skull. It is clear that these situations can be controlled by two haemodynamic effects; either an increase of blood outflow from the brain to the

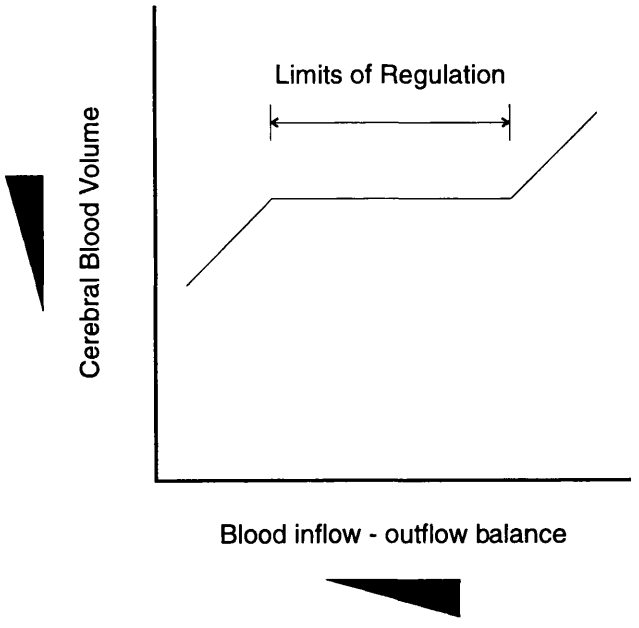

Figure 1.8 *Diagrammatic representation of CBV regulation. The active control system of the cerebral circulation maintains a constant CBV within certain limits in spite of changes in cerebral blood inflow-outflow balance.*

extracranial venous bed or a restriction of inflow of blood from the extracranial arteries, i.e. either active venous or arterial control must be exercised. It has been shown that although cranial veins will respond to sympathetic stimulation and vasoconstricting agents, the cerebral venous pressure is linearly related to the extracranial venous pressure[104]. This clearly indicates the absence of an active autoregulatory response in the cerebral venous system.

It is well known that cerebral arteries are both structurally and functionally equipped to control the inflow of blood into the brain and it is therefore no surprise that it is this arterial control which is responsible for maintaining CBV in the normal range and preventing potentially dangerous excessive accumulation of blood in the cerebral vasculature. Physical factors such as the rigidity of the skull, the CSF pressure and the mechanical properties of the brain do still play an important part in the maintenance of constant CBV particularly when the blood inflow-outflow balance is shifted to the negative side due to deficient blood inflow to the brain. Figure 1.8 demonstrates diagrammatically CBV regulation in terms of the blood inflow-outflow balance[40].

Animal studies have shown that if all the jugular veins are simultaneously occluded at the neck the total blood inflow to the brain is decreased. This effect was shown to be due to constriction of the major cerebral arteries (the internal carotid and vertebral arteries) rather than the pial or intracerebral arteries[105, 106]. It is the major arteries therefore which act as vascular affectors and are responsible for protecting the brain against excessive blood accumulation and maintaining CBV constant. This effect appears to be more well defined than the regulatory mechanisms controlling CBF.

Although the regulation of CBF and CBV are believed to be derived from different mechanisms they may operate synergistically and activators of the same effectors of regulation will combine to maintain constant cerebral blood flow, volume and pressure.

1.5.2 The Relationship between CBV and CBF

A fundamental equation which is often used in theoretical calculations of CBF was derived in 1954 by Meier and Zierler[107]:

$$\bar{t} = \frac{V}{F_t} \qquad \textbf{(1-15)}$$

where t is the mean transit time of a tracer through the brain, V is the volume of distribution of tracer in the organ and F_t is the blood flow per minute through the organ. For a non diffusible tracer the mean transit time of the tracer will approximate the mean cerebral vascular transit time and the volume distribution will approximate CBV. The CBF/CBV ratio is therefore equivalent to the reciprocal of the mean vascular transit time. This is also known as the Stewart Hamilton relationship.

Under certain conditions CBV can provide an index for CBF. Grubb et al. showed a linear relationship between CBV and $PaCO_2$ in rhesus monkeys[108]. However under conditions of induced hyper- or hypocapnia CBV displays a significant, though non linear, relationship with CBF[109]. During induced hypo- or hypertension CBV changes are completely independent of changes in CBF[110]. In fact from combinations of independent CBV and CBF changes it is possible to classify certain haemodynamic changes. The CBF/CBV ratio can be used to represent specific haemodynamic conditions within certain regions of the brain and in different pathological states.

1.5.3 The Relationship Between $PaCO_2$ and CBV

As already demonstrated in section 1.2.2 $PaCO_2$ has a potent effect on the cerebral vasculature. An increase in $PaCO_2$ produces the most marked vasodilation of any known agent whilst a reduction in $PaCO_2$ produces a profound vasoconstriction[29, 44]. Greenberg et al.[111] found a linear relationship between $PaCO_2$ and CBV in the range 2.5 - 5.5 kPa in both the grey and white matter using PET to measure local cerebral blood volume (LCBV) in normal human awake volunteers. The results yielded a slope of 3.68 $ml.100g^{-1}.kPa^{-1}$ for the entire brain. Other investigators have shown linear responses over a range of $PaCO_2$ values in the rhesus monkey[31, 108], goats[112] and rats[113]. It has also been shown in animal studies that removal of the skull bone allows the brain to swell freely and augment the increase in CBV with hypercapnia[110].

1.5.4 The Measurement of CBV

The techniques used to measure CBV fall into three catogeries; ex vivo methods, in vivo methods and transit time methods.

The ex vivo method has its basis in the autoradiographic method which has already been described in detail in section 1.4.2.5. It involves the injection of an intravascular tracer which is injected into an animal which is then killed. The brain is excised and the CBV is calculated by comparing the concentration of the tracer per weight of brain sample to the concentration per weight of blood.

The in vivo method requires the measurement of the concentration of the intravascular indicator in the brain tissue in vivo with reference to the blood concentration by means of external detectors once equilibrium has been reached.

$$rCBV = \frac{C_T}{C_a \cdot r} \qquad \textbf{(1-16)}$$

where r is the ratio of brain to capillary large-vessel haematocrit. Early studies were performed on cats by Risberg et al.[114] who used ^{131}I-labelled human serum albumin as a tracer for continuous monitoring of CBV. Relative changes in CBV have been carried out by reflectrometry of haemoglobin in superficial areas of the brain[115] and by the photoelectric method[116]. The first method to succeed in providing quantitative measurements of CBV in humans was developed by Ter-Pogossian, Grubb and Phelps using the X-ray fluorescence of iodinated contrast material[117-119]. This led to the measurement of rCBV using positron emitting intravascular tracers which selectively label the red blood cells for the duration of a PET study. Kuhl et al. [120] and Greenberg[111] used ^{99m}Tc-labelled red blood cells, and because of its affinity to haemoglobin, carbon monoxide compounds are also suitable tracers. Both ^{11}C-labelled carbon monoxide[121] and ^{15}O labelled carbon monoxide[122] have been used. In all these in vivo methods the CBV values obtained are derived from those of red cell volume and therefore tissue haematocrit must be known or accurately estimated to provide an absolute measurement of CBV. In addition the density of both blood and tissue must be known and account must be taken of tracer recirculation.

The transit time method involves measurement of the transit time of a non diffusible tracer (t_b) which remains in the blood and the transit time of a diffusible tracer (t_t) which

transfers into the tissue. Since t_b and t_t are proportional to the volume of tracer in the blood and tissue respectively CBV can be calculated from the ratio t_b of to t_t:

$$CBV = 100 \cdot \lambda \cdot \frac{t_b}{t_t} \qquad \textbf{(1-17)}$$

where λ is the partition coefficient of the diffusible indicator between the blood and brain tissue. This method has been used in man[123] with ^{99}Tc-labelled red blood cells and ^{133}Xe and with indocyanine green and ^{85}Kr[112]. In the monkey $H_2{}^{15}O$ and $C^{15}O$ labelled red blood cells[109] have been used. This method is seen to be clinically useful but errors include overlapping effects and unmatched spatial measuring volumes.

1.6 SUMMARY

This chapter has described the role of the cerebral circulation and the importance of reliable monitoring of cerebral haemodynamics. Table 1.i summarises the important attributes of those techniques which are currently in use for the clinical measurement of CBF and CBV. At present no single technique provides a combination of all the "ideal" requirements. In other words an inexpensive, easily managed bedside monitor which provides information on CBF and CBV with high temporal and spatial resolution has yet to be developed. The technique of near infrared spectroscopy has been included in the table, and in the following chapters its contribution to the assessment of cerebral haemodynamics will be detailed.

Table 1.i *Comparison of clinical methods currently available for the measurement of CBF. An asterix marks those techniques which can also be used to measure CBV.*

Technique	Spatial Resolution	Temporal Resolution	Tracer	Clinical Applicability	Advantages	Disadvantages
Kety-Schmidt	Global	Intermittent (minutes)	N_2O	Bedside	Inexpensive, minimal equipment, repeatable	No spatial resolution
^{133}Xenon	cm^3	Intermittent (minutes)	^{133}Xenon	Bedside	Regional, mobile,	Radioactive tracer limits repeatability
PET*	mm^3	Intermittent (minutes)	$C^{15}O_2$	Requires dedicated laboratory	Highly localised, produces CBF maps	Radioactive tracer limits repeatability, expensive, technically demanding
Thermal Clearance	mm^3	Continuous	Thermal bolus	Only used on exposed cortex	High temporal resolution, inexpensive	Craniectomy necessary, restricted to cortical measurements
Laser Doppler	mm^3	Continuous	-	Only used on exposed cortex	High temporal resolution	Quantitation of relative trends only, craniectomy necessary
Transcranial Doppler	cm^3	Continuous	-	Bedside	Non invasive, inexpensive	Non quantitative, signal influenced by large artery calibre variation
NMR	mm^3	Intermittent (minutes)	Spin labelled H_2O	Requires dedicated laboratory	Highly localised, also provides brain maps	Non quantitative, expensive
NIRS*	cm^3	seconds	$\Delta[HbO_2]$	Bedside	Non invasive high temporal resolution absolute quantitation	Low spatial resolution, not yet validated

1.7 REFERENCES

1. Jöbsis F.F. (1977) Noninvasive infrared monitoring of cerebral and myocardial oxygen sufficiency and circulatory parameters. *Science* 198;1264-1267
2. Brazy J.E., Lewis D.V., Mitnick M.H., Jöbsis F.F. (1985) Noninvasive monitoring of cerebral oxygenation in preterm infants: preliminary observations. *Pediatrics* 75;217-225
3. Brazy J.E. and Lewis D.V. (1986) Changes in cerebral blood volume and cytochrome aa3 during hypotensive peaks in preterm infants. *Pediatrics* 108;983-987
4. Ferrari M., De Marchis C., Giannini I., Nicola A., Agostino R., Nodari S., Bucci G. (1986) Cerebral blood volume and haemoglobin oxygen saturation monitoring in neonatal brain by near infrared spectroscopy. *Adv. Exp. Med. & Biol.* 200;203-212
5. Wyatt J.S., Cope M., Delpy D.T., Edwards A.D., Wray S.C., Reynolds E.O.R. (1986) Quantification of cerebral oxygenation and haemodynamics in sick newborn infants by near infrared spectrophotometry. *Lancet* ii;1063-1066
6. Edwards A.D., Wyatt J.S., Richardson C., Delpy D.T., Cope M., Reynolds E.O.R. (1988) Cotside measurement of cerebral blood flow in ill newborn infants by near infrared spectroscopy. *Lancet* 2;770-771
7. Wyatt J.S., Cope M., Delpy D.T., Richardson C.E., Edwards A.D., Wray S., Reynolds E.O.R. (1990) Quantitation of cerebral blood volume in human infants by near-infrared spectroscopy. *J. Applied Physiol.* 68;1086-1091
8. Peebles D.M., Edwards A.D., Wyatt J.S., Bishop A.P., Cope M., Delpy D.T., Reynolds E.O.R. (1991) Effect of oxytocin on fetal brain oxygenation during labour. *Lancet* 338;254-255
9. Peebles D.M., Edwards A.D., Wyatt J.S., Bishop A.P., Cope M., Delpy D.T., Reynolds E.O.R. (1992) Changes in human fetal cerebral haemoglobin concentration and oxygenation during labour measured by near infrared spectroscopy. *Am. J. Obstet. Gynecol.* 166;1369-1373
10. Aldrich C.J., Wyatt J.S., Spencer J.A.D., Reynolds E.O.R., Delpy D.T. (1994) The effect of maternal oxygen administration on human fetal cerebral oxygenation measured during labour by near infrared spectroscopy. *Br. J. Obst. & Gynaecol.*

101;509-513

11. Fox E.J., Harme M.H., Mitnick M.H., Jöbsis F.F. (1982) Non invasive monitoring of cerebral oxygen sufficiency during general anesthesia. *Anesthesiology* 57;A160
12. Ferrari M., De Marchis C., Giannini I., Sideri G., Fieschi C., Carpi A. (1986) Effects of carotid compression test on regional cerebral blood volume, haemoglobin oxygen saturation and cytochrome-c-oxidase redox level in cerebrovascular patients. *Adv. Exp. Med. & Biol.* 200;213-222
13. Chance B., Smith D.S., Nioka S., Miyoka H., Holton G., Maris M. (1989) Photon migration in muscle and brain. In "*Photon migration in tissues*", eds Chance B., Plenum Press, .
14. Hampson N.B., Camporesi E.M., Stolp B.W., Moon R.E., Shook J.E., Greibel J.A., Piantadosi C.A. (1990) Cerebral oxygen availability by NIR spectroscopy during transient hypoxia in humans. *J. Applied Physiol.* 69;907-913
15. Greely W.J., Bracey V.A., Ungerleider R.M., Greibel J.A., Kern F.H., Boyd J.L., Reves J.G., Piantadosi C.A. (1991) Recovery of cerebral metabolism and mitochondrial oxidation state is delayed after hypothermic circulatory arrest. *Circulation* 84;400-406
16. Solokoff L. (1960) Metabolism of the central nervous system in vivo. In "*Handbook of Physiology*", eds McGoun H.W., Williams and Wilkins, Washington D.C.
17. Williams L.R. and Leggett R.W. (1989) Reference values for resting blood flow to organs of man. *Clin. Phys. Physiol. Meas.* 10(3);187-217
18. Kety S.S. and Schmidt C.F. (1948) The nitrous oxide method for the quantitative determination of cerebral blood flow in man: theory, procedure, and normal values. *J. Clin. Invest.* 27;476-483
19. Xie Y., Mies G., Hossman K.A. (1984) Ischemic threshold of brain protein sysnthesis of the unilateral carotid artery occlusion in gerbils. *Stroke* 20;620-626
20. Astrup J., Symon L., Branston N.M., et al. (1977) Cortical evoked potential and extracellular K and H at critical levels of brain ischemia. *Stroke* 8;51-57
21. Scheinberg E. and Joyne H.W. (1952) Factors influencing cerebral blood flow and metabolism. *Circulation* 5;225-236
22. Peterson S.E., Fox P.T., Postner M.I., Mintum M., Raichle M.E. (1988) Positron emission tomographic studies of the cortical anatomy of single word processing. *Nature* 331;585-589

23. Phelps M.E., Kuhl D.E., Mazziotta J.C. (1981) Metabolic mapping of the brain's response to visual stimulation: studies in humans. *Science* 211;1445-1448

24. Hill L. (1896) *The Physiology and Pathology of the Cerebral Circulation.*, Churchill, London.

25. Lassen N.A. (1959) Cerebral blood flow and consumption in man. *Physiol. Rev.* 39;183-238

26. Kety S.S. (1960) The cerebral circulation. In "*Handbook of Physiology*", eds McCoun H.W., Williams and Wilkins, Washington D.C.

27. Harper A.M. (1990) Physiological control of the cerebral circulation. In "*Cerebral blood flow and metabolism*", eds Harper A.M. and Jennett S., Manchester University Press, Manchester.

28. Lassen N.A. (1978) Brain. In "*Peripheral Circulation*", eds Johnson P.C., John Wiley & Sons, New York.

29. Gibbs F.A., Gibbs E.L., Lennox W.G. (1935) Changes in human cerebral blood flow consequent of alterations in blood gases. *Am. J. Physiol.* 111;557-563

30. Kety S.S. and Schmidt C.F. (1948) The effects of altered arterial tensions of carbon dioxide and oxygen on cerebral oxygen consumption of normal young men. *J. Clin. Invest.* 27;484-492

31. Reivich M. (1964) Arterial PCO_2 and cerebral hemodynamics. *Am. J. Physiol.* 206(1);25-35

32. Symon L., Held K., Dorsch N.W.C. (1973) A study of regional autoregulation in the cerebral circulation to increased perfusion pressure in normocapnia and hypercapnia. *Stroke* 4;139-147

33. D'Alecy L.A., Rose C.J., Seller S.A. (1979) Sympathetic modulation of hypercapnia cerebral vasodilation in dogs. *Circ. Res.* 45;771-785

34. Severinghaus J.W. and Lassen N.A. (1967) Step hypocapnia to separate arterial from tissue PCO_2 in the regulation of cerebral blood flow. *Circ. Res.* 20;272-278

35. Raichle M.E. and Plum F. (1972) Hyperventilation and cerebral blood flow. *Stroke* 3;566-575

36. McDowall D.G. (1966) Interrelationships between blood oxygen tension and cerebral blood flow. In "*Oxygen Measurements in Blood and Tissues*", eds Payne J.P. and Hill D.W., Churchill, London.

37. Kogure K., Scheinberg P., Reinmuth O., Fujishima M., Busto R. (1970) Mechanisms

of cerebral vasodilation in hypoxia. *J. Applied Physiol.* 29;223-229

38. Hamer J., Hoyer S., Alberti E., Weinhardt F. (1976) Cerebral blood flow and oxidative brain metabolism during and after moderate and profound arterial hypoxemia. *Acta. Neurochir.* 33;141-150

39. Siesjo B.K. (1978) *Brain Energy and Metabolism.*, J. Wiley and Sons, New York.

40. Mchedlishvili G. (1986) *Arterial behavior and blood circulation in the brain.*, Plenum Press, New York.

41. Duvernoy H.M., Delon S., Vannson J.L. (1981) Cortical blood vessels of the human brain. *Brain Res. Bull.* 7;519-579

42. Mellander S. and Johannsson B. (1968) Control of resistance, exchange and capacitance vessels in the peripheral circulation. *Pharmacol. Rev.* 20;117-196

43. Lierse W. and Horstmann E. (1965) Quantitative anatomy of the cerebral vascular bed with especial emphasis on homogeneity and inhomogeneity in small parts of the gray and white matter. *Acta Neurol. Scand.* 14;15-19

44. Gibbs E.L., Lennox W.G., Nims L.F., Gibbs F.A. (1942) Arterial and cerebral venous blood. Arterial differences in man. *J. Biol. Chem.* 144;325-332

45. Kety S.S. and Schmidt C.F. (1945) The determination of cerebral blood flow in man by the use of nitrous oxide in low concentrations. *Am. J. Physiol.* 143;53

46. Edvinsson L., MacKenzie E.T., McCulloch J. (1993) *Cerebral Blood Flow and Metabolism.*, Raven Press, New York.

47. Robertson C. (1993) Measurements of cerebral blood flow and metabolism in severe head injury using the Kety-Schmidt technique. *Acta. Neurochir.* 59;25-27

48. Overgaard J., Molsdad C., Tweed W.A. (1981) Cerebral circulation after head injury. Part 3. Does reduced cerebral blood flow determine recovery of brain function after blunt head injury? *J. Neurosurg.* 55;63-74

49. Robertson C.S., Contant C.F., Gokaslan Z.L., Narayan R.K., Grossman R.G. (1992) Cerebral blood flow, arteriovenous oxygen difference, and outcome in head injured patients. *J. Neurol. Neurosurg. Psychiatry.* 55;594-603

50. Lassen N.A., Hoedt-Rasmussen K., Sorensen S.C., Skinhoj E., Cronquist S., Bodforss B., Ingvar D.H. (1963) Regional cerebral blood flow in man determined by krypton^{85}. *Neurology* 13;719-727

51. Obrist W.D., Thomson H.K., Wang H.S., et al. (1975) Regional cerebral blood flow estimated by ^{133} Xenon inhalation. *Stroke* 6;245-256

52. Hoedt-Rasmussen K., Svensdottir E., Lassen N.A. (1966) Regional cerebral blood flow in man determined by intra-arterial injection of inert gas. *Circ. Res.* 18;237-247

53. Meixensberger J. (1993) Xenon 133 - CBF measurements in severe head injury and subarachnoid haemorrhage. *Acta. Neurochir.* Suppl 59;28-33

54. Greisen G. (1990) Cerebral blood flow in mechanically ventilated preterm neonates. *Dan. Med. Bull.* 2;124-132

55. Greisen G. (1986) Cerebral blood flow in preterm infants during the first week of life. *Acta Paediatr. Scand.* 75;43-51

56. Jaggi J.L., Lipp A.E., Duc G. (1989) Measurement of cerebral blood flow with a noninvasive ^{133} Xenon method in preterm infants. In "*Physiological Foundations of Perinatal Care*", eds Stern L. and Fris-Hansen B., Elsevier, Amsterdam.

57. Pasztor E., Symon L., Dorsch N.W., Branston N.M. (1973) The hydrogen clearance method for assessment of blood flow in cortex, white matter and deep nuclei of baboon. *Stroke* 4;556-571

58. Skarphedinsson J.O., Harding H., Thoren P. (1988) Repeated measurements of cerebral blood flow in rats. Comparisons between the hydrogen clearance method and laser Doppler flowmetry. *Acta Physiol. Scand.* 134(1);133-142

59. Meyer J.S., Toyoda M., Schinohara Y., Kitamura A., Ryn T., Wiederholt J. (1968) Regional cerebral blood flow (carotid perfusion) measured by clearance of hydrogen from cerebral venous blood. *Scand. J. Clin. Lab. Invest.* Suppl 102;XIG

60. Uhl M.W., Kochanek P.M., Schiding J.K., Melick J.A., Nemoto E.M. (1992) The regional cerebral blood flow response to cortical microelectrode insertion is neutrophil dependent. *Adv. Exp. Med. & Biol.* 317;701-705

61. Tomida S., Wagner H.G., Klatzo I., Nowak T.S. (1989) Effect of acute electrode placement on regional CBF in the gerbil: a comparison of blood flow measured by hydrogen clearance, [^{3H}] nicotine, and [^{14}]iodoantipyrine techniques. *J. Cereb. Blood Flow & Metab.* 9;79

62. Nemoto E.M., Liping Y., Yonas H., Darby J. (1992) Active basal and whole brain blood flow, oxygen and glucose metabolism in monkeys. *Adv. Exp. Med. & Biol.* 317;695-699

63. Jones S.C., Korfali E., Marshall S.A. (1991) Cerebral blood flow with the indicator fractionation of [^{14}C] Iodoantipyrine : Effect of PCO_2 on cerebral venous appearance time. *J. Cereb. Blood Flow & Metab.* 11;236-241

64. Landau W.M., Freygang W.H., Rowland L.P., Solokoff L., Kety S.S. (1955) The local circulation of the living brain: Values in the unanesthetized and anesthetised cat. *Trans. Am. Neurol. Assoc.* 80;125-129

65. Reivich M., Jehle J., Solokoff L., Kety S.S. (1969) Measurement of regional cerebral blood flow with antipyrine-^{14} in awake cats. *J. Applied Physiol.* 27;296-300

66. Sakurada O., Kennedy C., Jehle J., Brown J.O., Garbin G.L., Solokoff L. (1978) Measurement of local cerebral blood flow with iodo-[14C]-antipyrine. *Am. J. Physiol.* 234;H59-H66

67. Goldman S.S., Hass W.K., Ransohoff J. (1980) Unsymmetrical alkayl thioureas compounds for use as cerebral blood flow tracers. *Am. J. Physiol.* 238;H776-H787

68. Kuhl D.E. and Edwards R.Q. (1963) Image separation radioisotope scanning. *Radiology* 80;653-662

69. Lassen N.A., Svensdottir E., Kanno I., Stokely E.M., Rommer P. (1978) A fast moving, single photon emission tomograph for regional cerebral blood flow studies in man. *J Comput. Assist. Tomogr.* 2;661-662

70. Stokely E.M., Svensdottir E., Lassen N.A., Rommer P. (1980) A single photon dynamic computer-assisted tomograph (DCAT) for imaging brain function in multiple cross sections. *J Comput. Assist. Tomogr.* 4;230-240

71. Anderson A.R. (1989) ^{99m}Tc-D,L-hexamthylene-propyleneamine oxime (^{99m}Tc-HMPAO): basic kinetic studies of a tracer of cerebral blood flow. *Cereb. Brain. Metab. Rev.* 1;228-318

72. Anderson A.R., Friberg L., Schmidt J.F., Hasselbalch S.G. (1988) Quantitative measurements of cerebral blood flow using SPECT and [^{99m}Tc]-d,l-HM-PAO compared to xenon^{133}. *J. Cereb. Blood Flow & Metab.* 8(6);S69-81

73. Lauritzen M. and Olesen J. (1984) Regional cerebral blood flow during migraine attacks by xenon-133 inhalation and emission tomography. *Stroke* 12;284-288

74. Lassen N.A., Henriksen L., Paulson O.B. (1981) Regional cerebral blood flow in stroke by 133-xenon inhaltion using emission tomography. *Stroke* 12;284-288

75. Decety J., Sjoholm H., Ryding E., Stenberg G., Ingvar D.H. (1990) The cerebellum participates in mental actvity: tomographic measurements of regional cerebral blood flow. *Brain Res.* 535;313-317

76. Frackowiak R.S., Lenzi G.L., Jones T., Heather J.D. (1980) Quantitative measurement of regional cerebral blood flow and oxygen metabolism in man using ^{15}O and positron

emission tomography: theory, procedure, and normal values. *J Comput. Assist. Tomogr.* 4;727-736

77. Huang S.C., Carson R.E., Hoffman E.J., Carson J., MacDonald N., Barrio J.R., Phelps M.E. (1983) Quantitative measurement of local cerebral blood flow in humans by positron emission tomography and ^{15}O-water. *J. Cereb. Blood Flow & Metab.* 3;141-153

78. Herscovitch P., Markham J., Raichle M.E. (1983) Brain blood flow measured with intravenous $H_2{}^{15}O$. I. Theory and error analysis. *J. Nucl. Med.* 24;782-789

79. Raichle M.E., Martin W.W.R., Herscovitch P., Mintun M.A., Markham J. (1983) Brain blood flow measured with intravenous $H_2{}^{15}O$. II. Implementation and Validation. *J. Nucl. Med.* 24;790-798

80. Lammertsma A.A., Jones T., Frackowiak R.S.J., Lenzi G.L., Pozzilli C. (1981) A theorectical study of the steady state model for measuring regional cerebral blood flow and oxygen utilisation using oxygen-15. *J Comput. Assist. Tomogr.* 5;544-550

81. Eichling J.O., Raichle M.E., Grubb R.L., Ter-Pogossian M.M. (1974) Evidence of the limitations of water as a freely diffusible tracer in brain of the rhesus monkey. *Circ. Res.* 35;358-364

82. Herscovitch P., Raichle M.E., Kilbourn M.R., Welch M.J. (1987) Positron emission tomographic measurement of cerebral blood flow and permeability-surface area product of water using [^{15}O]water and [^{11}C]butanol. *J. Cereb. Blood Flow & Metab.* 7;527-542

83. Iida H., Kanno I., Miura S., Murakami M., Takahashi K., Uemura K. (1986) Error analysis of a quantitative cerebral blood flow measurement using $H_2{}^{15}O$ autoradiography and positron emission tomography, with respect to the dispersion of the input function. *J. Cereb. Blood Flow & Metab.* 6;536-545

84. Marcus M.L., Heistad D.D., Ehrhardt J.D., Abbound F.M. (1976) Total and regional cerebral blood flow measurements with 7-, 10-, 15-, 25-, and 50 μm microspheres. *J. Applied Physiol.* 40;501-507

85. Marcus M.L., Bischof C.J., Heistad D.D. (1981) Comparison of microsphere and ^{133}Xenon clearance method in measuring skeletal muscle and cerebral blood flow. *Circ. Res.* 48;748-761

86. Fan F.C., Chen R.Y.Z., Schuessler G.B., Chien S. (1979) Comparison between the ^{133}Xe clearance method and microsphere technique in cerebral blood flow

determinations in the dog. *Circ. Res.* 44(5);653-659

87. Carter L.P., Weinand M.E., Oommen K.J. (1993) Cerebral blood flow (CBF) monitoring in intensive care by thermal diffusion. *Acta. Neurochir.* ;43-46

88. Gaines C., Carter L.P., Crowell R.M. (1983) Comparison of local cerebral blood flow determined by thermal and hydrogen clearance. *Stroke* 14;66-69

89. Schröder M.L. and Muizelaar J.P. (1993) Monitoring of regional cerebral blood flow (CBF) in acute head injury by thermal diffusion. *Acta. Neurochir.* ;47-49

90. Harper A.M., Lorimer A.R., Thomas D.L. (1974) Methods of measuring blood flow. In "*Scientific Foundations of Anaesthesia*", eds Scurr B. and Feldman S., Heinemann, London.

91. Cappelen C. and Hall K.V. (1967) Electromagnetic blood flowmetry in clinical surgery. *Acta Chir. Scand.* 368;1-27

92. Roberts V.S. (1969) Haematocrit variations and electromagnetic flowmeter sensitivity. *Biomed. Eng,* 4;408-412

93. Meyer J.S., Yoshida K., Sakamoto K. (1967) Autonomic control of cerebral blood flow measured by electromagnetic flowmeters. *Neurology* 17;638-648

94. Atkinson P. and Woodcock J.P. (1982) *Doppler Ultrasound and its use in Clinical Measurements.*, Academic Press, New York.

95. Newell D.W. and Aaslid R. (1992) *Transcranial Doppler.*, Raven Press, New York.

96. Paneri R.B., Coughtrey H., Rennie J.M., Evans D.H. (1993) A model of the instantaneous pressure-velocity relationships of the neonatal cerebral circulation. *Physiol. Meas.* 14(4);411-418

97. Stern M.D. (1975) *In vivo* evaluation of microcirculation by coherent light scattering. *Nature* 254;56-58

98. Diragl U., Kaplan B., Jacewicz M., Pulsinelli W. (1989) Continuous measurement of cerebral cortical blood flow by laser-doppler flowmetry in a rat stroke model. *J. Cereb. Blood Flow & Metab.* 9;589-596

99. Carter L.P. (1991) Surface monitoring of cerebral cortical blood flow. *Cereb. Brain. Metab. Rev.* 3;246-261

100. Eyre J.A., Flecknell P.A., Bartholomew P.H., Sinclair J.I. (1988) A comparison of measurements of cerebral blood flow in the rabbit using laser Doppler spectroscopy and radionuclide labelled microspheres. *Clin. Phys. Physiol. Meas.* 9(1);65-74

101. Stern M.D., Lappe D.L., Bowen P.D., Chimosky J.E., Holloway G.A., Kreiser H.R.,

Bowman R.L. (1977) Continuous measurement of tissue blood flow by laser-Doppler spectroscopy. *Am. J. Physiol.* 232;H441-448

102. Baker L.L., Kucharczyk J., Sevick R.J., Mintorovitch J., Moseley M.E. (1991) Recent advances in MR imaging/spectroscopy of cerebral ischemia. *AJR* 156;1133-1143
103. Turner R., Jezzard P., Wen H., Kwong K.K., Le Bihan D., Zeffiro T., Balaban R.S. (1993) Functional mapping of the human visual cortex at 4 and 1.5 tesla using deoxygenation contrast EPI. *Magn. Res. Med.* 29;277-279
104. Mchedlishvili G., Sikharulidze N.V., Itkus M.L., Janushewski S. (1980) Cerebral venous pressure, its relation to systemic venous pressure and brain edema development. *Byull. Eksp. Biol. Med.* 89;14-16
105. Mchedlishvili G. (1964) Vascular mechanisms pertaining to the intrinsic regulation of the cerebral circulation. *Circulation* 30;597-610
106. Mchedlishvili G. (1972) *Vascular Mechanisms of the Brain.*, Plenum Press, New York.
107. Meier P. and Zieler K.L. (1954) On the theory of the indicator-dilution method for measurement of blood flow and volume. *J. Applied Physiol.* 12;731-744
108. Grubb R.L., Raichle M.E., Eichling J.O., Ter-Pogossian M.M. (1974) The effects of changes in $PaCO_2$ on cerebral blood volume, blood flow, and vascular mean transit time. *Stroke* 5;630-639
109. Eichling J.O., Raichle M.E., Grubb R.L., Larson K.B., Ter-Pogossian M.M. (1975) In vivo determination of cerebral blood volume with radioactive oxygen-15 in the monkey. *Circ. Res.* 37;707-711
110. Raichle M.E. (1979) Quantitative in vivo autoradiography with positron emission tomography. *Brain Res. Rev.* 1;47-68
111. Greenberg J.H., Alavi A., Reivich M., Kuhl D.E., Uzzell B. (1978) Local cerebral blood volume in response to carbon dioxide in man. *Circ. Res.* 43(2);324-331
112. Smith A.L., Neufeld G.R., Ominsky A.J., Wollman H. (1971) Effect of arterial CO_2 tension on cerebral blood flow, mean transit time, and vascular volume. *J. Applied Physiol.* 31(5);701-707
113. Metzger H., Erdmann W., Thews G. (1971) Effect of short periods of hypoxia, hyperoxia, and hypercapnia on brain O_2 supply. *J. Applied Physiol.* 31(5);751-759
114. Risberg J., Ancri D., Ingvar D.H. (1969) Correlation between cerebral blood volume and cerebral blood flow in the cat. *Exp. Brain Res.* 8;321-326
115. Eke A., Hutiray G., Kovach A.B.G. (1979) Induced hemodilution detected by

reflectrometry for measuring microregional blood flow and blood volume in cat brain cortex. *Am. J. Physiol.* 236;H759-H768

116. Tomita M., Gotoch F., Sato T., et al. (1978) Photoelectric method for estimating hemodynamic changes in cerebral tissue. *Am. J. Physiol.* 4;322-328

117. Ter-Pogossian M.M., Phelps M.E., Grubb R.L., et al. (1971) Measure of regional cerebral blood volume in vivo by means of excited fluorescent X-radiation, and factors affecting this parameter. *Eur. Neurol.* 6;218-223

118. Grubb R.L., Phelps M.E., Ter-Pogossian M.M. (1973) Regional cerebral blood volume in humans. X-ray fluorescence studies. *Arch. Neurol.* 28;38-44

119. Phelps M.E., Grubb R.L., Ter-Pogossian M.M. (1973) In vivo regional cerebral blood volume by X-ray fluorescence: validation of method. *J. Applied Physiol.* 35;741-747

120. Kuhl D.E., Reivich M., Alavi A., Nyary I., Staum M. (1975) Local cerebral blood volume determined by three-dimensional reconstruction of radionuclide scan data. *Circ. Res.* 36;610-619

121. Grubb R.L., Raichle M.E., Higgins C.S., Eichling J.O. (1978) Measurement of regional cerebral blood volume by emission tomography. *Arch. Neurol.* 4;322-328

122. Martin W.W.R., Powers W.J., Raichle M.E. (1987) Cerebral blood volume measured with inhaled $C^{15}O$ and positron emission tomography. *J. Cereb. Blood Flow & Metab.* 7(4);421-426

123. Matthew N.J., Meyer J.S., Bell R.L., et al. (1972) Regional cerebral blood flow and blood volume with the gamma camera. *Neuroradiology* 4;133-140

CHAPTER 2

OPTICAL CHARACTERISTICS OF TISSUE

2.1 INTRODUCTION

The technique of near infrared spectroscopy involves the measurement of the concentration of certain chromophores by illuminating living tissue with near infrared light. To understand the physical principles of the technique we must first consider the basic interactions of light with tissue *in vivo*. When light enters tissue it is both scattered and absorbed. These phenomena will first be considered in isolation and then their combined effects will be discussed. Since the aim of this project is to demonstrate the use of NIRS for measurement of cerebral haemodynamics, particular attention will be paid to those chromophores present in brain tissue. This chapter will also define the terminology describing optical and physical characteristics which will be used throughout the thesis.

2.2 ABSORPTION OF LIGHT

The terminology used to describe the behaviour of light in a non-scattering homogeneous absorbing medium must first be considered. Imagine a solution comprised of a non-absorbing medium in which an absorbing compound of concentration c is dissolved. The amount of light that this compound absorbs is dependent upon the wavelength of the light which is incident upon it. This wavelength dependent absorption is described by the absorption spectrum of the compound, in which the specific extinction coefficient of the compound (α) is expressed as a function of wavelength.

In a non scattering solution, the optical pathlength of the light is purely the physical distance between the points where the light enters and leaves the medium (*d*). The intensity of the light incident on the solution is I_o and the intensity of the light transmitted through the solution is *I*. The loss of light intensity (attenuation) is usually measured in units of optical density (OD) and can be described using the Beer-Lambert law[1]. This law states that for an absorbing compound dissolved in a non-absorbing medium, the attenuation (*A*) is proportional to the concentration of the compound in the solution (*c*), the specific extinction coefficient of the compound (α) and the optical pathlength (*d*):

$$A = lg[\frac{I_o}{I}] = \alpha \cdot c \cdot d \qquad (2\text{-}1)$$

where A = attenuation measured in OD

I_o = the light intensity incident on the medium

I = the light intensity transmitted through the medium

α = specific extinction coefficient of the absorbing compound measured in $\mu molar^{-1}.cm^{-1}$,

c = the concentration of the absorbing compound in the solution measured in μmolar,

d = distance between the points where the light enters and leaves the solution measured in cm.

Note that this relationship only applies to a collimated beam and detector arrangement where all the light collected has travelled the same optical pathlength.

The product of αc is known as the absorption coefficient of the absorbing medium (μ_a). Equation 2.1 can therefore be expressed as:

$$A_n = \ln[\frac{I_o}{I}] = \mu_a \cdot d \qquad (2\text{-}2)$$

where A_n is the *natural* attenuation since μ_a is expressed in *natural* logarithm units.

The distinction between the term **specific extinction coefficient** and **absorption coefficient** must be made clear. Unfortunately the terminology used in this field has become somewhat confused and so a definition of the terms and representative symbols used is

necessary. Throughout this thesis α will be used to represent the specific extinction coefficient for unit absorber concentration in $\mu molar^{-1}.cm^{-1}$, i.e. the level of absorption per μmol of compound per litre of solution per cm. This definition has been used in order to match the units in which concentration and distance are most commonly measured clinically (i.e. μmolar and cm). μ_a is used to represent the absorption coefficient in cm^{-1}. Note that the difference between α and μ_a is purely a scaling factor due to the different base of the logarithm units used for the definition of each. The term extinction coefficient is described using base 10 logarithm units (lg) and absorption coefficient using natural logarithm units (ln). In this thesis, all spectra are presented as specific extinction coefficient versus wavelength and the term attenuation will refer to the definition given in equation 2.1. In line with common usage however the descriptive term "absorption" will generally be used in preference to the term "extinction".

In a solution containing several different absorbing compounds, except at very high concentrations not usually met in biological media, the overall extinction coefficient is simply the linear sum of the contributions of each compound:

$$A = [\alpha_1 c_1 + \alpha_2 c_2 + \alpha_3 c_3 + ...\alpha_n c_n]d \qquad \textbf{(2-3)}$$

The term used to describe a compound which absorbs light in the spectral region of interest is chromophore. Each chromophore has its own particular absorption spectrum (extinction coefficient versus wavelength) which dictates the level of absorption at each wavelength. There are obviously numerous chromophores in tissue and those which are of interest for the application of NIRS will now be considered.

2.2.1 Absorbers in Tissue

The technique of NIRS relies upon the relative transparency of biological tissue to light in the near infrared region of the spectrum. The total amount of light absorbed by tissue decreases significantly in the near infrared region of the spectrum between the wavelengths 650 - 1000nm. Near infrared spectroscopy targets those compounds whose absorption in the NIR region of the spectrum is well described, and that are present in living tissue in significant concentrations. Within this subset of compounds there are absorbers whose

concentration over a reasonable measurement period are fixed and whose presence merely adds to the total light attenuation (e.g. melanin, bilirubin, water). Of more interest are the absorbers whose concentration (and therefore light absorbance) vary with time or with oxygenation status. These compounds are oxyhaemoglobin (HbO_2), deoxygenated haemoglobin (Hb) and oxidised cytochrome oxidase (CtOx). It is the measurement of these compounds which can be used to provide information on cerebral oxygenation status.

2.2.1.1 *Water*

Figure 2.1 shows the extinction coefficients for water over the wavelength range (a) 200 - 2000 nm,[2] and (b) 650 - 1000 nm,[3]. It can be seen that the absorption of light by water is relatively low between 200 - 900nm with a minimum at around 500 nm. Beyond 900 nm absorption starts to rise with increasing wavelength with a spectral peak being visible at 970nm. A very strong absorption peak is also present beyond 1400nm. For the purposes of most clinical measurements the water concentration in tissue can be thought of as constant, and as such water acts as a fixed constant absorber, albeit a dominant one. The high concentration of water in living tissue, typically 80% in adult brain tissue[4], dictates the wavelength region in which spectroscopic techniques for tissue interrogation are possible by strongly limiting the tissue thickness through which light can penetrate. For this reason, the

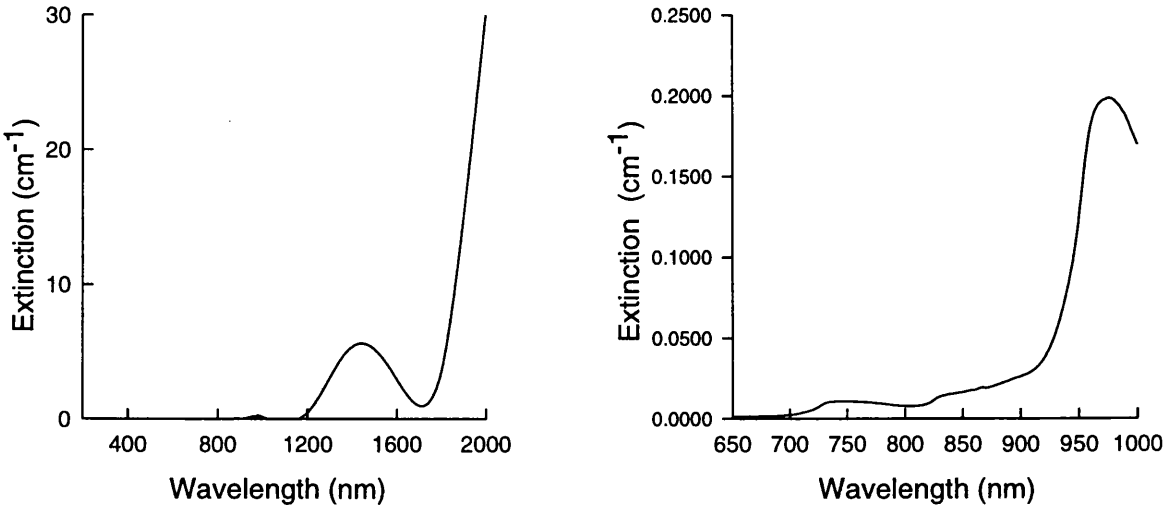

Figure 2.1 *The extinction spectra for pure water over the range (a) 200-2000nm and (b) 650-1000nm.*

water spectrum is said to demonstrate a "window" of transparency between 200 - 900 nm within which spectroscopic measurements can be made. However, as will be demonstrated in a later section (section 3.4.3), the presence of small water absorption peaks both within and beyond this "window" can also be used in the direct quantification of cerebral haemodynamic parameters in NIRS. For the purpose of most clinical measurements the water concentration in tissue can be thought of as constant, and as such water acts as a fixed constant absorber.

2.2.1.2 *Lipids*

Although the distribution of lipid in brain tissue is dependent upon tissue type, it can also be thought of as a constant absorber with changes in its concentration throughout the course of a clinical measurement being unlikely. Fillerup[5] measured the fat content within brain tissue to be 8% in grey matter and 17% in the myelinated white matter. Studies on pure pork fat have shown that water and lipid have extinction coefficients and spectra in the NIR region of similar magnitude, with the only significant spectral peak at 930nm. Since the percentage of lipid in living tissue is generally much lower than that of water, its absorption characteristics do not impose the same restrictions on tissue penetration that water does. Its effect is one of transparency since fatty tissue often contains few absorbers and it has a relatively low scattering effect. However, when making measurements on limbs, fat distribution over the illuminated area may be an important factor[6]. The significant differences between the spectra of water and fat have been used to make direct measurements of fat concentration in tissue[7].

2.2.1.3 *Haemoglobin*

Within the "window" of transparency the most important absorbers are the haemoglobin group. The specific extinction coefficients of oxygenated haemoglobin (HbO_2) and deoxyhaemoglobin (Hb) in the wavelength range 450 - 1000nm,[8] are shown in Figure 2.2. (These specific extinction coefficients are calculated per functional unit (tetrahaem) and not per haem group.) The difference in the absorption levels between the two compounds in the visible part of the spectrum can clearly be seen. This difference explains the well recognised phenomena of arterial blood (containing approximately 98% HbO_2) having a bright red appearance while venous or deoxygenated blood appears more purple or blue. In many ways

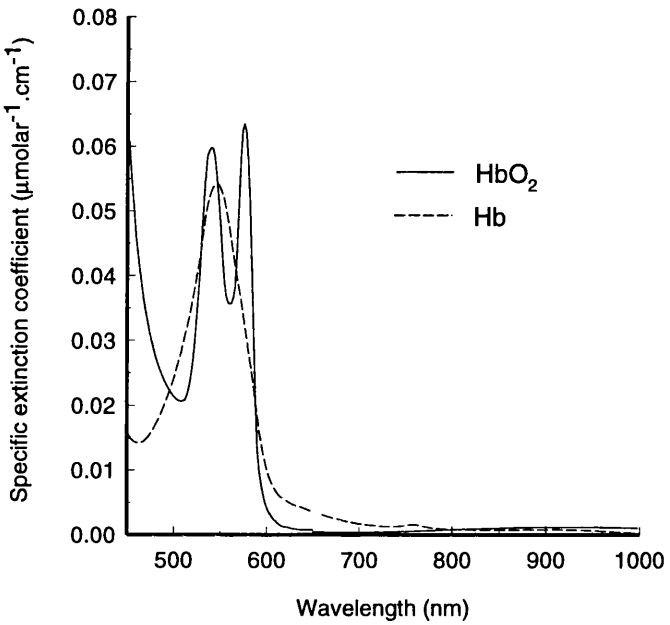

Figure 2.2 *The absorption spectrum for HbO_2 and Hb in the visible and NIR region.*

NIRS is an extension of this crude technique of colour coding tissue according to its oxygenation status. In the near infrared region of the spectrum the absorption of both chromophores decreases significantly compared to that observed in the visible region. However the absorption spectra of Hb and HbO_2 remain significantly different in this region

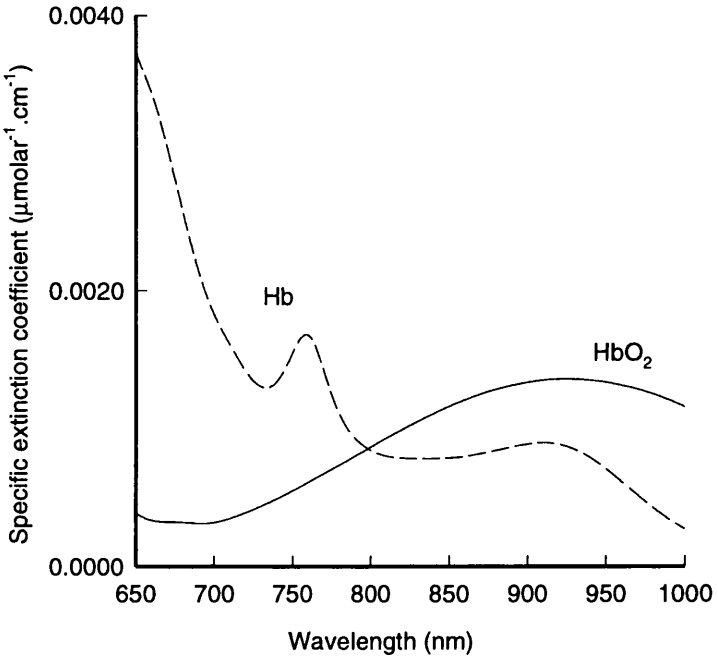

Figure 2.3 *The absorption spectrum for Hb and HbO_2 in the NIR region.*

(shown in Figure 2.3[9]) allowing spectroscopic separation of the compounds to be possible using only a few sample wavelengths. An isobestic point where the extinction coefficients of the two compounds are equal can be seen at 800nm, which can be used to calculate haemoglobin concentration independent of oxygen saturation. The typical value for haemoglobin concentration in, for example, adult brain tissue is 84 μmolar[9].

There are other haemoglobin compounds which have a characteristic absorption in the near infrared, although their levels in tissue are low and in many cases non existent in normal blood. These compounds include carboxyhaemoglobin, (HbCO), which although it can be present in significant quantities in tissue, has a low specific extinction coefficient rendering its effect on most in vivo measurements negligible. Haemiglobin (Hi) is present in very low concentrations and sulfhaemoglobin (SHb) is not present at all in normal blood. The combined error in ignoring these compounds in the measurement of the total haemoglobin signal is probably less than 1% in normal blood and the majority of clinical conditions encountered[9]. However it is worth remembering that some of these forms of haemoglobin, especially Hi, may become significantly raised in some diseases of the liver or in malaria.

2.2.1.4 *Cytochrome c oxidase*

The structure and physiological behaviour of cytochrome c oxidase and the other respiratory enzymes is the subject of much investigation and debate. Cytochrome oxidase (CtOx) is the terminal enzyme in the cellular respiratory chain, and is located in the mitochondrial membrane. The enzyme contains four metal centres, two heme units (*a* and a_3) and two copper atoms (Cu_A and Cu_B). These four metal centres change their redox state (i.e. accept or donate electrons) during electron turnover of the enzyme. The oxygen binding site of the enzyme is the binuclear unit which is formed of the Cu_B and heme a_3. It is donation of electrons from this unit to oxygen which accounts for the great majority of oxygen consumption in biological tissue. The Cu_A and heme-a centres donate electrons to this binuclear unit and are therefore not directly involved in reduction of oxygen. However absorption of near infrared light by cytochrome oxidase occurs primarily at the Cu_A centre, the oxidised spectrum having a characteristic shape, with a peak at 830 nm which is missing in the reduced enzyme. In the short term the total tissue CtOx concentration does not vary and NIRS measurements of changes in CtOx thus measure alterations in the redox state concentration of Cu_A within cytochrome oxidase.

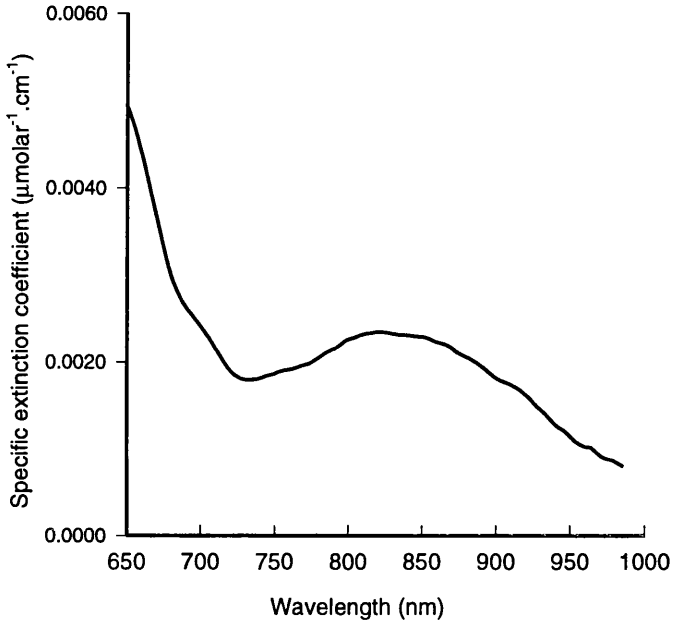

Figure 2.4 *The difference absorption spectrum between the oxidised and reduced forms of cytochrome oxidase.*

Since the total CtOx concentration does not alter, NIRS measurements need only be made of the *change* in redox state, so it is only necessary to know the *difference* spectrum between the oxidised and reduced forms of the enzyme. This difference spectrum is shown in Figure 2.4[9]. It can be seen that the magnitude of the specific extinction coefficients are similar to those of haemoglobin, but since the concentration of cytochrome oxidase in living tissue is usually at least an order of magnitude below that of haemoglobin[10-12], the measurement of cytochrome oxidase with optical techniques is by no means as easy as that of haemoglobin. When oxygen limits the rate of oxygen consumption by cytochrome oxidase, the Cu_A centre becomes more reduced. Therefore the absorbance of NIR light by cytochrome oxidase may be used as an indicator of oxygen availability at a cellular level and ultimately of cell metabolism. There are however numerous caveats to this statement as factors other than just oxygen concentration can affect the redox state of Cu_A. Details of the physiological mechanisms affecting the oxidation state of cytochrome oxidase are given elsewhere[13-16].

2.2.1.5 *Surface Tissues*

Most extracerebral tissues are important in spectroscopic measurements because of the contribution to total light attenuation of the chromophores they contain rather than any distinct characteristic absorption in the near infrared. An example of one such chromophore is melanin which is found in the epidermis layer of the skin. Melanin is a highly effective absorber of light, especially in the ultraviolet region of the spectrum, and although this absorption can be considered to be constant and oxygen independent, the concentration of melanin in tissue will directly affect the reflectance of light from the skin and therefore the transmission of light through the skin. This may become more noticeable when considering measurements on non caucasian subjects.

The epidermis can be divided into several layers. The outermost layer is the stratum corneum, a horny layer with high lipid and protein content and relatively low water content. This layer has a larger affect on attenuation than other layers in the epidermis. The much thicker skin layer, the dermis, is highly vascularised and contains the main NIR absorbers mentioned above, i.e. haemoglobin and cytochrome oxidase, and as such changes in its oxygenation status may interfere with measurements of cerebral oxygenation.

In the near infrared region bone is found to be more transparent than most other tissues. There is little general absorption in bone apart from that due to the haemoglobin present in the blood supply to the bone. Although literature is scarce, it is thought that the skull bone has a very low blood flow (0.5 - 4.0 $ml.100g^{-1}.min^{-1}$)[17], and as such will contribute only a small amount to absorption. Muscle layers over the skull such as the temporalis muscle, contain myoglobin which has an absorption spectra which is almost indistinguishable from haemoglobin. More important is the blood flow to this muscle which may be related to facial gestures or movement and is therefore unlikely to remain constant for long measurement periods.

It is known that the extracerebral compartments which are illuminated together with the brain during near infrared spectroscopy of the adult head account for a significant portion of the light path. The details of the effects of the various extracerebral compartments on the measured variables will be dealt with in later sections.

2.3 SCATTERING OF LIGHT

Now that the contribution of absorption to light attenuation has been detailed, it is necessary to consider the effect of scattering particles in tissue. The effect of scattering is to increase the observed attenuation at a single point above that to be expected from absorption alone. When light is absorbed its energy is dissipated as thermal energy throughout the absorber. When light is scattered the photons may undergo inelastic collisions in which the energy of the scattered photon is different to that of the incident photon, or they may undergo an elastic collision in which no energy is lost and the incident photon merely changes direction. In the NIR virtually all (approximately 99.99%) scatter events are elastic. All new possible directions which the scattered photon may take do not occur with equal probability. The direction in which the scattered photon travels is dependent upon both the size of the particle it collided with, the wavelength of the light and the refractive indices of the scattering medium through which it is travelling.

The terminology of the parameters which dictate the scattering of light, must first be considered. The ability of a particle to scatter light is expressed as an effective surface area and is called the total scattering cross-section, σ_s, and is measured in mm^2. The density of scattering particles within a solution is called the number density, ρ, and is measured in mm^{-3}. The angular dependence of scattering is known as the single scattering phase function, f. The scattering coefficient, μ_s, for a medium containing a single type of scattering particle of number density, ρ is given as

$$\mu_s = \rho \cdot \sigma_s \qquad \textbf{(2-4)}$$

μ_s is normally expressed in mm^{-1} and is a measure of the likelihood that a photon will be scattered as it passes through a given medium. ($1/\mu_s$ is the mean length a photon will travel between scattering events). For a scattering medium containing a mixture of scattering particles and the case of single scattering,

$$\mu_s = \sum_i \rho_i \cdot \sigma_{si} \qquad \textbf{(2-5)}$$

For a solution containing a single scatterer which does not absorb light, the natural

attenuation of light intensity due to scattering alone is given by the equation:

$$A = \ln\frac{I_o}{I} = \sigma_s \cdot \rho \cdot d = \mu_s \cdot d \qquad \textbf{(2-6)}$$

In general the scattering coefficient is not constant and can depend upon, among other things, the wavelength of light used.

A commonly used parameter is g, the anisotropy factor, which is the mean cosine of the scattering phase function, and as such a measure of the symmetry between forward and backward scattering. In the case of isotropic scattering, i.e. when all possible scattering angles occur with equal probability, g=0. When the total scatter is in the forward direction g=1, and conversely when the total scatter is in the backward direction g=-1.

The two theories most commonly used to describe the scattering of light by single scatterers are those given by Rayleigh and Mie. In order to decide which is the most appropriate theory to apply to a particular model it is important to know the size of the scattering particle in the medium, a, relative to the wavelength of light used. This is given by the size parameter, x, where:

$$x = k \cdot a = \frac{2\pi \cdot a \cdot n}{\lambda} \qquad \textbf{(2-7)}$$

and n is the refractive index of the medium, λ, the wavelength of the light and k, the wave number. Rayleigh theory can be applied to any shape of scattering particle, but is generally only used when x is $<<1$, and so is more suitable to the description of light scattering by molecules and smaller particles. Mie theory strictly applies only to light scattering by a sphere, but can be used to describe the scattering caused by larger structures where $a>>\lambda$. An approximation of the Rayleigh theory called the Rayleigh-Gans or Rayleigh-Debye theory can only be applied to large tenuous absorbers but can be extended to arbitrary shapes. Mie theory solutions for some non spherical shapes have been derived.

2.3.1 Multiple Scattering

Tissue is quite obviously not a single scatterer and models which predict the effects of multiple scattering due to spatially varying refractive index, must be considered. The calculation of light transport in tissue is by no means simple and to date three techniques have produced some favourable results; radiative transfer theory, Monte Carlo modelling and finite element modelling. The details of these models are subjects of a whole thesis in their own right and so will be dealt with only briefly here with an expanded discussion available from the theses of van der Zee[18] and Schweiger[19].

The radiative transfer theory is sometimes also referred to as the Transport Theory. The most popular approaches have been to use the so-called two flux approximation of Kubella-Monk and the P_n approximations[20]. Monte Carlo modelling is an exact analysis which simulates particle paths within a specified media which can be assigned spatially varying absorption and scattering parameters. Although the technique can cope with complex boundary conditions and distribution of optical characteristics, the computing time required to run realistic size models of tissue slabs is often prohibitive. The finite element method approximates the required function to a discrete function on a mesh of points. The domain of the function is divided into a number of sub-domains called finite elements. The power of this method for the modelling of light transport in tissue especially using the diffusion equation (the P_1 approximation) has been demonstrated over the last decade [21-23].

When considering multiple scattering a term commonly used is the transport scattering coefficient, μ_s' where:

$$\mu_s' = \mu_s (1 - g) \qquad \textbf{(2-8)}$$

This represents the isotropic scattering coefficient that would give rise to the same light distribution in tissue as the real μ_s and g.

The linear total attenuation coefficient for a single scatterer is given by μ_t where:

$$\mu_t = \mu_s + \mu_a \qquad \textbf{(2-9)}$$

and likewise for the equivalent scattering transport attenuation coefficient (μ_{tr}) can be defined:

$$\mu_{tr} = \mu_s' + \mu_a \qquad \textbf{(2-10)}$$

The values for μ_a, μ_s and g are then very important in defining the interaction of light with tissue. Unfortunately they are also very difficult to measure on selected tissue.

2.3.2 Scatterers in Tissue

Light scattering originates from mismatches in refractive index between different structures. When considering where the dominant scattering centres are in tissue, it is most sensible to try and identify the boundaries where this mismatch is likely to occur. In a complex structure such as the brain there are many micro and macroscopic boundaries which can give rise to scattering. These include membrane boundaries of the cells themselves as well as of various organelles inside the cell. Mismatching will occur between intra and extracellular fluid, or intracellular fluid and fluid inside the nucleus of the cell or other enclosed particles such as ribosomes, fat globules, glycogen and secretory globules. As with absorption, the volume of a particular scatterer within in the tissue is as important as its scattering ability. Evidence suggests that cell membranes are the most important source of scattering in brain tissue since they account for a large proportion of the solid content of brain tissue. Mitochondria are also important scatterers along with the remaining cell contents.

In brain the scattering effects are far more significant contributors to total attenuation than absorption as can be seen by the reported values for μ_a and μ_s' in human adult brain. van der Zee[18] reported the following values for human brain measured between 600 -1000 nm; for white matter μ_a = 0.05 - 0.09mm^{-1}, and μ_s'= 2 - 4mm^{-1}, for grey matter μ_a = 0.02 - 0.08mm^{-1}, and μ_s'= 11 - 7mm^{-1}.

Red blood cells account for approximately 2% of the solid content of tissue and as such the attenuation due to pure blood cell scattering is low. Pedersen[24], using the Mie scattering model at 685nm and assuming an haematocrit of 0.41 and haemoglobin content of normal blood, estimated μ_a at 0.2mm^{-1} and μ_s at 0.6mm^{-1}. The assumption that red blood cells are spherical is obviously in error since it is well known that they are capable of readily deforming their doughnut shape to flow through vessels of diameter less than their own, but experimental data shows surprisingly good agreement to theoretical predictions which assume an equivalent spherical volume[25].

Scattering is also responsible for significant attenuation in the extracerebral layers. In the dermis layer of the skin, collagen fibres in the connective tissue are thought to be the primary scatterers. Values of 2 - 4mm^{-1} for μ_s' and 0.2 - 0.5 for μ_a have been recorded[26, 27]. Bone causes significant scattering and recent measurements on adult skull gave values of μ_a = 0.04 mm^{-1} and μ_s' = 2.7 mm^{-1} at 650nm and μ_a = 0.05 mm^{-1} and μ_s' = 1.4 mm^{-1} at 950nm[28].

It should also be remembered that macroscopic boundaries between structures may also cause significant scattering particularly for example between healthy and diseased tissue, soft tissue and bone and large blood vessels. These effects are obviously specific to the actual tissue area illuminated and will be dealt with in more detail in further sections.

2.4 LIGHT ATTENUATION BY TISSUE

It is clear that when light travels through tissue it is attenuated due to the effects of both scatter and absorption, and hence both these parameters must be taken into account when considering spectroscopic measurements. In a non scattering medium, using the relationship given by the Beer-Lambert law (equation 2.1), the concentration of the absorber in the solution is given by:

$$c = \frac{A}{\alpha \cdot d} \qquad \textbf{(2-11)}$$

If both α and d are known in absolute units (μmolar^{-1}.cm^{-1} and cm respectively) then the concentration of absorber in the medium can be calculated absolutely in quantified units of μmolar.

In tissue illuminated with NIR light approximately 80% of the total attenuation is due to scattering and the remaining 20% is due to absorption. As such, tissue is considered a highly scattering medium whose optical characteristics deviate significantly from that described by the Beer-Lambert law. This high degree of scattering is the single biggest problem when attempting quantitative spectroscopy of tissue.

2.4.1 Modified Beer-Lambert Law

When a highly scattering medium is considered, the Beer-Lambert relationship must be modified to include (i) an additive term, G, due to scattering losses and (ii) a multiplier to account for the increased optical pathlength due to scattering. In a highly scattering medium such as tissue, the photons travel a mean distance which is far greater than the geometrical pathlength *d*. This true physical distance has been defined as the differential pathlength (DP) and differs from the geometrical distance by a scaling factor called the differential pathlength factor (DPF)[29]:

$$\beta = B \cdot d \qquad \textbf{(2-12)}$$

where β is the differential pathlength, B the differential pathlength factor and d the geometrical distance.

The modified Beer-Lambert law which incorporates these two additions is then expressed as:

$$A = lg\frac{I_o}{I} = \alpha \cdot c \cdot d \cdot B + G \qquad \textbf{(2-13)}$$

where G is the additive term due to scattering losses. For almost all physiological measurements in tissue the measured changes in chromophore concentration are relatively small and it can be assumed that the change in attenuation is approximately linear with respect to μ_a. A description of the full non linear mathematical model of multiple scattering in a media is given elsewhere[9, 30]

There are several reasons why this modified Beer-Lambert law will not yield an absolute measurement of concentration, in the same way that the original Beer-Lambert law does for a non scattering medium. The most important of these is that G is unknown and is dependent upon the measurement geometry and the scattering coefficient of the tissue interrogated. Without knowledge of G, equation 2.13 cannot be solved to provide a measure of *absolute* concentration of the chromophore in the medium from a measure of *absolute* attenuation. However if G does not change during the measurement period, it is possible to determine the *changes* in concentration of the chromophore from the measured *changes* in attenuation.

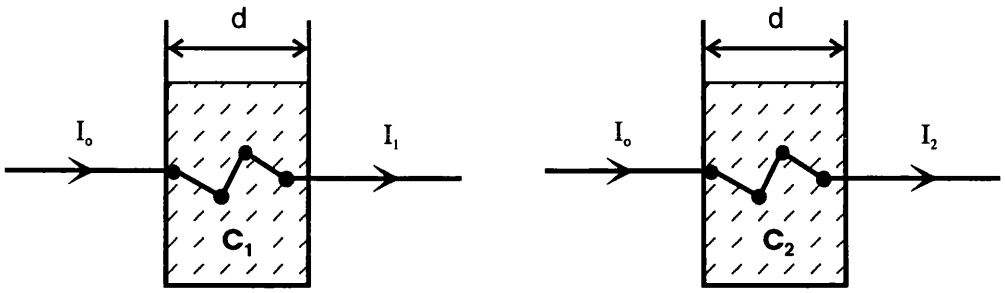

$A_1 = c_1.\alpha.d.B + G$ $\qquad$ $A_2 = c_2.\alpha.d.B + G$

Figure 2.5 *Differential attenuation demonstrated using a cuvette model with different concentrations of absorber, c_1 and c_2.*

Imagine a highly scattering medium containing an absorber in concentration c_1 (Figure 2.5). The attenuation of the medium, A_1, is measured but the concentration of the absorber cannot be quantified because the contribution of scattering, (G), to the total attenuation is unknown. If extra absorber is added to the medium and the concentration changes to c_2, the new attenuation of this solution is measured as A_2. The *change* in attenuation (A_2 - A_1) is measured and provided G remains constant, the *change* in concentration (c_2 - c_1) can be calculated:

$$\Delta A = \Delta c \cdot \alpha \cdot d \cdot B \qquad \textbf{(2-14)}$$

Note that the *differential* attenuation is actually measured, giving rise to the terminology *differential* pathlength and *differential* pathlength factor.

It is clear from equation 2.14 that the quantification of the *change* in concentration of the chromophore still depends upon the measurement of the geometrical distance, *d* and the differential pathlength factor *B*, i.e. true optical pathlength which the scattered light has travelled. *d* is simple enough to measure, as is it purely the geometrical distance between the point where the light enters and leaves the medium. Since *B* is dependent upon, among other factors, the amount of scattering in the medium, its measurement is not straightforward and

requires more thought. There are a number of different techniques which can be applied to the measurement of *B* including; the measurement of the direct time of flight of a picosecond light pulse travelling through tissue, monitoring the phase shift of a frequency modulated light source and measurement of tissue absorption from the known concentration of water in tissue. These techniques are described in more detail in section 3.4.

2.4.2 Relationship between μ_a and DPF

Assuming B can be measured absolutely, the application of the modified Beer-Lambert law is further complicated by the fact that in highly scattering media such as tissue the differential pathlength factor, is not only strongly dependent upon the modified scattering coefficient, μ_s'(as expected), but is also a weaker function of the absorption coefficient, μ_a. This relationship is perhaps also obvious, since in the limit where $\mu_a >> \mu_s$', the light which has been scattered and has taken a longer optical path is more likely to be absorbed before it is detected and its contribution to the mean pathlength estimate is negligible. Only unscattered light will avoid this increased absorption and will be detected having taken a much shorter

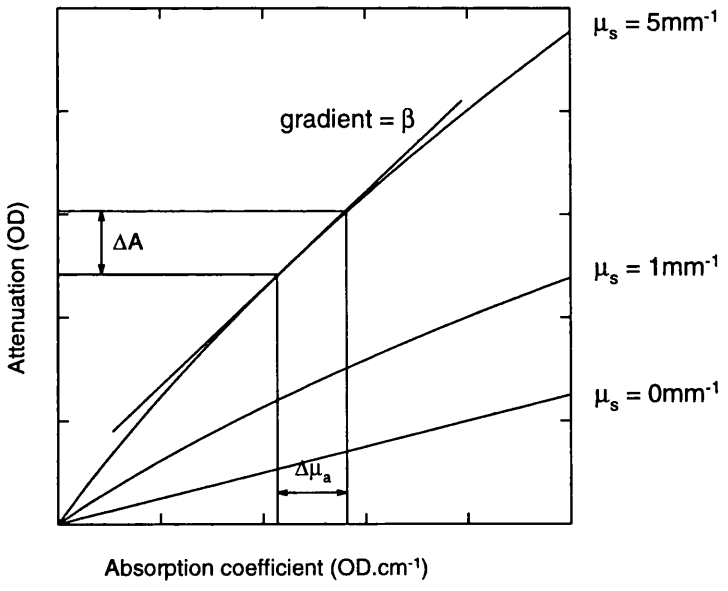

Figure 2.6 *Plot of attenuation (A) as a function of absorption coefficient (μ_a) for three different values of scattering coefficient (μ_s').*

optical path, meaning that the conventional Beer-Lambert law for non scattering medium can be applied. The relationship between μ_a and DPF can be demonstrated most clearly using theoretical data generated using a diffusion equation model of attenuation measured at varying μ_a, in a scattering ($\mu_s' \neq 0$) and non scattering ($\mu_s' = 0$) medium.

Figure 2.6 shows A as a function of μ_a for a medium of thickness *d* for three different scattering coefficient conditions. DP is then the local gradient of the curve. As expected, for $\mu_s' = 0$, the relationship between A and μ_a is linear and the slope of the line is simply the geometrical pathlength *d*. For non zero values of μ_s' A becomes increasingly non linear with increasing μ_s'. In general therefore DP will increase with increasing scattering coefficient and decrease with increasing absorption coefficient. It has been shown that the maximum extent of the absorption dependent variation in optical pathlength in physiological measurements in the NIR is < 15%. Therefore, in order to make quantified measurements of the changes in concentration, it has been assumed that since the measured change in attenuation is small compared to the large constant background attenuation in tissue, that DPF is approximately constant for a given tissue. Since μ_a and μ_s are wavelength dependent parameters, the DPF will obviously vary with the illuminating wavelength, λ, the geometry of the system and spatial variations in the optical characteristics of the scattering medium e.g. combination of healthy and diseased tissue. These relationships will be dealt with in section 3.5.

Assuming then that the geometrical distance *d*, the DPF, and the scattering term, G, remains constant during a measurement, the modified Beer-Lambert law given in equation 2.13 can be used to derive absolute changes in chromophore concentration in a highly scattering medium in non arbitrary units.

2.4.3 Spectroscopic Measurements of the Brain

Let us now briefly consider the transference of these theories into the measurements of adult cerebral haemodynamics and some of the terminology which is often used in clinical spectroscopy measurements. Figure 2.7 shows a schematic of the experimental set up for the spectroscopic measurement across an adult head. The fibres which carry the NIR light to and from the head are referred to as the *optical fibres*, and are truncated as small cylindrical *optodes* containing prisms which direct the light normally on to the surface of the tissue. In this case the highly scattering medium is the tissue which is illuminated between the two

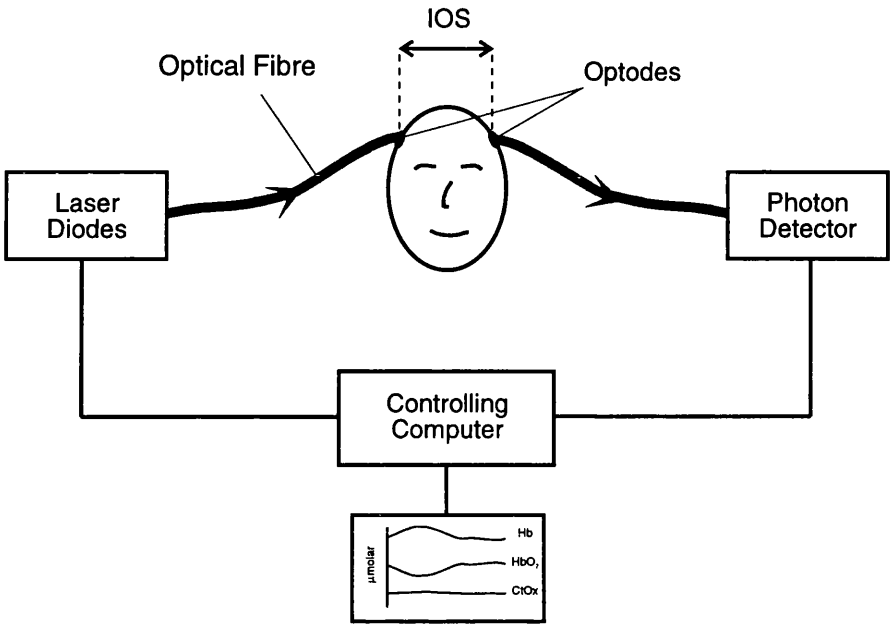

Figure 2.7 *Schematic of the experimental set up for NIRS measurements across the head. (In practice the optodes are rarely positioned directly opposite each other on the adult head.)*

optodes. For this reason the geometrical distance, *d*, is often referred to as the *interoptode spacing* (IOS) and is usually measured with a pair of callipers directly over the measurement site. Note this distance is the chord distance rather than the length of the arc between the two points. This assumption is based upon the fact that light inside the brain becomes essentially diffuse within a few millimetres of entering the tissue, at which point it becomes a unidirectional source, even if the angle between the source and detector is less than 180° [31]. DPF has been measured in the adult head using the time of flight method described in section 3.4.1 and a value of 5.93 was obtained. Therefore for an IOS of 4cm the mean distance which the light has actually travelled in the head is approximately 24cm.

The chromophores of interest within the tissue whose concentration varies with oxygenation are HbO_2, Hb and CtOx. The specific extinction coefficients (α) for these chromophores are expressed in units of per µmol of chromophore per litre of tissue per cm ($\mu molar^{-1}cm^{-1}$).

Once d, α and B are known the *change* in chromophore concentration (Δc) can easily be computed from the measured *change* in attenuation (ΔA) using the expression defined in equation 2.14. However for the simultaneous computation of the *changes* in concentration of a number of chromophores from the *changes* in attenuation at a number of wavelengths, a

matrix operation must be performed incorporating the relevant extinction coefficients for each wavelength and chromophore. For each wavelength it is assumed that the linear changes in attenuation for each chromophore can be linearly summed. If the number of wavelengths at which attenuation changes are measured is greater than the number of chromophores, the accuracy of the calculation may be improved by using multilinear regression to 'fit' to each chromophore spectra[9]. The result of these computations is the value of the absolute *change* in concentration of each chromophore in the non arbitrary units of μmol of chromophore per litre of tissue (μmolar).

Since the absolute concentration of chromophore is unknown (and is unable to be calculated due to the effects of light scattering within the tissue), all measurements are expressed as **absolute concentration *changes*** from an **arbitrary zero** at the start of the measurement period. Using NIRS therefore the quantified *changes* in tissue oxygenation can be non invasively monitored. It is the quantification of these *changes* in concentration of Hb and HbO_2 which makes possible the measurement of quantified cerebral haemodynamics which will be described in Chapter Four.

2.5 REFERENCES

1. Beer A. (1852) Bestimmung der Absorption des rothen Lichts in farbigen Flüssigkeiten. *Ann. Phys. u. Chem.* 163;78
2. Hale G.M. and Querry M.R. (1973) Optical constants of water in the 200-nm to 200-μm wavelength region. *Appl. Opt.* 12 (3);555-563
3. Wray S., Cope M., Delpy D.T., Wyatt J.S., Reynolds E.O.R. (1988) Characterisation of the near infrared absorption spectra of cytochrome aa_3 and haemoglobin for the non invasive monitoring of cerebral oxygenation. *Biochim. Biophys. Acta* 933;184-192
4. Woodard H.Q. and White D.R. (1986) The composition of body tissues. *Br. J. Radiol.* 59;1209-1219
5. Fillerup D.L. and Mead J.F. (1967) The lipids of aging human brain. *Lipids* 2(4);295-298
6. Matcher S.J., Cope M., Delpy D.T. (1994) Use of the water absorption spectrum to quantify tissue chromophore concentration changes in near-infrared spectroscopy. *Phys. Med. Biol.* 39;177-196

7. Conway J.M., Norris K.H., Bodwell C.E. (1984) A new approach for the estimation of body composition: infrared interactance. *Am. J. Clin. Nutr.* 40;1123-1130

8. Horecker B.L. (1943) The absorption spectra of hemoglobin and its derivatives in the visible and near infra-red regions. *J. Biol. Chem.* 148;173-183

9. Cope M. (1991) The development of a near infrared spectroscopy system and its application for non invasive monitoring of cerebral blood and tissue oxygenation in the newborn infant. *Ph.D., University College London.*

10. Brown G.C., Crompton M., Wray S. (1991) Cytochrome oxidase content of rat brain during development. *Biochim. Biophys. Acta* 1057;273-275

11. Van Kuilenburg A.B.P., Dekker H.L., Van Den Bogert C., Nieboer P., Van Gelder B.F., Muijsers A.O. (1991) Isoforms of human cytochrome-*c* oxidase. *Eur. J. Biochem.* 199;615-622

12. Sato N., Hagihara B., Kamada T., Abe H. (1976) A sensitive method for the quantitative estimation of cytochromes *a* and a_3 in tissues. *Anal. Biochem.* 74;105-117

13. Cooper C.E., Matcher S.J., Wyatt J.S., Cope M., Brown G.C., Nemoto E.M., Delpy D.T. (1994) Near infrared spectroscopy of the brain: relevance to cytochrome oxidase bioenergetics. *Biochem. Soc. Trans.* 22;974-980

14. Brown G.C. (1992) Control of respiration and ATP synthesis in mammalian mitochondria and cells. *Biochem. J.* 284;1-13

15. Babcock G.T. and Wikström M. (1992) Oxygen activation and the conservation of energy in cell respiration. *Nature* 356;301-309

16. Wilson D.F., Erecinska M., Drown C., Silver I.A. (1979) The oxygen dependence of cellular energy metabolism. *Arch. Biochem. Biophys* 195(2);485-493

17. Brookes M. (1971) *The blood supply to bone.*, Butterworth, London.

18. van der Zee P. (1993) Measurement and modelling of the optical properties of biological tissues in the near infrared. *Ph.D., University of London.*

19. Schweiger M. (1994) Application of the finite element method in infrared image reconstruction of scattering media. *Ph.D., University College London.*

20. Kubelka P. and Munk F. (1931) Ein Beitrag zur Optik der Farbanstriche. *Z. Tech. Phys.* 12;593-601

21. Schweiger M., Arridge S.R., Delpy D.T. (1993) Application of the finite-element method for the forward and inverse models in optical tomography. *J.M.I.V.* 3;263-283

22. Arridge S.R., Schweiger M., Hiraoka M., Delpy D.T. (1993) Performance of an

iterative reconstruction algorithm for near infrared absorption and scatter imaging. *Proc. SPIE* 1888;360-371

23. Arridge S.R., Schweiger M., Hiraoka M., Delpy D.T. (1993) A finite element approach for modelling photon transport in tissue. *Med. Phys.* 20;299-309
24. Pedersen G.D., McCormick N.J., Reynolds L.O. (1976) Transport calculations for light scattering in tissue. *Biophysics Journal* 16;199-207
25. Chadwick R.S. and Chang I.D. (1973) A laser study of the motion of particles suspended in a slow viscous shear flow. *J. Colloid. Interface Sci.* 42;516-534
26. Jacques S.L., Alter C.A., Prahl S.A. (1987) Angular dependence of HeNe laser light scattering by human dermis. *Las. Life. Science* 1;309-333
27. van Gemert M.J.C., Jacques S.L., Sterenborg H.J.C.M., Star W.M. (1989) Skin Optics. *IEEE transactions on Biomedical Engineering* 36;1146-1154
28. Firbank M., Hiraoka M., Essenpreis M., Delpy D.T. (1993) Measurement of the optical properties of the skull in the wavelength range 650-950nm. *Phys. Med. Biol.* 38;503-510
29. Delpy D.T., Cope M., van der Zee P., Arridge S.R., Wray S., Wyatt J.S. (1988) Estimation of optical pathlength through tissue from direct time of flight measurement. *Phys. Med. Biol.* 33(12);1433-1442
30. Cope M., van der Zee P., Essenpreis M., Arridge S.R., Delpy D.T. (1991) Data analysis methods for near infrared spectroscopy of tissue: problems in determining the relative cytochrome-aa_3 concentration. *Proc. SPIE* 1431;251-262
31. van der Zee P., Arridge S.R., Cope M., Delpy D.T. (1990) The effect of optode positioning on optical pathlength in near infrared spectroscopy of the brain. *Adv. Exp. Med. & Biol.* 277;79-84

CHAPTER 3

INSTRUMENTATION

3.1 INTRODUCTION

This chapter will describe the near infrared spectroscopy systems currently used to make the clinical measurements of haemodynamics and tissue oxygenation detailed in Chapter Two. As highlighted in that chapter, the optical characteristics of tissue as a highly scattering medium places important boundaries on the degree of quantification in NIRS measurements. The research instrumentation currently being used to investigate these effects, and in particular the nature of light scattering in tissue, is also detailed. Since the measurements of CBF and CBV which will be described in Chapter Four depend upon pulse oximetry, some details of this technology are also included.

3.2 PULSE OXIMETRY

Spectroscopic techniques have long been used for *in vitro* analysis of biochemical samples. The development of instruments for routine *in vivo* spectroscopy however is more recent, even though the first use of differential light absorption for oxygen measurements was made by Matthes in 1935[1]. Oximetry is the general term used to describe the spectrometric techniques which estimate haemoglobin oxygen saturation. Several types of non invasive oximeters have been developed including the Wood type ear oximeter, the reflection oximeter and the multi-wavelength oximeter. However the most commonly used clinical instrument is the pulse oximeter, first described by Nakajami in 1975[2].

Haemoglobin oxygen saturation (SO_2) is defined by the following ratio:

$$SO_2\% = \frac{HbO_2}{HbO_2 + Hb} \times 100 \qquad \textbf{(3-1)}$$

The technique uses the pulsatile component of the arterial blood flow for its measurement of absolute values of arterial haemoglobin oxygen saturation (SaO_2). As already discussed, when light travels through the body it is attenuated by all tissues in its path. In pulse oximetry a relatively thin section of tissue such as the finger or the ear is illuminated with light in the red and infrared region of the spectrum. It is assumed that the only factor causing a gross change in total attenuation of light in this thin sample over short periods is the pulsatile component of the arterial blood. Attenuation due to the remaining arterial blood, venous blood and other tissues such as skin and bone is assumed to remain constant during the period of a heartbeat. The total light absorbance therefore has a DC component due to the "static absorbers" and an AC component due solely to the pulse of arterial blood entering the field of view. Equation 2.13 can then be applied solely to the AC component to provide a measure of Hb and HbO_2 and SaO_2 can then be calculated from the ratio given in equation 3.1. By focusing purely on the attenuation due to the dynamic component, pulse oximetry conveniently circumvents the effects of other tissues in the field, and also simultaneously measures the pulse rate.

Probes incorporating two light emitting diodes (LED) emitting in the red and infrared regions (usually at 660nm and 940nm respectively) and a suitable photodiode are most commonly used. The probe design depends upon the site of measurement which may include the earlobe, fingertip, toe or in the case of the neonate the cheek or arm. Whichever site is chosen adequate perfusion and a good arterial pulse are essential. The pulsatile component of the total attenuation is small, with the AC component being typically 0.2% of the DC component. Many oximeters display a plethsymographic waveform to confirm the presence of a strong pulse. These indicators can be very useful since the accuracy of the measurements will be compromised by low cardiac output, local or core body cooling, and disturbed peripheral perfusion. Since measurement of the pulse is non-directional, exaggerated venous pulsations are not accounted for.

Secure fixation of the probe is also important because the measurement is usually interrupted when the fingertip or earlobe changes its position relative to the axis of the light beam. However if the probe is fastened too tightly, flow to the measurement site will be

restricted.

Pulse oximeters are usually calibrated using a co-oximeter as a standard blood gas analyser. Manufacturers generally quote accuracies of 2% in the 50-100% range. Data for accuracies of values below this is difficult to obtain *in vivo* (for obvious reasons) and is generally not quoted at all. Other calibration constants (i.e. to take account of optical pathlength or possible HbCO absorption) are derived empirically and may therefore not be consistent for all makes of pulse oximeter. Severinghaus[3] conducted a comparative study of six pulse oximeters and showed that the accuracy of the units differed widely.

In most pulse oximeters, SaO_2 is calculated 25 times per second. The large number of data points generated from this sampling rate allows the use of a comprehensive weighting programme for each sample. Weighting usually depends upon the signal strength of each sample (to take into account the point in the cardiac cycle when the data was collected), and the current average saturation. The purpose of most signal averaging is to minimise the effects of artefacts (e.g. due to movement or fluctuations in ambient light levels) and enhance the accuracy and stability of the readings. The data averaging period and update interval can be selected by the user, however the shortest data averaging period of most commercial oximeters is about 2 seconds. Over the last decade pulse oximeters have become a prerequisite for the monitoring of the majority of surgical and clinical procedures. Due to their routine use, particularly in the intensive care setting, most manufacturers are unwilling to provide a facility where this minimal signal averaging can be easily bypassed. This presents a significant problem to those research users who wish to monitor changes in SaO_2 faster than once every two seconds. The effects of the limitations of currently available pulse oximeters on CBF and CBV measurements using NIRS will be discussed in section 4.2.3. and 4.3.3.

3.3 NONPATHLENGTH MEASURING NEAR INFRARED SPECTROMETERS

A general overview of the instrumentation used in NIR spectrometers will be given, followed by details of the specific spectrometer used in the studies described in later chapters. All conventional nonpathlength measuring near infrared spectrometers are based on the instrumentation shown in Figure 3.1.

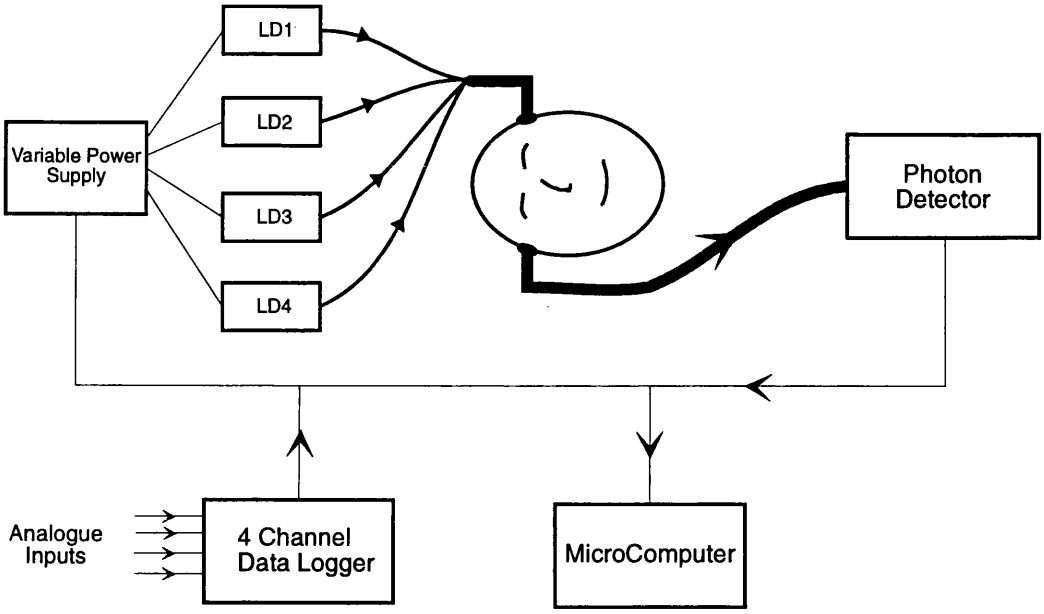

Figure 3.1 *Schematic of an NIR spectrometer. Details such as the number of laser diodes, and the method of photon detection may vary between systems.*

3.3.1 Optodes

Laser diodes produce light in the near infrared region of the spectrum which is carried to and from the spectrometer via fibre optic bundles or optodes. The truncation of these bundles and their housing depends upon the tissue to be interrogated. Most commonly the fibre bundle is butted up against a prism which bends the light through 90° so that the fibre optic can be placed along the surface of the skin and light is directed normally into the tissue. The glass fibre bundle is covered by a light proof protective sheath which must be strong enough to prevent damage to the fibres but flexible enough to allow easy attachment to the patient. Specific optodes have been designed for measurements on neonatal heads, adult heads, adult limbs and more recently on the fetal head during labour and childbirth. The housing of the optodes and their attachment to the skin surface is of prime importance in ensuring the clinical usefulness of the technique. Several different application methods have been tried by different companies, the most successful and well received appears to be a flexible black rubber unit which houses the optodes at a fixed spacing, shields them from ambient light and can be securely attached onto the surface of the tissue with adhesive tape. Most devices now have a fixed interoptode spacing to avoid errors due to movement of optodes with respect to

each other during a study.

3.3.2 Light Detection

When NIR spectrometers were first designed for clinical use, the light detection system was based around a photomultiplier tube (PMT). Currently, some companies are using the less expensive photodiodes as an alternative means of light detection. The original use of a PMT answered the need for a reliable, sensitive monitor of the non coherent light which emerges from the tissue and which is capable of running continuously for several hours. PMTs require protection from excessive light exposure and good temperature control since their quantum efficiency is temperature dependent, especially near the long wavelength region. In the early systems (Hamamatsu NIR 1000) a Peltier cooling system was installed to achieve the optimum working temperature for the PMT.

3.3.3 NIRO 500

The NIR spectrometer currently in use in this department for clinical and research studies is the Hamamatsu NIRO 500 (Hamamatsu Photonics KK, Japan) which is a commercial version of an instrument originally designed and built at the Medical Physics Department (University College London)[4]. This unit uses four pulsed laser diodes as the NIR light source. These diodes typically produce light at wavelengths 775, 825, 850 and 904 nm. Since the diodes are not produced specifically for the unit the wavelengths will vary between machines by a few nanometres, but will follow the same spectral distribution. The pulse frequency of each of the diodes is approximately 1.9kHz with each pulse having a duration of 100nsec. This produces a peak laser output power of 1W, with a average power of approximately 1mW at the patient attachment. The light is directed along a 3m fibre optic towards an optode with an emitting/detecting area of typically 25 -64mm^2. The power density of the light at the surface of the optode is more than one order of magnitude below international safety standards for skin exposure (IEC 825/BSEN 60825). The power levels are also less than the international safety limits for eye exposure for both "intrabeam" and "extended source" viewing.

The unit uses a Hamamatsu Photonics PMT (R1333) as its detector and is capable of sampling every 0.5, 1, 2, 5, 10, 30 or 60 seconds. The base sampling interval is 500 msec

and data is then averaged up into the sampling times given above. Data is displayed graphically or numerically on a front panel but can also be sent via an RS232 connection to an external PC. The data which is collected is the *change* in the raw optical density. A previously defined algorithm[5, 6] which incorporates the absorption characteristics of the three chromophores, is used to convert these measured changes in attenuation at each wavelength into equivalent changes in [HbO_2], [Hb] and [CtOx]. The continuous NIRS measurements are expressed as *absolute concentration changes* from an *arbitrary zero* at the start of the measurement period. The user has the choice of data format for the RS232 output, although the data is most commonly exported as a text file containing the raw optical density data so that if necessary a different algorithm can be applied to the data at a later date. A real time printout of the data displayed on the screen is also available.

The unit is also capable of collecting data from external monitors such as pulse oximeters and blood gas monitors. There are four analogue input channels with a voltage range ±3V which are recorded at the same sampling interval as the optical data.

The unit is essentially portable with dimensions (in mms) of 430W x 295H X 550D, however its weight (37kg) does mean it is usually transported on a trolley which can be positioned next to a cot on the neonatal unit, in adult intensive care or in an operating theatre.

3.4 PATHLENGTH MEASURING NEAR INFRARED SPECTROMETERS

The role of the DP in the quantification of NIRS concentration measurements has already been outlined. This section will describe the current methods employed for the measurement of DP and DPF. Each method has its own merits and can be used additionally to determine the relationship between DPF and for instance, wavelength or optode spacing.

3.4.1 Time of Flight System

The development of the synchronously pumped dye laser and synchronscan streak camera made possible the first direct measurement of the time of flight of an optical pulse through tissue[7]. A schematic of the experimental set up used for these measurements is shown in Figure 3.2. The system currently used at UCL is a picosecond laser system which comprises a 12-W Ar-ion laser pumping a Ti:sapphire laser. With suitable mirrors the laser can be tuned between 740 and 920nm. An electro-optical feedback mechanism supports the

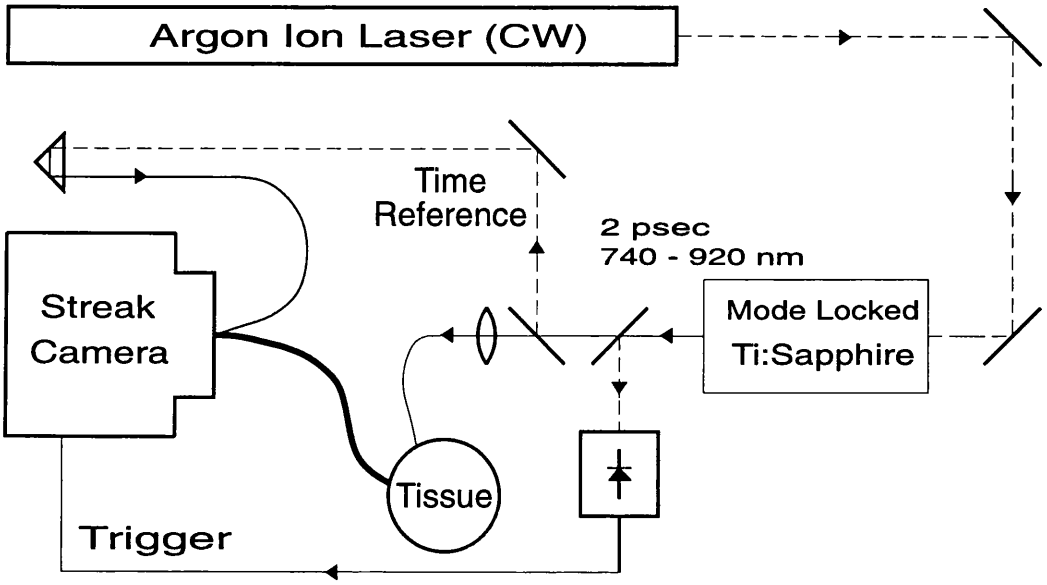

Figure 3.2 *Experimental system for the measurement of the TPSF of tissue.*

auto-mode-locking behaviour of the Ti:sapphire crystal producing stable mode locking at 82MHz and a full width at half maximum of a single pulse of approximately 2ps. The light from the laser is coupled into a single low-dispersion fibre with diameter 125μm and length 0.6m to allow easy application to the tissue. A beam splitter and similar optical fibre takes part of the laser output as a time reference and if required, as a trigger for the streak camera. The other part of the beam is directed through the tissue sample. Light emerging from the tissue is collected using a fibre bundle with a circular cross-section of diameter 1.9mm at the tissue end and a linear cross-section at the distal end to match the input slit of the streak camera. In order to minimize transit time differences, this fibre bundle is assembled using 100 single low-dispersion fibres 1m in length. The temporal reference and the sample are recorded simultaneously on the same streak image. The geometrical distance d between the centre of the transmitting fibre and the centre of the detecting fibre bundle is accurately measured. As with conventional spectroscopy measurements, it is important to minimise movement of the tissue between the fibres and various stereotactic devices have been used to stabilise the tissue under interrogation.

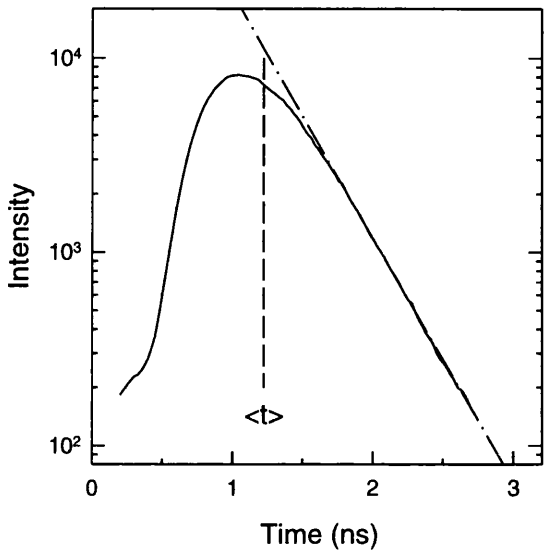

Figure 3.3 *A typical TPSF measured on the adult head, showing the mean time <t>, and the gradient of the decay used in the calculation of* K_{ls}.

3.4.1.1 *Temporal Point Spread Function*

As already described, when light travels through tissue it is both absorbed and multiply scattered. These effects are seen in the dispersion of the picosecond light source which has travelled through the tissue. Figure 3.3 shows this dispersed pulse or temporal point spread function (TPSF) for the adult head and demonstrates the considerable temporal dispersion due to multiple scattering. The TPSF is usually characterised by two parameters; the mean time <t>, i.e. the time of the mean integrated intensity, and the gradient of the decay of the logarithmic intensity (K_{ls}).

It is <t> which is used in the calculation of the differential pathlength factor, B, in a simple time of flight approximation:

$$B = \frac{\beta}{d} \approx \frac{c}{d \cdot n_t} \langle t \rangle \qquad \textbf{(3-2)}$$

where c_v is the speed of light in vacuum, n_t is the refractive index of the tissue (usually taken as 1.40)[8] and ß is the differential pathlength. The time of flight system described above is

situated in a dedicated optical laboratory which precludes any pathlength measurements being made clinically by this method. Measurements have therefore been made in normal healthy adult volunteers and on post mortem infants[9].

The logarithm of the final slope K_{ls} can be described by the following equation:

$$K_{ls} = -\frac{\Delta \log[I(t)]}{\Delta x} = -\frac{n_t}{c}\frac{\Delta \log[I(t)]}{\Delta x} \quad \textbf{(3-3)}$$

where:

$$\Delta x = \Delta t \cdot \frac{c}{n_t} \quad \textbf{(3-4)}$$

The slope of the decay of the TPSF is calculated from a predefined window related to the maximum intensity of the dispersed signal. It has been shown that in an infinite medium at infinite time K_{ls} will be equivalent to μ_a but, in real tissue this is an oversimplification since in these circumstances K_{ls} also depends upon μ_s and the measurement geometry[10]. More work is required in order to determine μ_a and hence the absolute concentrations of the chromophores in tissue from the TPSF[5].

3.4.2 Intensity Modulated Optical Spectrometer

As previously stated, quantification of NIR data requires an accurate measurement of interoptode spacing during the time of the study. This is particularly true of measurements made on the fetal head during labour and childbirth or the muscle during exercise where large changes in IOS are to be expected. The ultimate goal of a reliable accurate bedside spectrometer can therefore only realistically be achieved when real time measurement of the total light path can be incorporated. By considering the current spectroscopy measurements in the frequency rather than the time domain, it has been possible to develop a new method of continuously monitoring the total path which the NIR light has travelled in the tissue of interest. Figure 3.4 demonstrates schematically the principles of the time and frequency domain measurements of DPF.

The laser pulses used in the time of flight system described in section 3.4.1, have a duration of less than 4 ps, equivalent to a bandwidth of 250 GHz. Therefore if a continuous laser source, modulated at all frequencies from DC to 250 GHz was used and the resulting

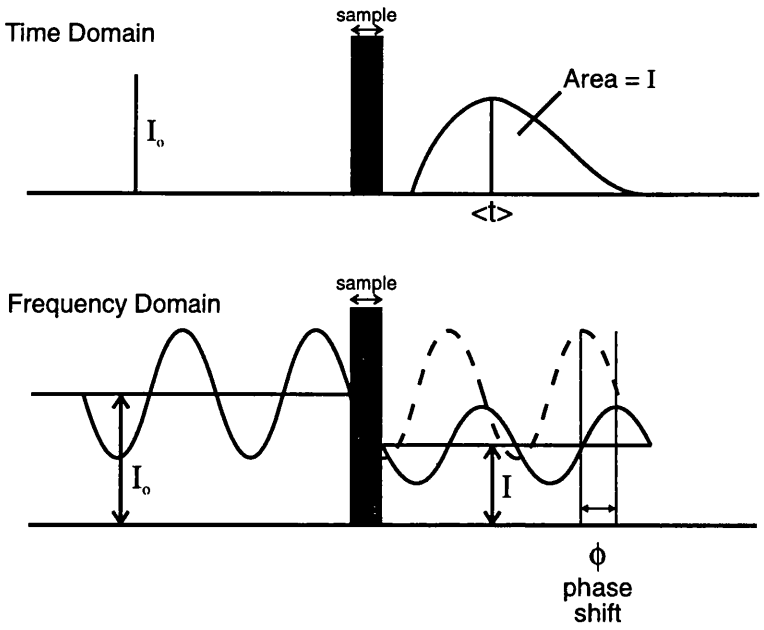

Figure 3.4 *Schematic comparison of the DPF measurement principles using the time (TPSF) and frequency (IMOS) domain.*

phase shift and modulation depth recorded, the result would be the Fourier transform of the TPSF. It has been shown that if ϕ is the phase shift measured in radians, the distance travelled through the tissue, β, is given by:

$$\beta = \frac{\phi c_v}{2\pi f n_t} \qquad (3\text{-}5)$$

where c_v is the speed of light in vacuo, f is the modulation frequency and n_t is the refractive index of tissue. If tissue sections of greater than 3 cm are studied the highest frequency required to reproduce the mean time of flight information is approximately 3 GHz, and optical pathlengths have been derived from a measurement of phase shift of light modulated at a single frequency of 220 MHz[11, 12].

An intensity modulated optical spectrometer capable of working over a range of frequencies has now been developed by Duncan et al.[13] for use in a number of clinical studies (particularly those where motion artefact is likely). The system consists of four laser diodes emitting at 690, 740, 804 and 829 nm. The diodes are modulated from one of two frequency synthesizers at between 1 - 500 MHz. Transmitted light is detected by a photomultiplier tube

with a fast rise time of 0.5 ns. After filtering, the DC component of the signal is amplified to provide the basic spectroscopic information of absorbance at each wavelength. The AC component, after further processing is analysed by a dual phase lockin amplifier and the resulting phase shift and modulation depth information is recorded simultaneously. Initial studies demonstrate noise characteristics of rms values of 0.0006 OD in attenuation, 0.0008% in modulation depth and 0.02mm in distance. Since the distance measured is the total optical pathlength (IOS x DPF), this instrument negates the need for manual IOS measurements and therefore represents a dramatic improvement in the accuracy of pathlength measurements. It is hoped that this enhanced performance will prove useful not only in studies where the optodes are likely to move (e.g. during fetal measurements or exercise studies) but also in improving the accuracy of oxidised cytochrome oxidase measurements which, due to the chromophore's relatively low concentration in tissue, are particularly vulnerable to errors in pathlength estimation. In addition, correction for pathlength variations known to occur with absorption coefficient, μ_a, (and hence wavelength) can also be made. Clinical measurements using this instrument are currently underway.

3.4.3 Water Peak measurements using CCD

The third method described for the measurement of optical pathlength in tissue requires neither time nor frequency resolved measurements of the type outlined in the previous sections. This novel method employs time resolved measurements of the attenuation of NIR light due to tissue water. Studies on the adult forearm have demonstrated the validity of the technique compared to the time of flight method[14].

Since the concentration of water in tissue is usually stable and can be estimated with reasonable accuracy it is possible that it may be used as a reference chromophore for the measurement of optical pathlength. The theoretical details of the technique are described in detail by Matcher et al.[14]. The technique relies upon the measurement and second differential analysis of the well defined spectral features in the NIR due to absorption by water (Figure 2.1). It is assumed that in a highly scattering medium the amplitude of the spectral features are scaled by the total optical pathlength. Therefore if the apparent water concentration is calculated from the amplitude of one of these spectral peaks and is then divided by the known water concentration for that tissue, an estimate of the total optical pathlength can be obtained. Due to the effects of other NIR absorbers, measurements are limited to the peak in water

absorption at 820nm which is usually fitted between 815 and 840nm. A previously described charged coupled device (CCD) spectrometer[15] with spectral range of 650 - 1000 nm sampled at 1.1 nm intervals is used to collect the necessary spectra. This method is therefore unable to provide information about the spectral dependence of optical pathlength on wavelength, but does have the important advantage of utilising less complex equipment than other methods thus increasing its clinical usefulness.

3.5 THE RELATIONSHIP BETWEEN OPTICAL PATHLENGTH AND OTHER VARIABLES

The importance of optical pathlength measurements has been made clear, but the relationship between DP and other experimental parameters must also be considered. It has been shown that the DP is dependent upon:

3.5.1 Tissue Type

Measurements of DPF have been made on the neonatal head and the adult head, forearm and calf and a marked difference is seen between the three tissues[9]. This difference is to be expected since DPF is directly dependent upon both the amount of light scatter and absorption in tissue, which in turn is dependent upon the proportion of, for example, soft tissue, muscle and bone in the illuminated tissue. The dependence of DPF on tissue type may contribute significantly to the measurement of adult cerebral haemodynamics where a heterogeneous field including skin, bone, and white and grey matter is illuminated. This effect is dealt with in more detail in section 4.2.7.3.

3.5.2 Absorption Coefficient

The time of flight system has been used to demonstrate the relationship between DP and wavelength of NIR light (and hence the absorption coefficient) in the adult head, forearm and calf (*in vivo*) and the infant head (*post mortem*)[5]. The DPF and logarithm slope, K_{ls}, were estimated from the TPSF measured between 740 and 840 nm. In all the tissues the DPF and the logarithmic slope showed a reciprocal relationship, as expected, and exhibit the absorption characteristics of haemoglobin. DPF falls with increasing wavelength with a variation of

typically 12%, while K_{ls} increases with wavelength.

3.5.3 Geometry of Optodes

van der Zee[16] demonstrated, with the aid of a computer simulation, that on a spherical object DPF is dependent upon angular position. DPF may vary significantly between an emitter-detector angle of 180° - 60°, and even more rapidly for angles of less than 60°. In contrast an experimental study by the same author[9], showed that in all tissues DPF initially fell with increasing interoptode spacing, the value becoming almost constant for spacings above 2.5cm. This discrepancy between the theoretical and experimental results can be explained in part by the fact that the theoretical model did not take into account the inhomogeneity of the tissue illuminated. This has been confirmed by modelling of multilayered tissues[17] where the DPF has been shown to vary with angle in the same way as observed experimentally. Much work is currently being done in further refining the models used for prediction of DPF, particularly in realistic tissue models[18].

3.6 REFERENCES

1. Matthes K. (1935) Untersuchungen über die Sauerstoffsättigungen des menschlichen Arterienblutes. *Arch Exp Path Pharmakol* 179;698-711
2. Nakajami S., Hirai Y., Takase H., et al. (1975) New pulse type ear oximeter. *Respiration and Circulation* 23;709-713
3. Severinghaus J.W. and Naifeh K. (1987) Accuracy of response to six pulse type oximeters to profound hypoxia. *Anaesthesiology* 67;551-558
4. Cope M. and Delpy D.T. (1988) A system for the long term measurement of cerebral blood and tissue oxygenation in newborn infants by near infrared transillumination. *Med. Biol. Eng. & Comp.* 26(3);289-294
5. Essenpreis M., Elwell C.E., Cope M., van der Zee P., Arridge S.R., Delpy D.T. (1993) Spectral dependence of temporal point spread functions in human tissues. *Appl. Opt.* 32(4);418-425
6. Wray S., Cope M., Delpy D.T., Wyatt J.S., Reynolds E.O.R. (1988) Characterisation of the near infrared absorption spectra of cytochrome aa_3 and haemoglobin for the non

invasive monitoring of cerebral oxygenation. *Biochim. Biophys. Acta* 933;184-192

7. Delpy D.T., Cope M., van der Zee P., Arridge S.R., Wray S., Wyatt J.S. (1988) Estimation of optical pathlength through tissue from direct time of flight measurement. *Phys. Med. Biol.* 33(12);1433-1442
8. Bolin F.P., Preuss L.E., Taylor R.C., Ference R. (1989) Refractive index of some mammalian tissues using a fiber optic cladding method. *Appl. Opt.* 28;2297-2302
9. van der Zee P., Cope M., Arridge S.R., Essenpreis M., Potter L.A., Edwards A.D., Wyatt J.S., McCormick D.C., Roth S.C., Reynolds E.O.R., Delpy D.T. (1992) Experimentally measured optical pathlengths for the adult head, calf and forearm and the head of the newborn infant as a function of interoptode spacing. *Adv. Exp. Med. & Biol.* 316;143-153
10. Nossal R. and Bonner R.F. (1991) Differential time-resolved detection of absorbance changes in composite structures. In "*Time-Resolved Spectroscopy and Imaging of Tissues*", eds Chance B., Proc. SOC. Photo-Opt. Instrum. Eng., 1431.
11. Chance B., Maris M., Sorge J., Zhang M.Z. (1990) A phase modulation system for dual wavelength difference spectroscopy of hemoglobin deoxygenationbin tissues. *Proc. SPIE* 1204;481-491
12. Weng J., Zhang M.Z., Simons K., Chance B. (1991) Measurement of biological tissue metabolism using phase modulation spectroscopic technology. *Proc. SPIE* 1431;161-170
13. Duncan A., Whitlock T., Cope M., Delpy D.T. (1993) A multiwavelength, wideband, intensity-modulated spectrometer for near-IR spectroscopy and imaging. *Proc. SPIE* 1888;248-257
14. Matcher S.J., Cope M., Delpy D.T. (1994) Use of the water absorption spectrum to quantify tissue chromophore concentration changes in near-infrared spectroscopy. *Phys. Med. Biol.* 39;177-196
15. Cope M., Delpy D.T., Wray S., Wyatt J.S., Reynolds E.O.R. (1989) A CCD spectrometer to quantitate the concentration of chromophores in living tissue utilising the absorption peak of water at 975nm. *Adv. Exp. Med. & Biol.* 247;33-40
16. van der Zee P., Arridge S.R., Cope M., Delpy D.T. (1990) The effect of optode positioning on optical pathlength in near infrared spectroscopy of the brain. *Adv. Exp. Med. & Biol.* 277;79-84
17. Hiraoka M., Firbank M., Essenpreis M., Cope M., Arridge S.R., van der Zee P., Delpy

D.T. (1993) Simulation of light distribution in inhomogeneous tissue by a Monte Carlo method. *Phys. Med. Biol.* 38;1859-1877

18. Schweiger M., Arridge S.R., Delpy D.T. (1993) Application of the finite-element method for the forward and inverse models in optical tomography. *J.M.I.V.* 3;263-283

CHAPTER 4

MEASUREMENT OF ABSOLUTE CBF AND CBV IN ADULTS USING NIRS

4.1 INTRODUCTION

The previous chapters have established the role and principles of cerebral haemodynamic measurements. As already discussed, the technique of NIRS can measure the *changes* in concentration of the chromophores Hb, HbO_2 and CtOx from an arbitrary zero baseline in an intact organ. These measurements, which can currently be made using a non invasive bedside monitor, are of limited clinical importance since they merely provide trend information about the haemodynamic status of the patient. However it is possible to perform certain manoeuvres which allow these quantitative *changes* to be used to provide useful clinical information in the form of absolute haemodynamic parameters. A few studies of the use of these qualitative changes in cerebral oxygenation have been published[1-5], but to date no quantitative measurements on adults have been reported. This chapter will describe the theoretical details, experimental procedures and data analysis involved in the measurements of CBF and CBV using NIRS. Particular emphasis will be placed on the considerations of applying these theories to the monitoring of adult haemodynamics. The role of pulse oximetry in the measurements of CBF and CBV is also detailed.

4.2 MEASUREMENT OF CEREBRAL BLOOD FLOW

The measurement of CBF using NIRS was first devised by Edwards et al. in 1988 [6], for use in the non invasive assessment of neonatal cerebral haemodynamics. Like many other CBF techniques the method employs a modification of the Fick principle which has already been described in section 1.4.2.1.

4.2.1 Theory

It would first be sensible to recall the equation that Kety derived for the measurement of CBF using an inert tracer:

$$\frac{F_t}{W} = \frac{C_T}{\int_0^t (C_a - C_v)\, dt} \qquad \textbf{(4-1)}$$

where F_t = blood flow through the brain

W = unit weight of the brain tissue

C_a = arterial tracer concentration

C_v = venous tracer concentration

C_T = accumulation of tracer concentration in the brain tissue

t = time over which tracer concentration is varying

It can be seen that tissue *perfusion* (i.e. flow per unit weight of tissue) is actually measured rather than the total blood flow to the whole brain. Now, taking this equation one step further, if the measurements of the accumulation of the tracer are made within the minimum transit time of that tracer through the brain, T_t, the venous tracer concentration (C_v) will be zero. Flow (or more accurately perfusion) can then be calculated from the ratio of the quantity of tracer accumulated to the quantity of tracer introduced during time t:

$$\frac{F_t}{W} = \frac{C_T}{\int_0^t C_a(t)\, dt} \quad \textit{where } t < T_t \qquad \textbf{(4-2)}$$

In NIRS the tracer used is *a change in concentration* of the near infrared "dye" oxyhaemoglobin. When a sudden increase is induced in fractional arterial oxygen saturation (ΔSaO_2), the resulting initial increase in cerebral [HbO_2] represents the accumulation of tracer C_T. If excessive changes in arterial oxygen tension (PaO_2) are avoided, the contribution of dissolved oxygen in the plasma can be disregarded and the actual quantity of tracer introduced is given by the integral of ΔSaO_2 with respect to time multiplied by the total concentration of haemoglobin in the whole blood ([tHb]). At this point it is interesting to note that unlike other CBF techniques, NIRS has the advantage of directly measuring the concentration of the tracer in the tissue (C_T). In methods such as PET and ^{133}Xenon washout, errors can be introduced in the estimation of the constant of proportionality which is required to relate the measured C_v to the desired C_T.

If $\Delta[HbO_2]$ is expressed in μmolar and [tHb] in $g.ml^{-1}$, cerebral blood flow can then be derived in units of $ml.100g^{-1}.min^{-1}$ from the equation:

$$CBF(ml.100g^{-1}.\min^{-1}) = \frac{K \cdot \Delta[HbO_2]}{[tHb] \cdot \int_0^t \Delta SaO_2 \, dt} \qquad \textbf{(4-3)}$$

where

$$K = \frac{MW_{Hb} \cdot 10^{-6}}{D_t \cdot 10} \qquad \textbf{(4-4)}$$

MW_{Hb} is the molecular weight of haemoglobin and D_t is the cerebral tissue density in $g.ml^{-1}$, assumed to be 1.06[7]. Total haemoglobin flow (F_{Hb}) in $\mu molar.min^{-1}$ may then be calculated using:

$$F_{Hb}\ (\mu molar.\min^{-1}) = \frac{\Delta[HbO_2]}{\int_0^t \Delta SaO_2 \, dt} \qquad \textbf{(4-5)}$$

Note that the NIRS technique monitors cerebral haemoglobin flow without the need for additional constants and when multiplied by four (the O_2 capacity of a haemoglobin functional

unit) gives the oxygen flow to the tissue (neglecting dissolved O_2 in the plasma). Unfortunately, μmolar units are not commonly accepted as the clinical units of blood flow through an organ and the conversion to $ml.100g^{-1}.min^{-1}$ is almost always necessary.

When the total cerebral haemoglobin concentration ([tcHb]) is constant it may be assumed that the changes in $[HbO_2]$ and [Hb] are equal and opposite. The signal representing the difference between the change in $[HbO_2]$ and [Hb] is thus twice the amplitude of the corresponding signal representing the change in $[HbO_2]$ alone. Therefore to improve the signal to noise ratio of the NIRS data, equation 4.3 can be modified to :

$$CBF(ml.100g^{-1}.\min^{-1}) = \frac{K \cdot (\Delta[HbO_2] - \Delta[Hb])}{2 \cdot [tHb] \cdot \int_0^t \Delta SaO_2 \, dt} = \frac{K \cdot \Delta[Hb_{diff}]}{2 \cdot [tHb] \cdot \int_0^t \Delta SaO_2 \, dt} \qquad \textbf{(4-6)}$$

The term $[Hb_{diff}]$ is used to represent the difference between the HbO_2 and Hb concentrations and the term $[Hb_{sum}]$ to represent their sum.

To obtain data from which to calculate CBF, simultaneous arterial pulse oximetry (to measure SaO_2) and NIRS measurements are made while the subject's inspired oxygen fraction (FiO_2) is first slowly reduced to provide a stable baseline and then rapidly increased to produce the required sudden rise in SaO_2 (i.e. the delivery of the tracer $\Delta[HbO_2]$).

This method of measuring blood flow has been successfully validated in the neonate by comparison with the ^{133}Xenon washout method[8] and in the adult forearm by comparison with venous occlusion plethysmography[9]. These studies have showed that the technique is accurate for measurements up to approximately 40 $ml.100g^{-1}.min^{-1}$ and its use in neurological assessment of neonates has since flourished[10-13].

4.2.2 Problems Associated with NIRS CBF measurements in Adults

A typical value for average CBF in a neonate is 18 $ml.100g^{-1}.min^{-1}$[16], compared to a value of $50ml.100g^{-1}.min^{-1}$ in the adult. The problems associated with measuring these higher flow rates with the same technique must therefore be identified and addressed. Since the method requires accurate measurement of the rapid change in arterial [HbO_2] concentration by the NIR spectrometer, and of the change in arterial SaO_2 by a pulse oximeter, limitations in the performance of both these monitors can contribute errors to the calculation of CBF. These errors will be considered in turn:

4.2.2.1 *Sampling rate of the NIR spectrometer*

NIRS measures the increase in cerebral [HbO_2] and thus quantifies the tracer accumulation, Q. Since the NIR light illuminates the whole of the vascular field the measured changes in [HbO_2] do not differentiate between arterial inflow and venous outflow of tracer. Therefore in order to justify the assumption that the changes in cerebral [HbO_2] are due to arterial accumulation of the tracer in the brain, all measurements must be made within the minimum transit time of blood through the brain. Cerebral blood flow and vascular transit time will vary according to the relative amounts of grey and white matter in the field of view. If a mean value of 5.5 seconds is taken[14] with perhaps a range of ±2 seconds, then it is clear that the NIRS data must be collected over short time periods in order to obtain a sufficient number of data points before the minimum transit time is reached.

4.2.2.2 *Sampling rate of the pulse oximeter*

With the relatively short adult cerebral vascular transit time, the success of the NIRS flow measuring technique depends upon the sudden input of the tracer, oxyhaemoglobin, into the brain. As discussed in section 3.2, in many pulse oximeters some degree of signal averaging is performed which will damp the monitored SaO_2 input function and thus lead to an underestimate of the actual quantity of tracer introduced to the brain during time, t. To obtain SaO_2 values which will accurately monitor the step change, a pulse oximeter which performs minimal signal averaging is needed. This can be achieved by measuring SaO_2 on every heart beat.

4.2.2.3 *Pulse oximetry measurement site*

$\Delta[HbO_2]$ and SaO_2 are measured by NIRS and pulse oximetry respectively at two different sites on the body. Thus, the induced change in oxyhaemoglobin concentration may be seen first by the NIR spectrometer or by the pulse oximeter depending upon the time taken for the oxygenated blood to reach the brain and the pulse oximetry site respectively. To minimise this delay the ear is usually chosen as the monitoring site for SaO_2, but the delay will be exaggerated by the choice of a more distal site such as the finger for the oximetry measurements. The Fick principle involves calculating the ratio of the tracer accumulated to the tracer introduced during a given time period. Any delay between the detection of the signals must therefore be accurately compensated for since temporal mismatch of the signals will introduce errors into the calculation.

4.2.2.4 *Delivery of rapid step input of tracer*

Whether measurements are being made on normal volunteers or ventilated patients it is important to deliver the rapid step input of $[HbO_2]$ tracer as quickly as possible, i.e. to change FiO_2 by approximately 5% in 0.5 seconds. In spontaneously breathing adult volunteers this can be achieved by a breathing circuit described in section 4.2.4.1 which uses separate supplies for the hypoxic and oxygenated mixtures. However in ventilated adult patients, undergoing intensive care or anaesthetic procedures, the dead space of the ventilation circuit significantly impedes the rapid input of tracer. The step change in FiO_2 is controlled upstream of the ventilator which can act to disperse the input function. Methods used to overcome this problem include transiently increasing the flow rate of gas to the patient or manually ventilating the patient with 100% O_2 for a short period.

Once a step input of tracer has been successfully delivered to the patient, it is then important that the change in FiO_2 produces an equally rapid change in $[HbO_2]$ in the lungs. This requires a minimum level of lung function by the patient and most importantly an efficient transfer factor indicating the uptake of gas by the pulmonary circulation. In patients where lung function is compromised slurring of the step input will occur.

4.2.3 Pulse oximetry requirements for measurements of CBF

As can be seen from the previous description, pulse oximetry measurements are inherent in the quantification of CBF. The most important features of a pulse oximeter needed for these type of NIRS measurements are:

4.2.3.1 *Beat to beat collection*

For measurements of CBF the oximeter must be capable of working in beat to beat mode. Any signal averaging by the pulse oximeter will slur the recording of the step input function of SaO_2.

4.2.3.2 *Signal/noise performance and artefact rejection*

The oximeter must work with minimal signal averaging and yet is being used to monitor changes of only a few percent in saturation. This requires an oximeter with excellent signal to noise ratio (and signal processing) characteristics. The oximeter must also be immune to artefact (eg. movement, changes in ambient light etc.) since signal averaging and software rejection routines cannot be employed to reduce the effect of such artefacts.

4.2.3.3 *Ear Probe*

For both CBV and CBF measurements an ear probe is essential. Both measurements involve a direct correlation between systemic and cerebral oxygenation and the time delay between these two signals can be greatly reduced by making oximetry measurements at the ear. The problem of time delay is particularly pronounced in the adult where measurements of SaO_2 at the finger may lag those at the ear by up to 15 seconds[15].

4.2.3.4 *Analogue output of signals*

During measurements signals from the oximeter and other monitors are fed into the spectrometer for simultaneous real time display and storage along with the NIRS data. Most spectrometers will only accept analogue transfer of the oximetry (or any other) external data.

Unfortunately, these specifications are not met by any of the currently available clinical pulse oximeters of the type described in section 3.2. For this reason SaO_2 readings are often seen as the "weak link in the chain" during clinical NIRS studies and are responsible for the rejection of large sections of data.

4.2.4 Experimental Details

Five measurements of CBF were made on each of 10 male subjects (age range 24-36 years, median 27.5) who had no known respiratory or circulatory disorders. The study was approved by the University College London Faculty of Clinical Science Committee on the Ethics of Clinical Investigation, and informed consent was obtained from the subjects before each investigation.

4.2.4.1 *Instrumentation*

Near infrared light was carried to and from the NIRO 500 spectrometer along fibre optic bundles. The optodes were positioned high on the left side of the forehead 4 - 5 cm apart. Positions near the temporalis muscle may lead to significant contamination of the NIRS signal by surface tissues[16]. The sinuses were also avoided since light can be channelled by these away from the brain. The exact position of the optodes was dependent upon the level of the hairline in each subject, but did not vary by more than ±1 cm for all the subjects (Figure 4.1). The optodes were held in position with double sided adhesive rings and self adhesive tape and the head was then wrapped in black cloth to reduce background light. The prototype NIRO 500 used in these studies used pulsed laser diodes at three wavelengths (775, 829, 909 nm) as its light source and a photomultiplier tube for detection. Data were collected every 0.5s and the changes in $[HbO_2]$ and [Hb] were calculated using the method described in section 2.4.3.

SaO_2 and heart rate were monitored with a pulse oximeter (Novametrix 500, USA) modified to measure in "beat to beat" mode and employing a probe positioned on the right ear. A transcutaneous blood gas electrode (Novametrix 850, USA) was placed on the medial aspect of the left upper arm for monitoring transcutaneous carbon dioxide tension ($TcPCO_2$) continuously. The analogue outputs of both the oximeter and transcutaneous monitor were linked directly to the spectrometer for real time display and storage along with the NIRS data.

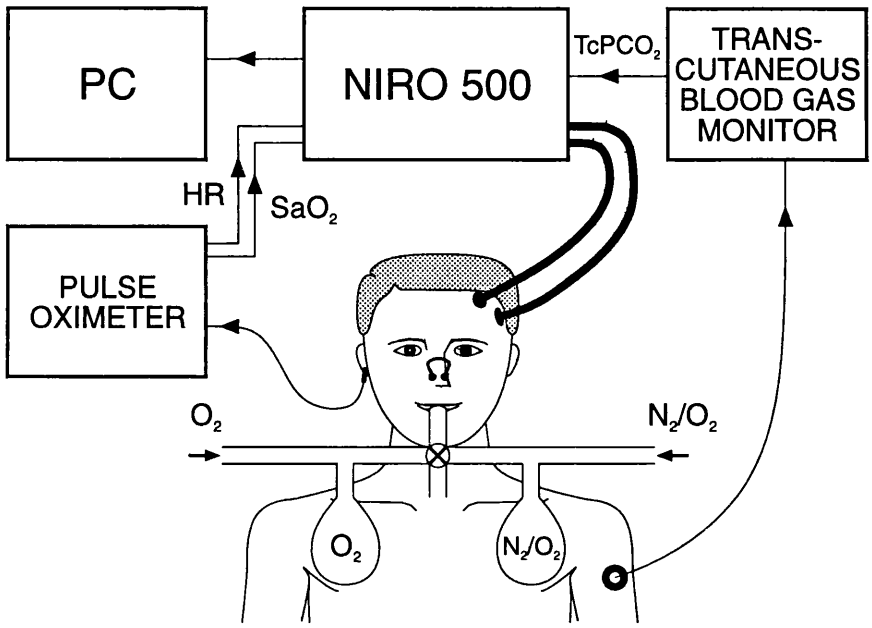

Figure 4.1 *Schematic of the experimental set up for the NIRS CBF measurement in spontaneously breathing adult volunteers.*

A modified anaesthetics trolley supplied a controlled mixture of nitrogen and oxygen to the subject via a Waters bag and mouthpiece (shown in Figure 4.1). A separate circuit supplied 100% oxygen to a second Waters bag. Both bags were connected to the mouthpiece by a two way switch valve which allowed the gas the subject was breathing to be changed from a hypoxic mixture to 100% O_2 virtually instantaneously. The subject wore a nose clip to ensure that the inspired oxygen concentration was well controlled, and a flap valve vented expired gas to the atmosphere to prevent rebreathing.

4.2.4.2 *Procedure*

All measurements were made with subjects lying flat on a couch. The subject initially breathed through the mouthpiece from the first Waters bag. The FiO_2 in this circuit was then gradually reduced over 3 - 4 minutes until a baseline SaO_2 of 85-90% was achieved. This baseline was maintained for 1 - 2 minutes and then at the end of an expiration the valve was switched to allow the subject to inspire 100% O_2 for the next breath which caused the SaO_2 to rise to 98-99% within 1.5 - 2 seconds. After one or two breaths of 100% O_2 the nose clip was removed so that the subject could breathe room air. This method allowed him to maintain

a constant breathing rate while SaO_2 was both lowered and then rapidly increased for the CBF manoeuvre, but avoided PaO_2 rising to very high levels which might cause cerebral vasoconstriction[17].

A venous blood sample was taken from each subject and [tHb] was measured by Coulter Counter.

4.2.5 Data Analysis

Figure 4.2 shows one set of data collected from one subject during a CBF measurement. The step change in SaO_2 can be more clearly seen on an expanded scale in Figure 4.3, where each point represents a 0.5 second sample. To calculate CBF both the integral of the SaO_2 rise and the change in $[Hb_{diff}]$ must be evaluated over a given time t. To do this, the start point for the rise in SaO_2 was defined by inspection of the data. However when SaO_2 was reduced to about 90%, oscillations were clearly seen in SaO_2 which appeared to be related to respiration. Although these are only partially transmitted to the cerebral circulation a mean value of three respiratory cycles was taken as the baseline for measuring the change in SaO_2. (The origin and implications of these oscillations was investigated further in a separate study which is described in Chapter Five.) The cumulative SaO_2 integral at each

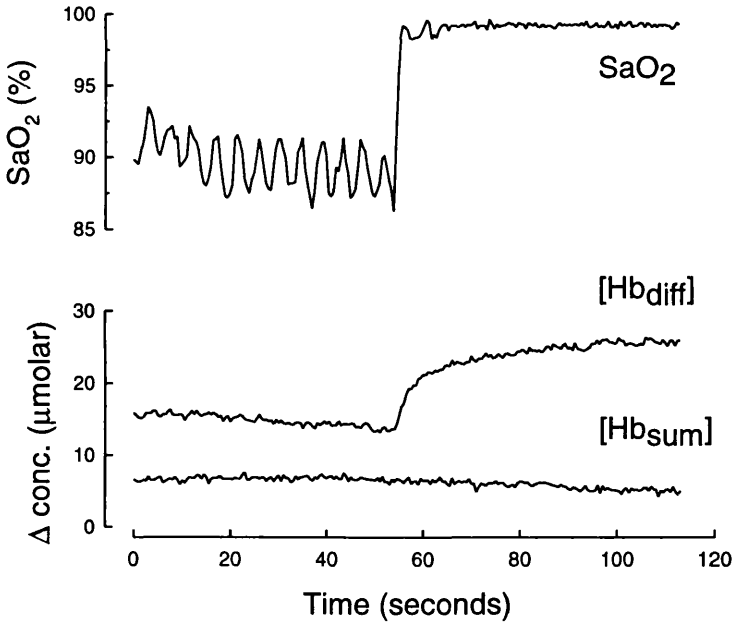

Figure 4.2 *NIRS and SaO_2 data collected during a measurement of CBF in a normal adult.*

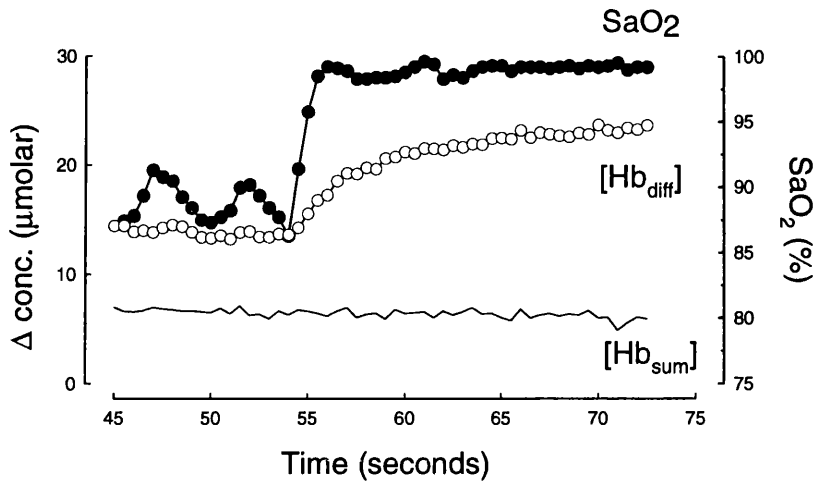

Figure 4.3 *Data collected during a CBF measurement (as shown in Figure 4.2) with an expanded time scale to demonstrate the step change in SaO_2 and respiratory linked oscillations.*

point over time t was estimated by Simpson's rule, and was then plotted against the equivalent $[Hb_{diff}]$ data for the same period (Figure 4.4). A fourth order polynomial was fitted to this data and the first order differential of this used to calculate a set of values for CBF over the time period, t (Figure 4.5).

To estimate the true value of the time difference between the ear (SaO_2) and the brain ($[Hb_{diff}]$), a range of CBF calculations were made. The cumulative SaO_2 integral over time t was fixed as above and then plotted against the measured $[Hb_{diff}]$ for the same time duration, but beginning 0.5 second away from the point of the initial rise in SaO_2. This procedure was then repeated changing the offset point by 0.5 second each time until CBF had been calculated on the data up to 5 seconds before and 10 seconds after the initial rise in SaO_2. This produced a set of calculated CBF values for every 0.5 second shift within this 15 second period. The point at which the change in $[Hb_{diff}]$ is correctly temporally matched with the SaO_2 step change was defined by the resulting CBF - time curve which had the maximum initial CBF value. Five CBF measurements were performed on each subject, and the mean CBF - time curves calculated from the analysis of these measurements were averaged to produce a mean curve for each subject.

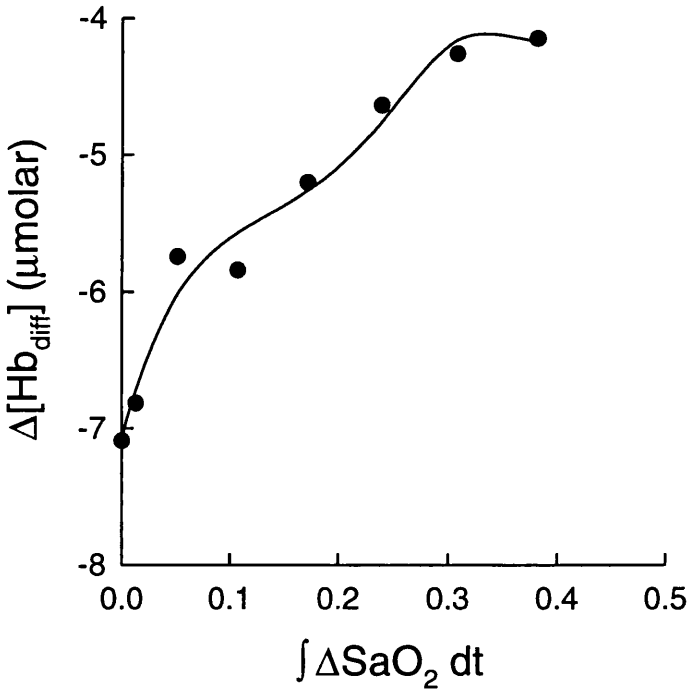

Figure 4.4 *Plot of the change in [Hb_{diff}] versus the cumulative integral of the fractional change in SaO_2 for the previously shown CBF measurement. A 4th order polynomial has been fitted to the data.*

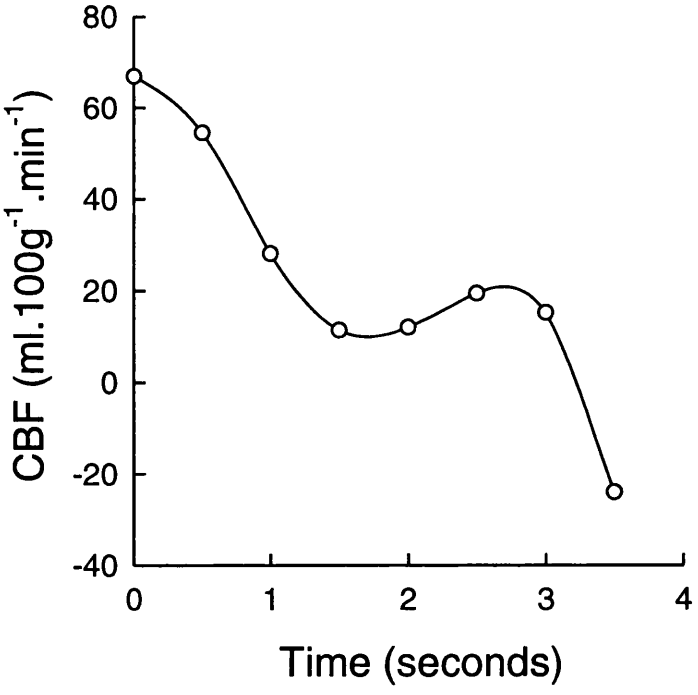

Figure 4.5 *Resulting CBF versus time curve for the data shown in Figure 4.4.*

The time over which the integral of the SaO_2 rise and the corresponding change in $[Hb_{diff}]$ are measured will depend upon the vascular transit time of the adult human brain. To investigate the dependence of the calculated CBF on the estimation of this parameter, the analysis procedure described above was initially performed over a period of 3 seconds and then repeated on the same data for periods of 4, 5 and 6 seconds.

To quantify the effects of signal averaging of the oximetry data, a rolling average over 1.5, 2.5 and 3.5 seconds was applied in software to the non averaged "beat to beat" SaO_2 data. The analyses described above were then repeated for each degree of averaging.

The effect of a deliberate temporal mismatch of the $[Hb_{diff}]$ rise and SaO_2 step was investigated by comparing the CBF - time curves obtained 1 and 2 seconds before and after the curve which produced the maximum initial CBF.

4.2.6 Results

Figure 4.6 shows the mean CBF - time curves, calculated over periods of 3, 4, 5 and 6 seconds, for each subject, and the overall mean for all ten subjects for each time period. The negative flow values of the final point of each curve are an artefact due to the effects of the polynomial fit, and are included only to demonstrate the high and low flow component trend seen on each measurement. From a total of 50 measurements (five measurements per subject), nine were rejected and excluded from further analysis. Criteria for rejection included conditions where CBV was changing significantly during the measurement. This was defined as a change in $[Hb_{sum}]$ of 30% or more of the change in $[Hb_{diff}]$. The intra subject coefficient of variation ranged from 4% to 57% (mean 20%), whilst the inter subject coefficient of variation ranged from 30% to 34% (mean 32%). The absolute values of $TcPCO_2$ did not vary by more than 0.53kPa during any of the CBF measurements. The mean (±SD) change in total cerebral haemoglobin concentration ($[Hb_{sum}]$) as a percentage of the change in $[Hb_{diff}]$ was 22 ± 5%.

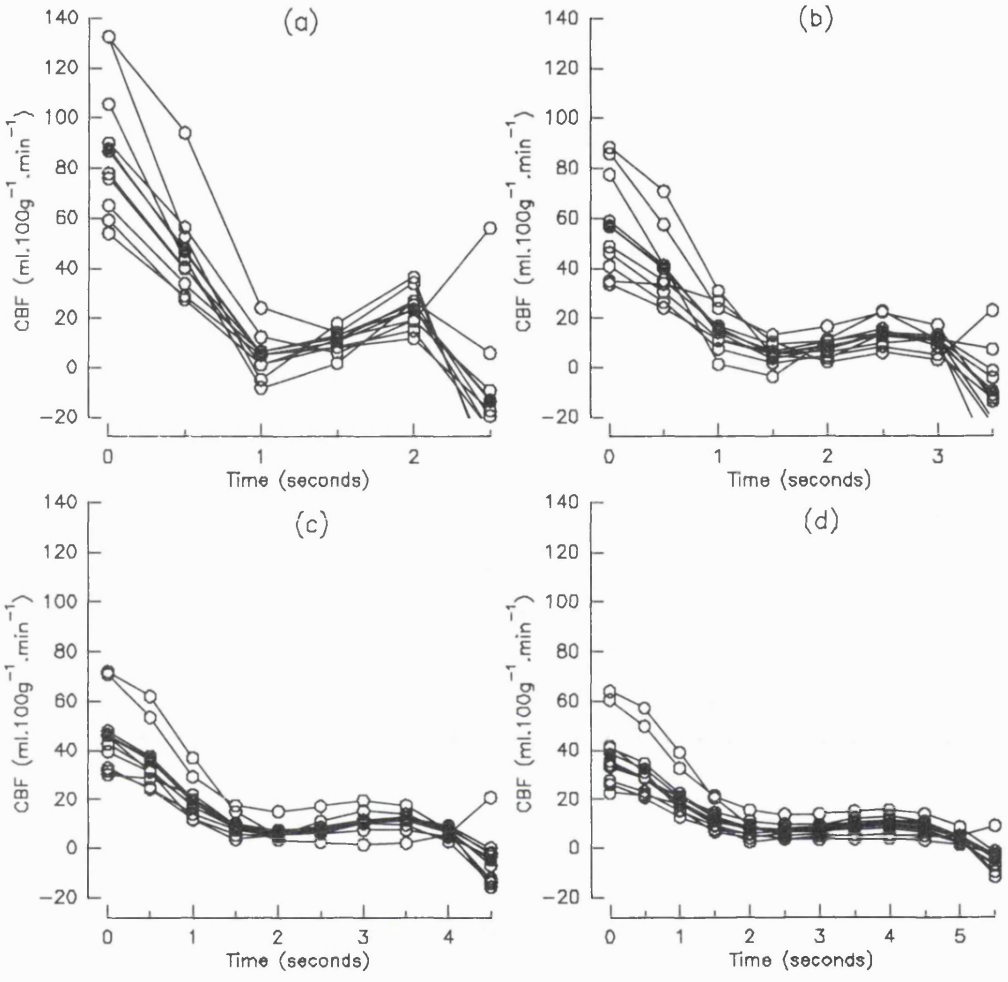

Figure 4.6 *Mean CBF time curves for each subject for (a) t=3s, (b) t=4s, (c) t=5s and (d) t=6s (hollow circles). The overall mean for all ten subjects in each time period are shown with filled circles.*

The relative effects of SaO_2 signal averaging on the mean CBF - time curve for all subjects over 6 seconds is shown in Figure 4.7. Table 4.i summarises the effects of SaO_2 averaging upon the calculated maximum flow. Figure 4.8 shows a plot, for each period, of the maximum CBF against temporal offset from the previously defined maximum CBF. The percentage decrease in calculated maximum CBF due to +2, +1, -1 and -2 second offsets are shown in Table 4.ii.

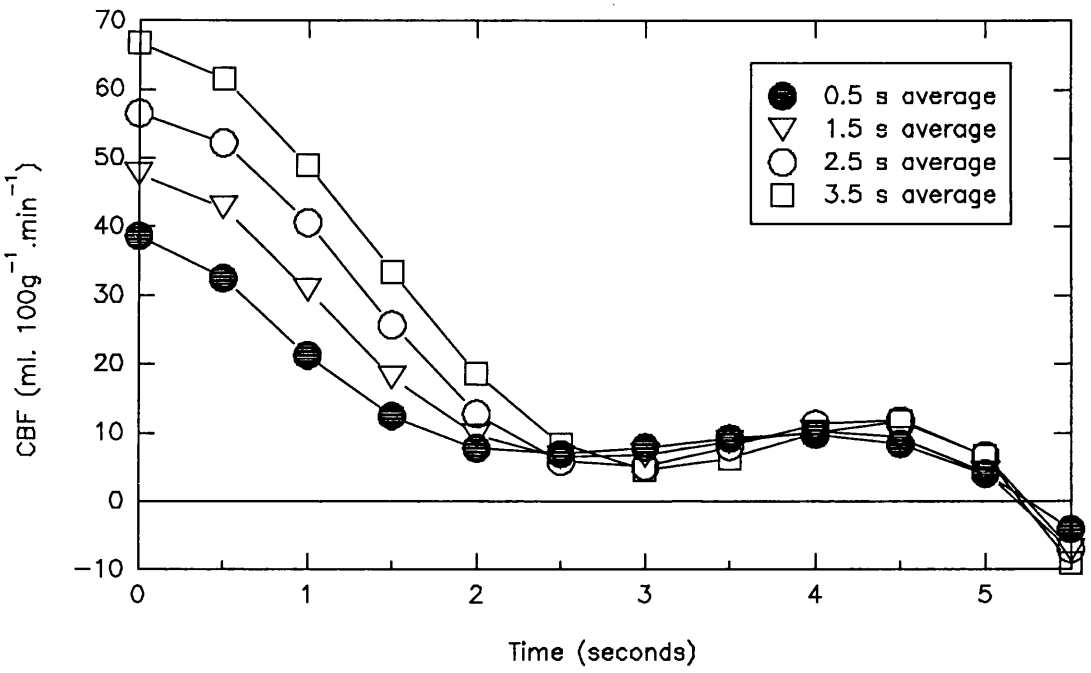

Figure 4.7 *The effect of SaO_2 averaging on the mean CBF-time curves for all subjects for t = 6s.*

Table 4.i *Percentage increase in calculated maximum CBF due to 1.5, 2.5, and 3.5 second averaging of the SaO_2 data.*

	t = 3 s	t =4 s	t = 5 s	t = 6 s
1.5 second SaO_2 averaging	45.8%	34.9%	26.7%	23.3%
2.5 second SaO_2 averaging	95.7%	64.0%	51.1%	46.3%
3.5 second SaO_2 averaging	122.4%	91.3%	75.7%	72.8%

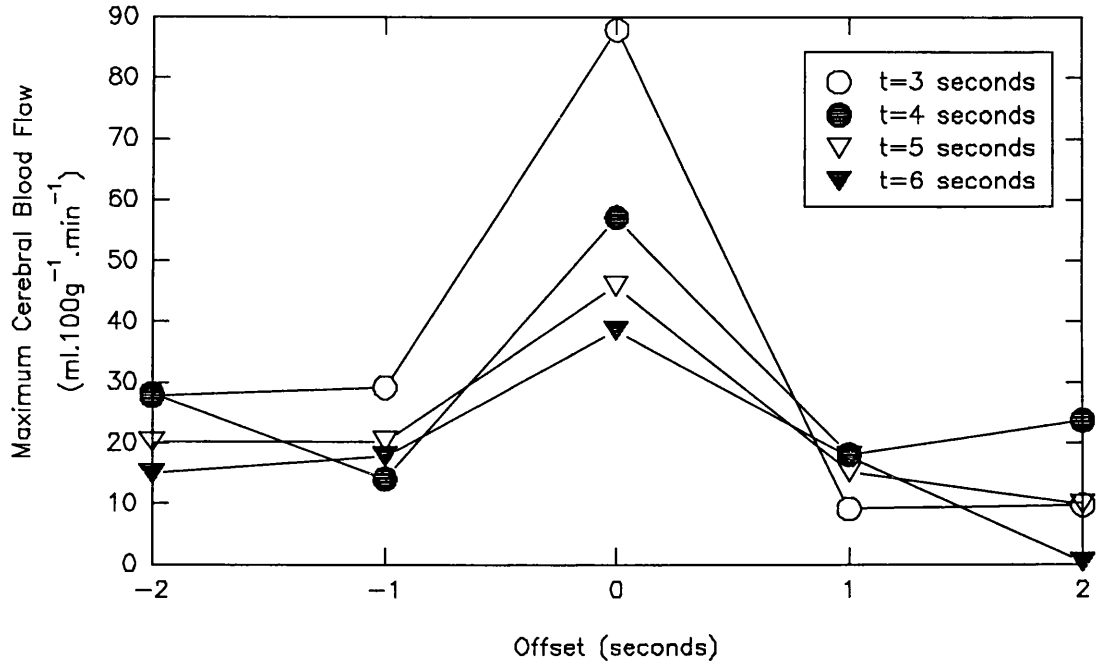

Figure 4.8 *The effects of temporal offset on the calculated maximum CBF (mean from all ten subjects).*

Table 4.ii *Percentage decrease in the calculated maximum CBF due to +2, +1, -1, and -2 second offset from the correctly temporally matched CBF calculations.*

OFFSET	t = 3 s	t = 4 s	t = 5 s	t = 6 s
+ 2 second	89.0%	58.7%	78.7%	99.2%
+ 1 second	89.6%	68.4%	66.8%	53.9%
- 1 second	66.9%	75.3%	55.8%	54.0%
- 2 second	68.4%	50.8%	55.9%	61.2%

4.2.7 Interpretation of CBF results

When interpreting the CBF data obtained it is necessary to consider the various theoretical, practical and analytical aspects of the study. An important question is whether in adult measurements NIR light adequately penetrates the cerebral compartment. Extracerebral tissue has an effect of the vascular field being interrogated but also on the assumed optical pathlength for the brain. Uncertainties due to methods of data collection and analysis and violations of the theoretical basis of the technique must all be considered. These points will be dealt with in turn in the following sections.

4.2.7.1 *Distribution of transit time and CBF*

These measurements of adult CBF by NIRS show a consistent pattern of variation of CBF at different time intervals following the wash in of the tracer, with absolute values depending on the period over which the measurement is made. On all measurements there is an immediate fall from a peak value, and then a slight rise to a second peak. The average of the flows measured on normal subjects where t = 3 seconds show an initial maximum flow of 88 $ml.100g^{-1}.min^{-1}$ falling within 1.5 seconds to a lower mean flow of 13 $ml.100g^{-1}.min^{-1}$. The most consistent explanation of this phenomenon is that the distribution of cerebral vascular transit times is bimodal, and that the early measurements (within the first 0 - 1 second) detect a rapid transit compartment while the later values represent slower transit times, with the tracer having already reached a steady state in tissue where the transit time is rapid. There is evidence to support this conjecture. Measurements of ^{133}Xenon clearance curves have shown that at least two exponential curves are needed to fit the data[18] and this has been widely interpreted as representing different flow rates in grey and white matter. A similar bimodal distribution has been shown to exist in the cerebral microcirculation[19]. If the ^{133}Xenon data are combined with measurements of cerebral blood volume by PET[14], mean transit times for grey and white matter can be calculated to be about 3.5 seconds and 9 seconds respectively. Measurements of regional cerebral transit time using radionuclide cerebral angiography[20] give a mean value over all regions of 3.2 $\pm$0.67 seconds. As the minimum transit time must be less than this, these values are consistent with the hypothesis that the variation in NIRS measurements is due to a bimodal distribution of transit times which may

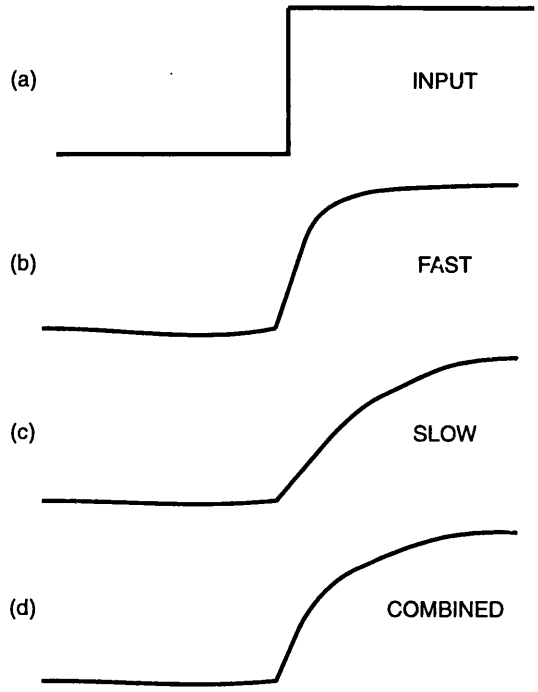

Figure 4.9 *Schematic showing (a) an ideal tracer input function, (b) the cerebral response due to fast transit time only, (c) the cerebral response due to slow transit time only and, (d) a convolution of both responses.*

represent the perfusion of cerebral grey and white matter. Figure 4.9 shows a schematic representation of the effect of a convolution of transit times on the perfect input function. The effect of a distribution of transit times within a single CBF measurement has obvious implications on the definition of mean CBF over that period. The use of multiple linear regression techniques to extract transit time information from the data shown in Figure 4.5 forms the basis of Chapter Six of this thesis.

An alternative explanation for the variation of measured CBF with measurement time is that the minimum cerebral transit time is less than one second and the initial plateau region of the flow curve cannot be defined using 0.5s data collection. However, studies in animals have shown that this is unlikely[21].

On the basis of a minimum transit time of 1.5 - 2 seconds, and assuming that transit times were normally distributed, a constant calculated value for CBF during the first 1 - 1.5 seconds would be expected. However, a different pattern was observed, with an immediate fall from the maximum calculated value. The likely reason for this is that the NIRS measurement is made over a relatively large volume of tissue in which there is not only a

distribution of transit times, but also a distribution of arrival times of the [HbO_2] tracer. This latter distribution is also likely to vary by up to ±1 second, although there seems to be little information on this aspect of the cerebral circulation. The measured data represents a convolution of these two distributions, and hence the calculated flow is unlikely to show a constant value if the data sampling period is 0.5 second.

4.2.7.2 *Vascular effects of extracerebral tissue*

Since the changes in [HbO_2] and [Hb] measured using NIRS may come from any compartment in the illuminated tissue the contribution of bone blood flow and scalp blood flow to CBF measurements must be considered. Given the short period over which the NIRS measurements are made, and the relatively low values of bone blood flow[22], it is possible that the rise in [HbO_2] in the bone blood will not have commenced and thus bone blood flow will not be detected over the period chosen for CBF calculation. A prolonged 'low flow' component can be seen in the NIRS data (Figure 4.2), and it may be possible to attempt a separate calculation for this region.

A study has now been completed where the contribution of scalp flow has been quantified. Parallel measurements of CBF using NIRS were made in subjects wearing a tourniquet inflated to arterial pressure around the base of the skull and around the forehead to occlude scalp circulation which was monitored using laser doppler flowmetry. The results of this study on 9 subjects are shown in Table 4.iii.

Table 4.iii *Effects of scalp occlusion on CBF, CBV and skin blood flux. Values shown are median (range). (H. Owen-Reece, 1994)*

	Before Occlusion	After Occlusion
CBF ($ml.100g^{-1}.min^{-1}$)	14 (9 - 24)	13 (8 - 38)
CBV ($ml.100g^{-1}$)	2.3 (1.8 - 3.0)	2.5 (1.4 - 2.8)
skin blood flux (arbitrary units)	29 (12 - 55)	12 (4 - 50)

It can be seen that there was no statistically significant difference between CBF and CBV measured with and without scalp blood flow occlusion (Private Communication, H. Owen-Reece 1994). In addition, Friberg et al.[23] estimated subcutaneous scalp blood flow in the frontal region to be as low as 5 - 8 $ml.100g^{-1}.min^{-1}$. Villringer and coworkers (1993)[24] used NIRS to study the haemodynamic changes during brain cell function in human adults. Epileptic patients were examined during spontaneously occurring complex-partial seizures and large increases in both $[HbO_2]$ and $[Hb_{sum}]$ were seen only with the optodes placed over the epileptic focus region. Laser doppler flowmetry was used to confirm that the haemodynamic changes did not originate from the scalp thus providing more evidence that NIRS monitors predominantly the brain. The spatial localization of the NIRS signal is still undetermined, but the technique has been successfully applied transcranially through intact skin and skull to detect the presence of intracranial haematomas in adult head injured patients[25].

4.2.7.3 *Optical pathlength effects of extracerebral tissue*

An essential parameter in the quantification of absolute CBF is an estimate of the pathlength of the light propagated through the tissue. The light entering and leaving the head will pass through a proportion of skin, fat, muscle and bone as well as brain tissue before being detected. In neonates where the skull thickness and calcification is less developed the contribution to scattering and absorption by these tissues is not thought to be significant. For example, during NIRS studies of cerebral oxygenation in the neonatal pig, the contribution of skull and surface tissues to the detected signal has been estimated to be less than 10% [26]. In adults however the thickness of skin, bone and muscle is greater and will therefore be more likely to effect the pathlength and distribution of light in the head. The practical limitations of light detection with currently available systems requires that an optode spacing of 4 - 6 cm must typically be employed. This relatively small optode spacing (in proportion to the size of the adult head) may reduce the thickness of brain tissue in the light path. This problem can be minimised by careful siting of the optodes. In this, and all subsequent studies on the adult head, the optodes were deliberately placed high on the forehead where the overlying tissue thickness is at a minimum, and the skull is relatively poorly perfused.

The presence of a proportion of effectively avascular tissue in the light path has direct effects on the calculated absolute values for CBF and CBV. It is likely that this tissue acts as static "dead space" with a near constant attenuation and therefore does not contribute to the

changing NIRS signals. However, the differential pathlength factor (DPF) used in these calculations (5.93) assumes that all tissues in the light path are contributing equally to the changes in [Hb] and [HbO_2]. The effect of this is significant. For instance, if we assume that the effective cerebral pathlength is approximately 50% of the total, the calculated absolute CBF and CBV would be doubled. Further modelling of the contribution to the NIRS signals of non cerebral tissue is needed to clarify the accuracy of absolute measurements.

4.2.7.4 *Data Collection and Analysis*

In order to make the measurement of CBF, SaO_2 must have both a stable baseline and a rapid change. The technique requires that the change in arterial saturation is determined continuously, and this was approximated by measuring arterial saturation on every heart beat. Any systematic error due to the pulse oximeter will compromise the accuracy of the CBF measurement, particularly if the data is processed to produce a rolling average over more than one heart beat. The current data show that the averaging likely to be performed by most commercial pulse oximeters causes significant artificial increase in the calculated CBF, and confirms the necessity for a non-averaging oximeter for these measurements. Shielding the oximeter probes from changes in ambient light and minimising sensor movement during the measurement period allowed sufficiently stable measures of SaO_2 to be obtained without averaging between heartbeats.

This study also found that slight temporal mismatching of the SaO_2 and [Hb_{diff}] signals caused a significant error in the calculated CBF. If no time delay existed between the measured SaO_2 and [Hb_{diff}] signals (as shown in Figure 4.3), the calculated SaO_2 integral could simply be matched directly with the equivalent [Hb_{diff}] rise over the same time period. However, time delays in the order of seconds are seen even when the oximeter probe is sited on the ear. Several calculations of CBF with different time offsets are then necessary to determine the correct CBF, and at high flow rates, a temporal mismatch of even one second can cause a gross underestimation of the true value. This means that all data must be sampled at intervals of 0.5 second or less.

The demonstration of the CBF versus time curve is a useful indicator of the sensitivity of the technique to measuring a distribution of flow rates within tissue. Chapter Six presents a novel analysis method for the derivation of a single mean CBF value from the data given in section 4.2.6.

4.2.7.5 *Theoretical Considerations*

The technique described here for the measurement of CBF using NIRS relies upon using a *small change in oxyhaemoglobin* as an inert intravascular tracer and assumes that (i) a significant proportion of the tracer is not consumed during the measurement period and (ii) the change induced in arterial oxygen concentration does not have a significant effect directly upon the parameters being measured. The validity of these assumptions requires consideration.

During a measurement of CBF any diffusion of the added oxygen from the capillary bed will cause the arterial measure of the total tracer input to be an overestimate of the quantity of tracer delivered, thus resulting in a underestimate of the calculated CBF. However it can be shown that for a small step change in SaO_2 within the physiological range (90% - 95%) the proportion of oxygen delivered to the cerebral circulation which is lost due to diffusion into the cerebral tissue during the measurement period is less than 3% (see Appendix A). The resulting error in CBF calculation is directly dependent upon the size of the step change in SaO_2 and at the levels quoted is acceptable.

The relationship between arterial oxygen content and cerebral blood flow has been thoroughly investigated over the last few decades. As discussed in Chapter One it has been demonstrated both in humans and animals that small changes in arterial blood oxygenation close to the normal range has little effect upon CBF or cerebral oxygen extraction [17, 27]. Specifically the effects of high normal values for PaO_2 are small so long as they remain below 14 kPa. The exact mechanisms of the cerebrovascular response to PaO_2 are still unclear as is the time taken for the response to occur. NIRS itself continuously monitors the changes in total cerebral haemoglobin concentration, $[Hb_{sum}]$, and as such gives a direct indication of the effect of changes in PaO_2 on CBV. It was seen during the CBF measurements that in most subjects the sudden increase in SaO_2 was associated with an immediate small decrease in $[Hb_{sum}]$. Over all ten subjects this decrease represented a mean fall in cerebral blood volume of 2% and as such is unlikely to have contributed a significant error to the calculation of CBF. It is possible that the changes seen in $[Hb_{sum}]$ during the step input of oxygen were in fact related to small changes in the subjects breathing pattern or changes in flow resistance and hence thoracic pressure. The relationship between breathing manoeuvres and changes in cerebral haemodynamics is dealt with in more detail in Chapter Five.

The CBF measurement depends upon the cerebral metabolic rate ($CMRO_2$) remaining constant during the small changes in SaO_2. It is reasonable to assume that in healthy resting adults $CMRO_2$ does not change over the short measurement period necessary for calculation of CBF.

The measurements described in this study were performed on healthy adult volunteers who could tolerate SaO_2 levels of around 90%. However, in clinical studies where subjects are likely to be more vulnerable to desaturation, changes in SaO_2 of as little as 3 - 4% have been successfully used to provide data from which to calculate CBF and CBV. Although using smaller changes in SaO_2 is obviously preferable, it does depend upon the performance of the pulse oximeter to accurately and reliably record these changes and highlights again the importance of having an instrument which meets the minimum requirements detailed in section 4.2.3.2.

4.3 Measurement of Cerebral Blood Volume

NIRS provides a continuous measurement of the *changes* in total haemoglobin concentration simply from the summation of $\Delta[HbO_2]$ and $\Delta[Hb]$ and this can be used to reflect the *changes* in CBV. The first description of the method used to *absolutely quantify* CBV using NIRS was given by Wyatt et al.[28] in 1990.

4.3.1 Theory

As with the CBF method, the measurement relies upon using oxyhaemoglobin as a NIR dye which can be measured in both the peripheral and cerebral circulation. A small slow change in the subject's SaO_2 is induced (usually 4-8% over 2-5 minutes). If CBF, CBV and oxygen consumption remain constant during the manoeuvre, then the consequent change in cerebral [HbO2] is equivalent to the product of ([tcHb]) and the change in fractional SaO_2:

$$\Delta\,[HbO_2] \;=\; [tcHb] \cdot \Delta SaO_2 \qquad \textbf{(4-7)}$$

If CBV is constant, the $[Hb_{diff}]$ term can be introduced into the equation such that:

$$[tcHb]\ (\mu molar) = \frac{\Delta[Hb_{diff}]}{2.\Delta SaO_2} \qquad \textbf{(4-8)}$$

To convert the data from units of μmolar to $ml.100g^{-1}$ the same constant K described for equation 4.4 is used, together with a value of 0.69 for the cerebral large to small vessel haematocrit ratio (CLVHR)[29]:

$$CBV\ (ml.100g^{-1}) = \frac{K \cdot [Hb_{diff}]}{2 \cdot [tHb] \cdot \Delta SaO_2 \cdot CLVHR} \qquad \textbf{(4-9)}$$

The CLVHR is used to take into account the relative lowering of haematocrit in the cerebral circulation. This is due to many factors including the migration of erythrocytes towards the centre of small blood vessels, reducing the number of red cells entering the capillaries, and differences in the viscosity of plasma and red cell flow in capillaries.

To obtain data from which to calculate CBV, FiO_2 is altered over a period of a few minutes to produce a gradual change in SaO_2 (measured by a pulse oximeter) and cerebral $[Hb_{diff}]$ (measured by the NIR spectrometer) with a period of equilibrium maintained at each level of SaO_2. The resulting $\Delta[Hb_{diff}]$ is plotted against ΔSaO_2 and the gradient of the regression line in equation 4.9 was used to calculate CBV.

This method of measuring cerebral blood volume has been applied predominantly in the neonatal field[11-13, 30-32]. A direct validation has not to date been performed, but values for CBV obtained in studies of human neonates are similar to the only other available data, which were obtained by PET[33].

4.3.2 Problems associated with NIRS CBV measurements in adults

Although neonatal values of CBV (2 $ml.100g^{-1}$)[28] differ from those of adults (5 $ml.100g^{-1}$)[34] this difference does not impose the same problems as seen in CBF measurements. CBV measurements are made over a much longer time period (minutes rather than seconds) and therefore do not require maximum sampling rates from the instrumentation. Dead space in the ventilation circuit does not present the same problem seen with the CBF measurements since slow changes in FiO_2 rather than a step change is required. However it is still important that the subject's lung function is adequate to provide slow changes in $[HbO_2]$ from the changes in FiO_2.

4.3.3 Pulse oximetry requirements for measurements of CBV

Again, since CBV measurements are made over a much longer time period, considerations of signal averaging and rapid response time of the pulse oximeter are not applicable. However since the oximetry and NIRS data must be correlated directly, temporal mismatch between the signals must be avoided, as discussed in section 4.2.2.3. The requirement for analogue outputs is also as stated in section 4.2.3.4.

4.3.4 Experimental Details

The instrumentation and procedures used for CBV measurements were very similar to those described in section 4.2.4 and measurements were made on the same set of subjects. Since minimal signal averaging was not required, the pulse oximeter was not operated in "beat to beat" mode. A controlled mixture of hypoxic gas was supplied by the circuit described in section 4.2.4.1 and in Figure 4.1. FiO_2 was gradually decreased from 21% to approximately 14% over 3 - 4 minutes prior to the step increase required for the measurement of CBF. This was repeated five times in each of the ten subjects.

4.3.5 Data Analysis

CBV was calculated from the initial gradual reduction of SaO_2. Ten seconds of data at the beginning and at the end of the FiO_2 decrease were averaged to produce mean values for SaO_2 and $[Hb_{diff}]$. The changes in $[Hb_{diff}]$ and SaO_2 were then incorporated into equation 4.9 and CBV was calculated in $ml.100g^{-1}$.

4.3.6 Results

From a total of 50 measurements only 28 proved suitable for calculation of CBV. Rejection criteria were as described for CBF measurements in section 4.2.6. The mean (±SD) CBV from all ten subjects was 2.85 ± 0.97 $ml.100g^{-1}$. The intra subject coefficient of variation for the CBV measurements ranged from 6% to 38% (mean 24%), while the inter subject coefficient of variation was 34%. The mean (±SD) change in $TcPCO_2$ during each measurement was 0.09 ± 0.08 kPa.

4.3.7 Interpretation of CBV results

The measurement of CBV using NIRS is intrinsically a less complex technique than that of CBF. Problems associated with transit time assumptions and instrument response time are not relevant, but the effects of extracerebral tissue, methods of data collection and other theoretical assumptions must still be considered.

4.3.7.1 *Vascular effects of extracerebral tissue*

Unfortunately studies documenting CBV measurements in bone (and in particular skull) are even more scarce than those on CBF, however it is reasonable to assume that like CBF, the values for skull CBV will be considerably less than those of brain tissue. The study to determine the contribution of scalp blood flow described in section 4.2.7.2 also included measurements of CBV pre and post scalp occlusion. As can be seen from Table 4.iii scalp flow had no significant effect on the measurement of CBV.

4.3.7.2 *Optical pathlength effects of extracerebral tissue*

The effects of extracerebral tissue acting as static "dead space" described in section 4.2.7.3 apply as much to CBV measurements as to CBF measurements. There have been many studies involving the measurement of CBV in normal adult humans[35, 36], notably in 1985 Sakai et al.[37] measured a mean CBV in a group of normal adults of 4.81 ± 0.37 ml.100g^{-1}. Overestimation of the differential pathlength used in the CBV calculation may well have caused the CBV values presented here to be lower than expected.

4.3.7.3 *Data Collection and Analysis*

As described in section 4.3.1, CBV is usually calculated by regressing a section of SaO_2 data against the equivalent section of $[Hb_{diff}]$ data during an increase or decrease in oxygenation. Due to the oscillations seen on the SaO_2 signal this was not possible and effectively a two point regression was performed using data from the top and bottom of the desaturation. Further studies are being devised to investigate the validity of using a two point volume calculation, compared to a full regression over several points. The relationship between the oscillations seen on the SaO_2 and in the cerebral circulation were also further investigated (Chapter Five).

Although in the adult there is considerable variation between measured $TcPCO_2$ and PaO_2[38], the transcutaneous blood gas monitor provided trend information to show that $TcPCO_2$ did not change appreciably during the course of the measurements. Arterial blood gas samples for analysis of absolute blood gases were not obtained. Some of the inter subject variation could therefore be attributed to different $PaCO_2$ levels in each subject.

4.3.7.4 *Theoretical Considerations*

The theoretical considerations detailed in section 4.2.7.5 apply equally to the measurement of CBV as to the measurement of CBF, since the same tracer (a *small* change in oxyhaemoglobin concentration) is used for both measurements. During measurements of CBV the system is allowed to reach an equilibrium state so that the effect of diffusion of tracer will merely be a time offset between the change in SaO_2 and $[Hb_{diff}]$.

4.4 REFERENCES

1. Chance B., Smith D.S., Nioka S., Miyoka H., Holton G., Maris M. (1989) Photon migration in muscle and brain. In "*Photon migration in tissues*", eds Chance B., Plenum Press, .
2. Ferrari M., De Marchis C., Giannini I., Sideri G., Fieschi C., Carpi A. (1986) Effects of carotid compression test on regional cerebral blood volume, haemoglobin oxygen saturation and cytochrome-c-oxidase redox level in cerebrovascular patients. *Adv. Exp. Med. & Biol.* 200;213-222
3. Fox E.J., Harme M.H., Mitnick M.H., Jöbsis F.F. (1982) Non invasive monitoring of cerebral oxygen sufficiency during general anesthesia. *Anesthesiology* 57;A160
4. Greely W.J., Bracey V.A., Ungerleider R.M., Greibel J.A., Kern F.H., Boyd J.L., Reves J.G., Piantadosi C.A. (1991) Recovery of cerebral metabolism and mitochondrial oxidation state is delayed after hypothermic circulatory arrest. *Circulation* 84;400-406
5. Hampson N.B., Camporesi E.M., Stolp B.W., Moon R.E., Shook J.E., Greibel J.A., Piantadosi C.A. (1990) Cerebral oxygen availability by NIR spectroscopy during transient hypoxia in humans. *J. Applied Physiol.* 69;907-913
6. Edwards A.D., Wyatt J.S., Richardson C., Delpy D.T., Cope M., Reynolds E.O.R. (1988) Cotside measurement of cerebral blood flow in ill newborn infants by near infrared spectroscopy. *Lancet* 2;770-771
7. Woodard H.Q. and White D.R. (1986) The composition of body tissues. *Br. J. Radiol.* 59;1209-1219
8. Skov L., Pryds O., Griesen G. (1991) Estimating cerebral blood flow in newborn infants : comparison of near infrared spectroscopy and ^{133} Xenon clearance. *Pediatr. Res.* 30;570-573
9. Edwards A.D., Richardson C.E., van der Zee P., Elwell C.E., Wyatt J.S., Cope M., Delpy D.T., Reynolds E.O.R. (1993) Measurement of haemoglobin flow and blood flow by near infrared spectroscopy. *J. Applied Physiol.* 75,;1884-1889
10. Pryds O., Griesen G., Skov L.L., Fris-Hansen B. (1990) Carbon dioxide related changes in cerebral blood volume and cerebral blood flow in mechanically ventilated preterm neonates. Comparison of near infrared spectroscopy and ^{133}Xenon clearance.

Pediatr. Res. 27;445-449

11. Edwards A.D., Wyatt J.S., Richardson C.E., Potter L.A., Cope M., Delpy D.T., Reynolds E.O.R. (1990) Effects of indomethacin on cerebral haemodynamics in very preterm infants. *Lancet* 335;1491-1495
12. Edwards A.D., McCormick D.C., Roth S.C., Elwell C.E., Peebles D.M., Cope M., Wyatt J.S., Delpy D.T., Reynolds E.O.R. (1992) Cerebral hemodynamic effects of treatment with modified natural surfactant investigated by near infrared spectroscopy. *Pediatr. Res.* 32;532-536
13. Bucher H.U., Wolf M., Keel M., von Siebenthal K., Due G. (1994) Effect of aminophylline on cerebral hemodynamics and oxidative metabolism in premature infants. *European Journal of Pediatrics* 153;123-128
14. Leenders K.L., Perani D., Lammertsma A.A., Heathers J.D., Buckingham P., Healy M.J.R., Gibbs J.M., Wise R.J.S., Hatazawa J., Herold S., Beaney R.P., Brooks D.J., Spinks T., Rhodes C., Frackowiak R.S.J., Jones T. (1990) Cerebral blood flow, blood volume and oxygen utilisation. Normal values and effect of age. *Brain* 113;27-47
15. Elwell C.E. (1991) Measurements in the diagnosis and treatment evaluation of obstructive sleep apnoea. *M.Phil, University of Exeter.*
16. Harris D.N.F., Cowans F.M., Wertheim D.A. (1994) NIRS in the temporal region - strong influence of external carotid artery. *Adv. Exp. Med. & Biol.* 345;825-828
17. Siesjo B.K. (1978) *Brain Energy and Metabolism.*, J. Wiley and Sons, New York.
18. Ginsberg M.D. (1986) Cerebral circulation and its regulation and pharmacology. In "*Diseases of the nervous system*", eds Asbury A.K., McKann G.M., McDonald W.I., W.B. Saunders, Philadelphia.
19. Hudetz A.G. (1992) Computer simulation of erthrocyte transit in cerebrocortical capillary network. *Adv. Exp. Med. & Biol.* 317;659-670
20. Carlsen O. and Hedegard O. (1987) Evaluation of regional cerebral circulation based on absolute mean transit times in radionuclide cerebral angiography. *Phys. Med. Biol.* 32,11;1457-1467
21. Jones S.C., Korfali E., Marshall S.A. (1991) Cerebral blood flow with the indicator fractionation of [^{14}C] Iodoantipyrine : Effect of PCO_2 on cerebral venous appearance time. *J. Cereb. Blood Flow & Metab.* 11;236-241
22. Brookes M. (1971) *The blood supply to bone.*, Butterworth, London.
23. Friberg L., Kastrup J., Hansen M., Bulow J. (1986) Cerebral effects of scalp cooling

and extra cerebral contribution to calculated blood flow values using the intravenous ^{133} Xe technique. *Scand. J. Clin. Lab. Invest.* 46;375-379

24. Villringer A., Planck J., Hock C., Scleinkofer L., Diragl U. (1993) Near infrared spectroscopy (NIRS) - a new tool to study hemodynamic changes during activation of brain function in human adults. *Neuroscience Letters* 154;101-104

25. Gopinath S.P., Robertson C.S., Grossman R.G., Chance B. (1993) Near infrared spectroscopic localization of intracranial hemotomas. *J. Neurosurg.* 79(1);43-47

26. Kurth C.D., Steven J.M., Benaron D., Chance B. (1993) Near infrared monitoring of the cerebral circulation. *J. Clin. Monitoring* 9(3);163-170

27. Kogure K., Scheinberg P., Reinmuth O., Fujishima M., Busto R. (1970) Mechanisms of cerebral vasodilation in hypoxia. *J. Applied Physiol.* 29;223-229

28. Wyatt J.S., Cope M., Delpy D.T., Richardson C.E., Edwards A.D., Wray S., Reynolds E.O.R. (1990) Quantitation of cerebral blood volume in human infants by near-infrared spectroscopy. *J. Applied Physiol.* 68;1086-1091

29. Lammertsma A.A., Brooks D.J., Beaney R.P., Turton D.R., Kensett M.J., Heather J.D., Marshall J., Jones T. (1984) In vivo measurement of regional cerebral haematocrit using positron emission tomography. *J. Cereb. Blood Flow & Metab.* 4;317-322

30. Livera L.N., Spencer S.A., Thorniley M., Wickramasinghe Y., Rolfe P. (1991) Effects of hypoxaemia and bradycardia on neonatal cerebral haemodynamics. *Arch. Dis. Child.* 66;376-380

31. Shah A., Pohl K., Elwell C.E., Matthew D.J., Edwards A.D., Kirkham F.J. (1992) Variation in cerebral blood volume during intracranial pressure spikes in children in coma. *British Paediatric Association* 64th Annual Meeting;Warwick

32. Owen-Reece H., Elwell C.E., Edwards A.D., Wyatt J.S., Reynolds E.O.R. (1992) Effect of mask ventilation on cerebral blood volume (CBV) in preterm infants studied by near infrared spectroscopy (NIRS). *Pediatr. Res.* 32(5);129

33. Altman D.I., Perlman J., Volpe J.J., Powers W.J. (1993) Cerebral oxygen metabolism in newborns. *Pediatrics* 92;99-104

34. Martin W.W.R., Powers W.J., Raichle M.E. (1987) Cerebral blood volume measured with inhaled $C^{15}O$ and positron emission tomography. *J. Cereb. Blood Flow & Metab.* 7(4);421-426

35. Grubb R.L., Raichle M.E., Higgins C.S., Eichling J.O. (1978) Measurement of regional cerebral blood volume by emission tomography. *Arch. Neurol.* 4;322-328

36. Kuhl D.E., Reivich M., Alavi A., Nyary I., Staum M. (1975) Local cerebral blood volume determined by three-dimensional reconstruction of radionuclide scan data. *Circ. Res.* 36;610-619

37. Sakai F., Nakazawa K., Tazaki Y., Katsumi I., Hino H., Igarashi H., Kanda T. (1985) Regional cerebral blood volume and haematocrit measured in normal human volunteers by single emission computed tomography. *J. Cereb. Blood Flow & Metab.* 5;207-213

38. Mindt W., Eberhard P., Schaefer R. (1983) Methodological factors affecting the relationship between transcutaneous and arterial PCO_2. In "*Continuous transcutaneous blood gas monitoring*", eds Huch R. and Huch A., Marcel Dekker Inc., New York.

CHAPTER 5

MEASUREMENTS OF OSCILLATIONS IN THE CEREBRAL CIRCULATION USING NIRS

5.1 INTRODUCTION

Due to the rapid sampling rate (2Hz) of current NIRS systems it has been possible to detect changes in cerebral haemodynamics which are not readily measurable by other techniques such as PET or ^{133}Xenon which have longer acquisition times. During the course of making the measurements of absolute CBF and CBV in adults using NIRS described in Chapter Four, oscillations were noted on both the oximetry and the NIRS signals. Studies were devised to investigate the nature of these oscillations in cerebral [Hb] and [HbO_2] and in particular their relationship to respiratory manoeuvres. This chapter will describe these studies and the measurement of another absolute cerebral haemodynamic parameter, mean cerebral oxygen saturation ($SmcO_2$).

5.2 MEASUREMENT OF MEAN CEREBRAL OXYGEN SATURATION ($SMCO_2$)

As demonstrated by equation 3.1, tissue saturation purely describes the proportion of haemoglobin in a given region which is oxygenated. Since NIRS can continuously measure changes in both the oxygenated and total haemoglobin concentration, calculation of cerebral oxygen saturation is in principle possible. If the total haemoglobin concentration of the brain ([Hb_{sum}]) changes by a small amount, with no concurrent alteration of blood flow or oxygen

consumption, the mean cerebral oxygen saturation of this changing cerebral volume can be calculated from the following equation:

$$SmcO_2\% = 100 \times \frac{\Delta[HbO_2]}{\Delta[HbO_2] + \Delta[Hb]} = 100 \times \frac{\Delta[HbO_2]}{\Delta[Hb_{sum}]} \qquad \textbf{(5-1)}$$

NIRS does not differentiate between light absorbed by blood in the arterial, venous and capillary compartments, so the measured $SmcO_2$ represents the saturation of a global region of tissue consisting of the average of all three compartments where a change in $[Hb_{sum}]$ occurs. In neonates changes in $[Hb_{sum}]$ have been induced by tilting the head slightly below the body, thus reducing venous return. In this case the measured saturation is likely to reflect mixed venous saturation[1]. The following sections will describe how, in adults, spontaneous changes in $[Hb_{sum}]$ related to respiration can be used to calculate $SmcO_2$.

5.2.1 Experimental Details

It was observed during the course of the experiments described in section 4.2 that as FiO_2 was reduced to produce mean SaO_2 values of approximately 90%, oscillations were evident on both the SaO_2 signal measured by the pulse oximeter and the $[HbO_2]$ and [Hb] signals measured by NIRS. At least two minutes of data in which the oscillations were evident was recorded for each of the ten subjects to enable the calculation of $SmcO_2$. To investigate whether the cycling was related to the respiratory frequency an additional set of experiments was performed on one subject (Subject A). The output from a pulse generator was fed into a loudspeaker to produce an audio signal with a controllable frequency. The subject was then requested to breathe in time with the audible pulse whilst the FiO_2 was held at a reduced level to produce a mean value for SaO_2 of 90% and maintained at that level for about 5 minutes. This allowed breathing to be controlled at a constant and known rate. The pulse generator frequency was altered and the procedure was repeated for breathing rates of 2, 3, 4, 6, 8 and 10 bpm.

5.2.2 Data Analysis

5.2.2.1 *Calculation of SmcO2*

The instantaneous $SmcO_2$ of the changing blood volume was calculated throughout five cycles for each of the ten subjects. To do this a section of $[HbO_2]$ data the length of one oscillation was regressed with the equivalent $[Hb_{sum}]$ data for that time period. $SmcO_2$ was then calculated from the gradient of this regression as indicated in equation 5.1. To investigate whether the calculated saturation varied throughout the oscillation, the procedure was then repeated using data blocks of the same length but shifted along by 0.5s for each regression. This built up a "rolling average" of $SmcO_2$ over several oscillations. $SmcO_2$ was plotted for each subject and the mean $SmcO_2$ for all ten subjects was also calculated.

5.2.2.2 *Oscillation of NIRS and SaO_2 signals*

To investigate the relation between respiratory frequency and the oscillations seen on both the oximetry and NIRS data at lower values of FiO_2 (Figure 4.2), a fast Fourier transform (FFT) was performed on the SaO_2 signal from the oximetry data of Subject A, and the dominant frequency was correlated with breathing rate (i.e. the frequency of the signal generator).

5.2.3 Results

5.2.3.1 *Measurement of $SmcO_2$*

For all ten subjects the mean calculated $SmcO_2$ was 59.4 ± 12.4 % at a mean SaO_2 of 91.8 ± 2.4 %. The instantaneously calculated $SmcO_2$ exhibited no significant periodicity when plotted over several respiratory cycles.

5.2.3.2 *Cycling of NIRS and SaO_2 data*

An example of the oscillating [HbO_2] and SaO_2 signals from the data recorded from Subject A is shown in Figure 5.1. Figure 5.2 shows a plot of the signal generator frequency (equivalent to breathing rate) against the dominant frequency of the FFT of the SaO_2 and [HbO_2] signals respectively. The line of identity is also plotted to illustrate the correlation. The regression of the SaO_2 cycling frequency (y) on the breathing rate (x) for all data points was $y = 0.99\ x + 0.001$; $r = 1.00$, and for the [HbO_2] cycling frequency (y_1) on the breathing rate (x) for all data points was $y_1 = 0.98x + 0.00$; $r = 0.99$. There was a mean time offset between the cerebral [HbO_2] and SaO_2 signals of 2.1 ± 0.9 seconds with cerebral [HbO_2] leading.

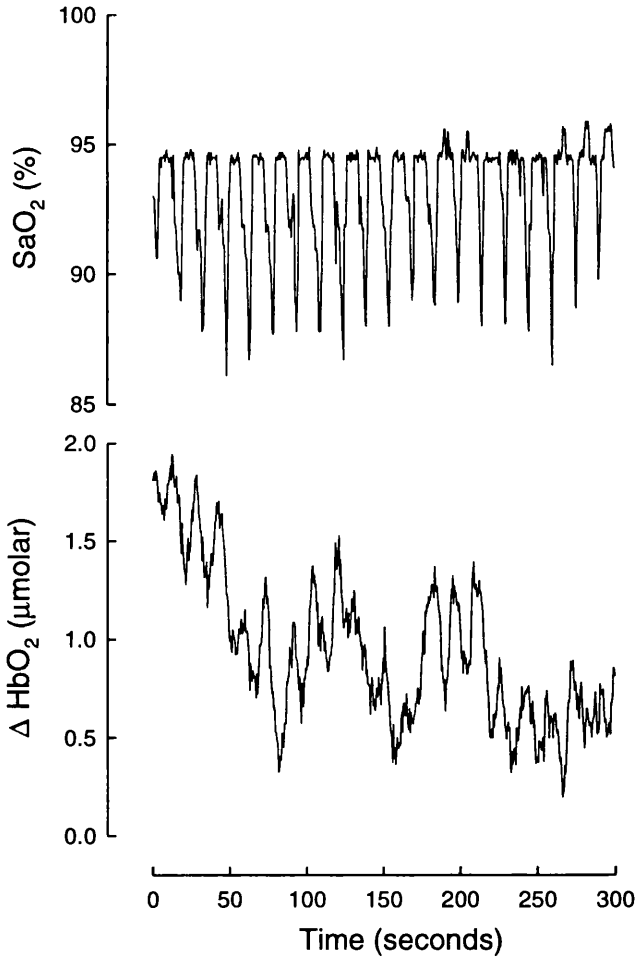

Figure 5.1 *Graph showing the SaO_2 (upper plot) and cerebral [HbO_2] (lower plot) data from Subject A breathing at a rate of 4bpm.*

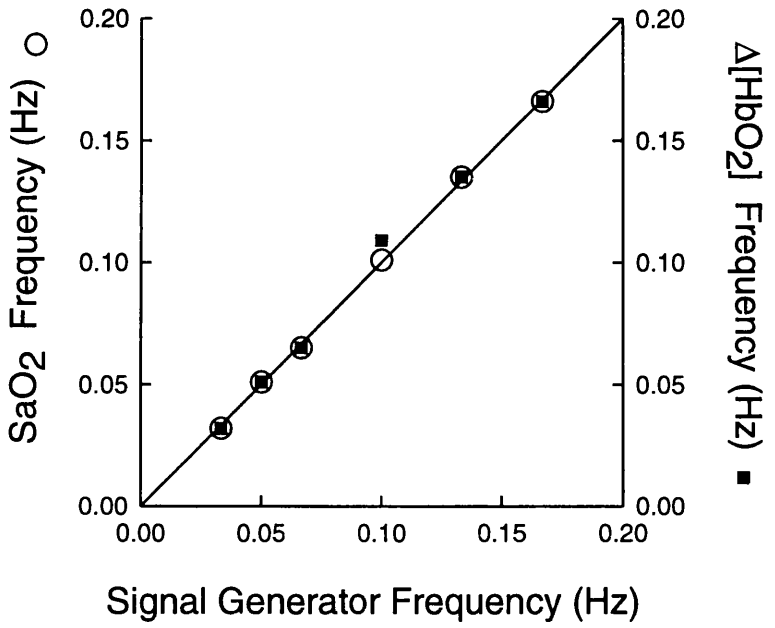

Figure 5.2 *Correlation between signal generator frequency (breathing rate) and dominant FFT frequency of the SaO_2 (hollow circles) and cerebral [HbO_2] (filled squares) with the line of identity.*

5.2.4 Interpretation of results

5.2.4.1 *Measurement of $SmcO_2$*

The [HbO_2] and [Hb] signals were calculated from the total absorption of light within a field of view incorporating arterial, capillary and venous compartments. Although the changes in [HbO_2] and [Hb] could be separated, the relative contribution of each of the three compartments to the calculated $SmcO_2$ could not be estimated. However the mean calculated $SmcO_2$ of all subjects agreed well with values for cerebral mixed venous saturation measured at the jugular bulb[2]. $SmcO_2$ was calculated at a lower than normal SaO_2 (91.8 ± 2.4 %) and as such will have underestimated the normoxic value. If it is assumed that, in equilibrium, when SaO_2 was increased the oxygen saturation of all compartments changed equally, then the $SmcO_2$ would have been 67.6 ± 13.8% at a normoxic SaO_2 of 98%.

The oscillations in [Hb_{sum}] and [Hb_{diff}] were very small (approximately 0.5 μmolar when subjects were breathing room air). Since cycling of heart rate and venous return was still occurring with respiration, this implies that neither of these factors significantly affects CBV or CBF under normal resting conditions in healthy subjects.

5.2.4.2 *Cycling of SaO_2 and NIRS data*

In the experiment performed on Subject A the frequency of the cycling of SaO_2 and [HbO_2] corresponded very closely with the respiratory rate. Considering the dissociation curve for normal healthy adults (Figure 5.3), an SaO_2 of 90% is equivalent to the elbow of the curve where a small change in PaO_2 produces a large change in SaO_2. With each breath alveolar PO_2 transiently increases and decreases with inspiration and expiration respectively[3]. These small changes in alveolar PO_2 are enough to produce fluctuations in PaO_2 levels which in turn are recorded as more significant swings in SaO_2. As soon as FiO_2 is increased to normal levels the PaO_2 values are equivalent to those found on the upper flat region of the dissociation curve. SaO_2 then becomes far less sensitive to small changes in PaO_2, and the small respiratory fluctuations in alveolar PO_2 have no recordable effect[4]. Because the SaO_2 cycling observed here was related directly to breathing rate (approximately 0.25Hz) even the basic

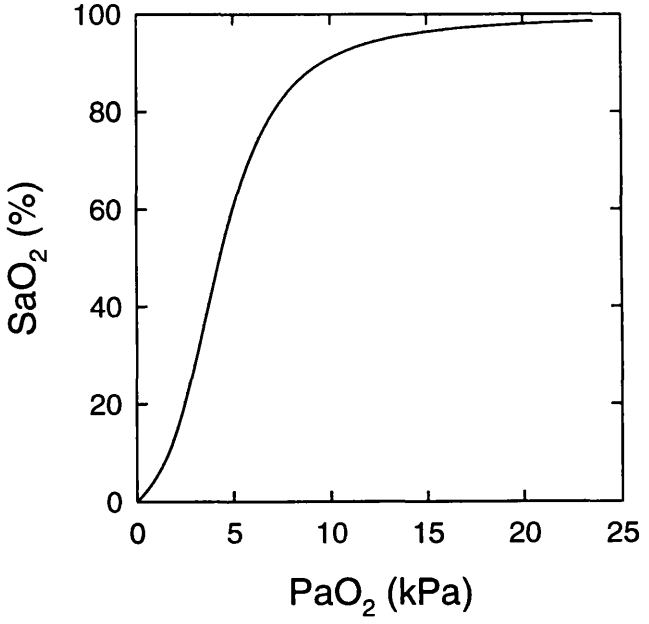

Figure 5.3 *The oxygen dissociation curve for haemoglobin.*

signal averaging incorporated in most pulse oximeters (typically 3 - 8 seconds) would smooth out the signal making this 'respiratory cycling' barely noticeable during routine clinical monitoring at hypoxic levels.

Assuming that the time delay between the [HbO_2] and SaO_2 signals represents transit times from the common carotid artery to the cerebral microcirculation in healthy adults it could perhaps be used as an indicator of cerebral circulatory efficiency or vessel patency.

There are at least three well defined physiological effects contributing to the cycling seen on both the [Hb] and [HbO_2] traces: (a) changes in [HbO_2] at SaO_2 <90% due to alveolar PO_2 swings with respiration discussed above, (b) changes in venous [HbO_2] and [Hb] due to respiratory swings in venous back pressure from the heart[5], (c) changes in arterial [Hb] and [HbO_2] due to cardiac output changes which may occur with respiration[6]. Since NIRS provides a global measure of tissue oxygenation, separation of these effects is not possible.

5.3 MEASUREMENT OF CHANGES IN [HbO_2] AND [Hb] DURING INSPIRATION AND EXPIRATION

Following the results of the previous studies it was decided that the changes in cerebral haemodynamics during respiration should be investigated more fully. A study was therefore devised to determine the haemodynamic effects of respiratory and cardiac manoeuvres over the period of a single breath. Pulsus paradoxus is the term used to describe the changes in mean arterial blood pressure (MAP) and cardiac output (CO) seen during inspiration and expiration[5]. The effects are known to be accentuated in patients with increased airways obstruction e.g. patients with asthma or those undergoing positive expiratory pressure ventilation. NIRS can then be used to investigate whether these cardiovascular changes known to occur with ventilation against an increased expiratory pressure (IEP), are reflected in the cerebral circulation.

5.3.1 Physiological Theory

Both heart rate (HR) and stroke volume are subject to changes on inspiration and expiration which are mediated by both neural and mechanical mechanisms. Resulting variations in cardiac output are synchronous with the respiratory rate of the subject. During inspiration the diaphragm moves downwards and intrathoracic pressure falls. This pressure

drop is transmitted via the thin walls of the low-pressure right heart to the whole right sided circulation, whereas the thick walled left ventricle, as a high pressure system remains largely immune to the change. Venous return to the right side of the heart increases, so the amount of blood pumped onwards into the pulmonary circulation increases. Therefore while the pressure in the left ventricle changes very little, the pressure in the pulmonary circulation becomes more negative and blood pools in the lungs. Blood flow from the lungs into the left heart falls and this effect is magnified by pulmonary vasodilation. As stroke volume falls, heart rate does not rise fast enough to compensate and cardiac output falls for the duration of the inspiration.

On expiration, the rise in intrathoracic pressure is again transmitted to the right sided circulation. This effect is enhanced when an expiratory resistance is applied. The blood in the pulmonary circulation is squeezed out of the lungs into the left heart and the stroke volume increases. The heart rate does not entirely compensate and so cardiac output rises. Thus, during expiration, an increase in MAP and HR is expected which is reversed on inspiration.

5.3.2 Experimental Details

The subjects for this study comprised six healthy adult males (age range 25-44, median 27) with no known respiratory or cardiovascular disorders. The NIRO 500 spectrometer described in Chapter Three was used to measure changes in [Hb] and [HbO_2] every 0.5 second and the optodes were set up as described in section 4.2.4.

The cuff of a non invasive continuous blood pressure monitor (Finapress 2300, Ohmeda, USA) was placed on the second finger of the left hand which was kept stationary at the level of the heart. The monitor, working in beat to beat mode, recorded both MAP and HR. $TcPCO_2$ was monitored as previously described and recorded with the MAP and HR data via the spectrometer.

The breathing circuit, shown in Figure 5.4, comprised a mouthpiece and T piece with a one way valve on the expiratory side. The inspiratory arm was left open to room air and atmospheric pressure. The IEP was introduced into the circuit by placing the expiratory line under water in a measuring cylinder at a depth which was varied between 5 and 20 cmH_2O in 5cm increments.

All subjects wore a nose clip and lay supine on a couch. They breathed room air initially against atmospheric pressure to familiarise themselves with the equipment and to

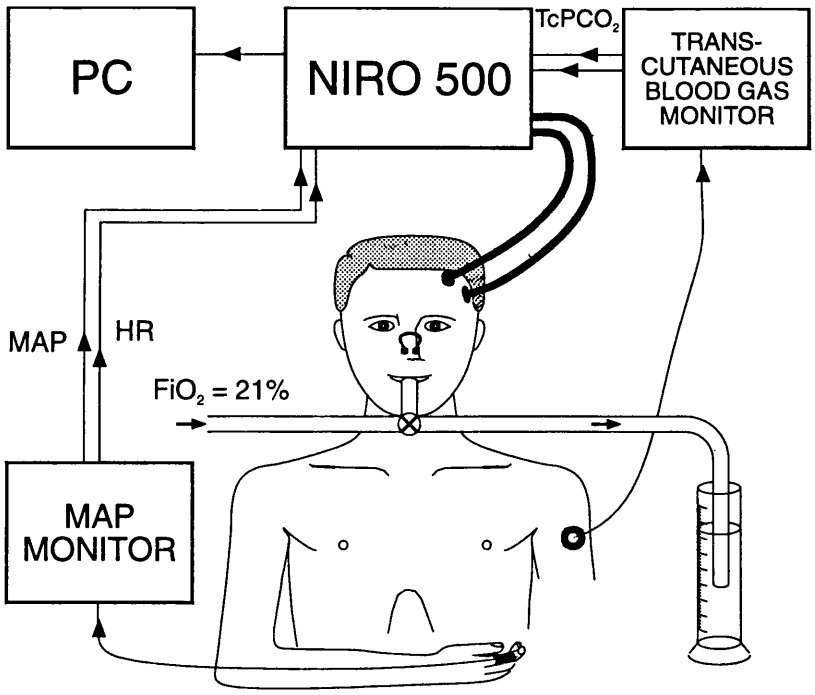

Figure 5.4 *Experimental set up for investigation of cerebral haemodynamic effects of increased IEP.*

provide baseline data. Once the subject was comfortable the expiratory arm was placed in the water and the subjects breathed against IEP of 5, 10, 15 and 20 cmH_2O, for approximately 2 minutes at each level. Respiratory rate was not experimentally controlled.

5.3.3 Data Analysis

Data were smoothed in software by applying a rolling average over three points. After inspection and rejection of obvious artefact (usually due to movement) three representative sections of data during the expiratory period were selected from each level of IEP in all six subjects. Where possible three consecutive periods were chosen. The positions of maxima and minima [HbO_2] were defined and the magnitude and direction of the changes in [Hb], [HbO_2], [Hb_{sum}] and [Hb_{diff}] between those points were calculated. A time offset of between 0.5 and 1.5 second was present between the MAP and NIRS data. This was accounted for in the calculation by defining the maxima and minima of the MAP trace independently from that of the NIRS data.

The magnitude and direction of the changes in MAP and HR were then calculated (measured peak to peak) and in addition, the baseline MAP was calculated by taking the

average MAP for the same period. $\Delta[HbO_2]$, $\Delta[Hb]$, $\Delta[Hb_{sum}]$, $\Delta[Hb_{diff}]$, ΔMAP, ΔHR and baseline MAP were averaged for each level of IEP for all six subjects. The level of IEP was then correlated with both $\Delta[Hb_{sum}]$ and ΔMAP.

5.3.4 Results

Figure 5.5 shows the NIRS, MAP and HR data collected from one subject breathing against an IEP of 20 cmH_2O. The section of data between the two vertical lines is expanded in Figure 5.6 to highlight the changes seen during one breath. All traces commence at the start of an expiration.

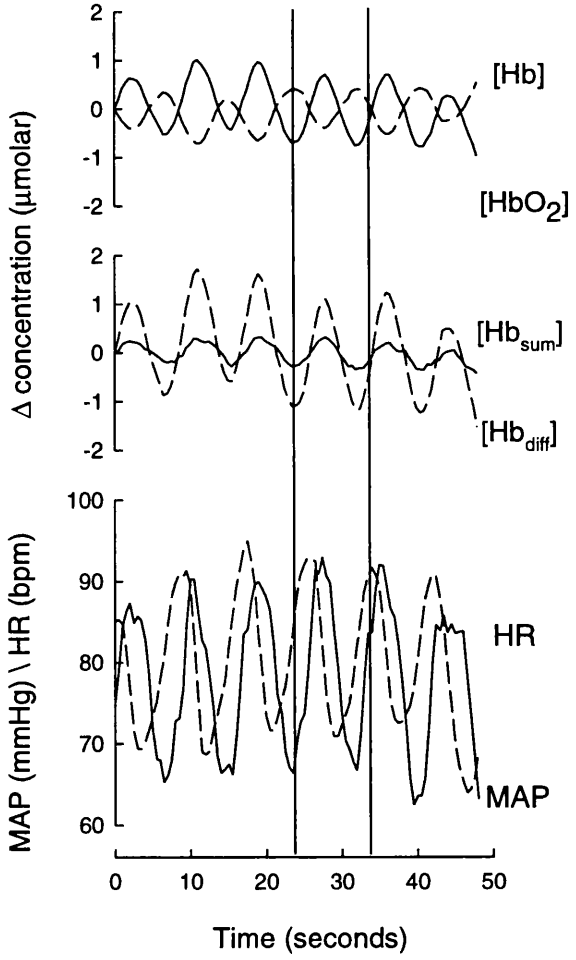

Figure 5.5 *NIRS, MAP and HR data collected from one subject breathing against an IEP of 20 cmH_2O. The trace starts at the beginning of an expiration.*

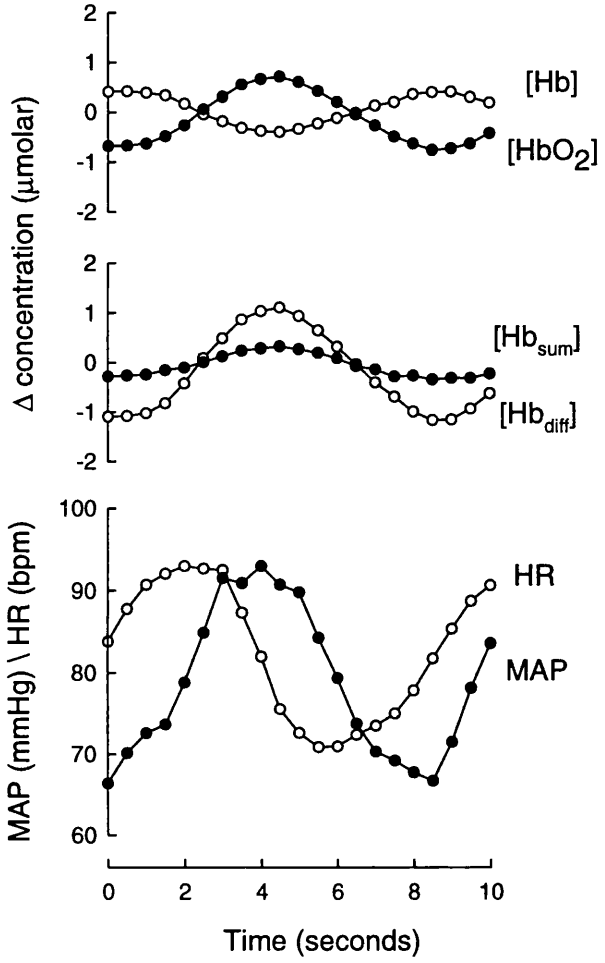

Figure 5.6 *NIRS, MAP and HR data collected from one subject breathing against an IEP of 20 cmH_2O during one breath. The trace starts at the beginning of expiration.*

Table 5.i shows the magnitude and direction of the changes recorded during expiration in the NIRS, MAP and HR data. Assuming a cerebral haemoglobin volume (CHV) of 84μmolar[7] the changes in [Hb_{sum}] can be expressed as a percentage change in total cerebral haemoglobin volume. Likewise ΔMAP can be expressed as a percentage of the baseline MAP for the equivalent period. These percentage changes are shown in Table 5.ii.

The regression of Δ[Hb_{sum}] (y) on the IEP level (x) for all points was $y = 19.6x - 4.1$; r = 0.96, and for ΔMAP (y_1) against IEP was $y_1 = 1.3x - 8.9$; r = 0.96.

Table 5.i : *The mean changes in the NIRS, MAP and HR data recorded during expiration at each level of IEP on all subjects (mean ± S.D.).*

IEP cmH_2O	$\Delta[HbO_2]$ µmolar	$\Delta[Hb]$ µmolar	$\Delta[Hb_{sum}]$ µmolar	$\Delta[Hb_{diff}]$ µmolar	ΔMAP mmHg	ΔHR bpm
0	0.4 ± 0.1	0.0 ± 0.2	0.4 ± 0.2	0.6 ± 0.1	5.8 ± 2.9	3.3 ± 3.1
5	0.7 ± 0.4	-0.4 ± 0.3	0.4 ± 0.2	1.1 ± 0.7	13.7 ± 1.9	9.0 ± 5.3
10	1.0 ± 0.5	-0.5 ± 0.2	0.6 ± 0.4	1.5 ± 0.8	14.1 ± 2.8	12.8 ± 7.2
15	2.0 ± 1.3	-1.0 ± 0.8	1.0 ± 0.7	2.8 ± 2.0	18.9 ± 3.4	15.1 ± 6.3
20	2.3 ± 1.3	-1.1 ± 0.7	1.2 ± 0.7	3.5 ± 2.0	21.1 ± 4.9	17.1 ± 7.7

Table 5.ii : *Percentage changes in CHV and MAP for each level of IEP (mean ± S.D.)*

IEP (cmH_2O)	ΔCHV (%)	ΔMAP (%)
0	0.5 ± 0.3	6.2 ± 0.3
5	0.4 ± 0.2	14.5 ± 3.6
10	0.7 ± 0.5	15.7 ± 4.3
15	1.2 ± 0.8	19.3 ± 4.3
20	1.5 ± 0.9	21.9 ± 6.7

5.3.5 Interpretation of Results

As shown above the changes in cerebral haemodynamics measured by NIRS were, on expiration, an increase in [HbO_2] accompanied by a smaller decrease in [Hb]. These changes were reversed on inspiration. The magnitude of these changes showed a strong correlation with the level of IEP.

Although the changes in [Hb] and [HbO_2] can be separated, the relative contribution of the three compartments to the total signal cannot be measured. It is however possible to make some deductions concerning firstly the changes in CBV and CBF that occur during ventilation, and secondly which compartments contribute to the [Hb_{sum}] signal.

Cardiovascular changes associated with expiration must first be considered. In the venous circulation there is an increase in central venous pressure and hence intracranial pressure, whilst the arterial changes described by pulsus paradoxus include an increase in MAP and CO. It would be expected that these pressure changes would increase CBV by (i) distending the arterial part of the cerebral circulation and (ii) impeding venous return and promoting venous distension. However, if the observed increase in [Hb_{sum}] was solely due to distention of the vessels then [HbO_2] and [Hb] would change in parallel. They do not, and if oxygen extraction is constant for this brief period, this can only be interpreted as an alteration in CBF.

The decrease in [Hb] can be explained as an increase in CBF, which, as well as increasing the delivery of arterial [HbO_2], effectively washes deoxygenated blood out of the venous compartment (approximately 30% of which is Hb). Although [HbO_2] and [Hb] can be expected to rise due to the increase in mean arterial and central venous pressure, the "pulse" of increased MAP appears to be associated with a significant increase in CBF which overrides the volume effect, producing a net decrease in [Hb]. This explanation is supported by the correlation of the level of IEP with both [Hb_{sum}] and MAP changes.

Depending upon the breathing rate of the subject, the mean time taken for the MAP to go from a minimum to a maximum was four seconds. There are few data documenting the time response of global (i.e. non microcirculatory) homeostatic control mechanisms in the cerebral circulation over such short time periods. Other quantitative non invasive methods of measuring changes in cerebral haemodynamics cannot achieve the temporal resolution necessary to detect the effects of transient changes in MAP and the cardiovascular system. Laser doppler flowmetry is one technique which can continuously monitor changes in CBF,

although absolute quantification of these changes is not yet possible. In 1992, Florence et al.[8] described a study measuring the time course of CBF during rapid hypovolaemic hypotension. In the figures of this paper oscillations in CBF and MAP during baseline conditions can be seen which appear to be compatible with the respiratory linked changes we have observed, although they are not commented upon in the text.

The changes in $[Hb_{sum}]$ observed are very small, on average 1% of the total blood volume despite the increase in MAP with each level of IEP. These small changes are clearly reproducible and as such indicate the sensitivity of the NIRS technique for monitoring subtle changes in cerebral haemodynamics. It is interesting to note that since the adult skull is effectively a sealed box, the increase in blood volume observed can only be achieved by displacement of an equal volume of cerebrospinal fluid (assuming the tissues to be incompressible). Although there may be many errors in both the latter assumption and in the conversion of $\Delta[Hb_{sum}]$ to change in CBV, this NIRS method may allow this parameter to be monitored.

This study demonstrates particularly the use of the high temporal resolution which can be achieved using NIRS. The near continuous monitoring of cerebral haemodynamics described above shows reproducible, consistent, respiratory linked oscillations, which although small can still be recorded non invasively and repeatedly with this technique.

5.4 REFERENCES

1. Skov L., Pryds O., Greisen G., Lou H. (1993) Estimation of cerebral venous saturation in newborn infants by near infrared spectroscopy. *Pediatr. Res.* 33(1);52-55
2. Gibbs E.L., Lennox W.G., Nims L.F., Gibbs F.A. (1942) Arterial and cerebral venous blood. Arterial differences in man. *J. Biol. Chem.* 144;325-332
3. Beneken-Kolmer H.H. and Kreuzer F. (1969) Recording and interpolation of oxygen pressure in respiratory air of man by the PO_2. In "*Progress in Respiratory Research*", eds Herzog H., Karger, Basel.
4. Sykes M.K., Vickers M.D., Hull C.J. (1991) *Principles of measurement and monitoring in anaesthesia and intensive care.*, Blackwell Scientific Publications, Oxford.
5. Weatherall D.J., Ledingham J.G.G., Warrel D.A. (1987) *Oxford Textbook of Medicine.*,

Oxford University Press, Oxford.

6. McGregor M. (1979) Current concepts : pulsus paradoxus. *New Engl. J. Med.* 301;480-482

7. Sakai F., Nakazawa K., Tazaki Y., Katsumi I., Hino H., Igarashi H., Kanda T. (1985) Regional cerebral blood volume and haematocrit measured in normal human volunteers by single emission computed tomography. *J. Cereb. Blood Flow & Metab.* 5;207-213

8. Florence G. and Seylaz J. (1992) Rapid autoregulation of cerebral blood flow: a laser-doppler flowmetry study. *J. Cereb. Blood Flow & Metab.* 12;674-680

CHAPTER 6

FURTHER DEVELOPMENT OF CBF ANALYSIS

6.1 INTRODUCTION

A major portion of this thesis has been concerned with the measurement of CBF in adults using NIRS. The data presented in Chapter Four demonstrates that these measurements are indeed possible, but that consideration must be given to the data analysis routines employed. If NIRS is to be fully exploited as a practical, accurate and reliable method for assessing CBF in adults it is important that any data analysis method should satisfy at least the following criteria. The method should;

(i) provide accurate and reproducible measurement of a single (mean) CBF value which can be directly related to some physiological criteria,

(ii) take into account different noise levels on the data,

(iii) be incorporated into software which can be used in real time at the bedside and not rely upon subjective opinions of the user.

In practice, these criteria are compromised to some degree in most analytical techniques. The following chapter describes the first steps towards the development of such a technique for analysing NIRS CBF data. The following sections will describe the analytical problem presented by the data described in Chapter Four and the current regression models which are used to deal with such data. The modifications to one of these models and the practical implementation of the analysis method are then described. The method has then been tested using sets of simulated data and finally used to reanalyse the data collected from the ten adult volunteers presented in Chapter Four.

6.2 THE ANALYTICAL PROBLEM

Three important points can be raised regarding the CBF data previously presented:

(i) Using the polynomial fitting routine and subsequent differentiation over 3,4,5 or 6 seconds the presence of two flow compartments was clearly demonstrated. These compartments are assumed to represent a high and low flow distribution within the cerebral circulation,

(ii) In a group of ten normal volunteers, measured at rest, the inter subject variation, using the above analysis method ranged from 30 - 34%,

(iii) The intra subject variation, based on up to five measurements in each subject, had a mean value of 20%.

For a technique to be useful as a clinical tool, a single descriptive value is almost always needed. This is demonstrated in the field of pulse oximetry where the information about blood oxygenation is condensed into a simple percentage value, to which upper and lower limits can be assigned. The same is true, although to a lesser degree, in the field of CBF measurements. Increasing interest in assessing the effects of visual, auditory and other sensory stimuli on the cerebral circulation is highlighting the demand for simple descriptive parameters for sometimes complex physiological measurements.

An important question therefore is, if a single CBF value is to be measured from the data set as shown in Figure 4.5, how is this value to be calculated, i.e. which "measurement period" should be used? If we return to the physical principles on which the measurement technique is based (described in section 4.2.1), the single most important assumption is that in a specified measurement period, the tracer (in this case a small change in $[HbO_2]$) is present only in the arterial part of the circulation and the effect of venous outflow (P_v) can therefore be ignored. The conclusions drawn about the distribution of flow rates suggest that the choice of the exact measurement period is crucial in determining a single mean CBF value.

It would appear therefore that in order to answer the above question it is necessary to interrogate more closely the response function, i.e. the rate of change of $[Hb_{diff}]$ ($[\Delta Hb_{diff}]$) versus the cumulative integral of the fractional change in SaO_2 ($\int \Delta SaO_2$). Figure 6.1 shows the theoretical response in (a) a single and (b) a dual flow compartment to a step change in tracer input. (Note that this model assumes a single arrival time for the bolus). The assumptions in the modified Fick principle used for the measurement of CBF using NIRS, are only valid when none of the tracer is leaving the field of view, i.e. in Figure 6.1(b) within the

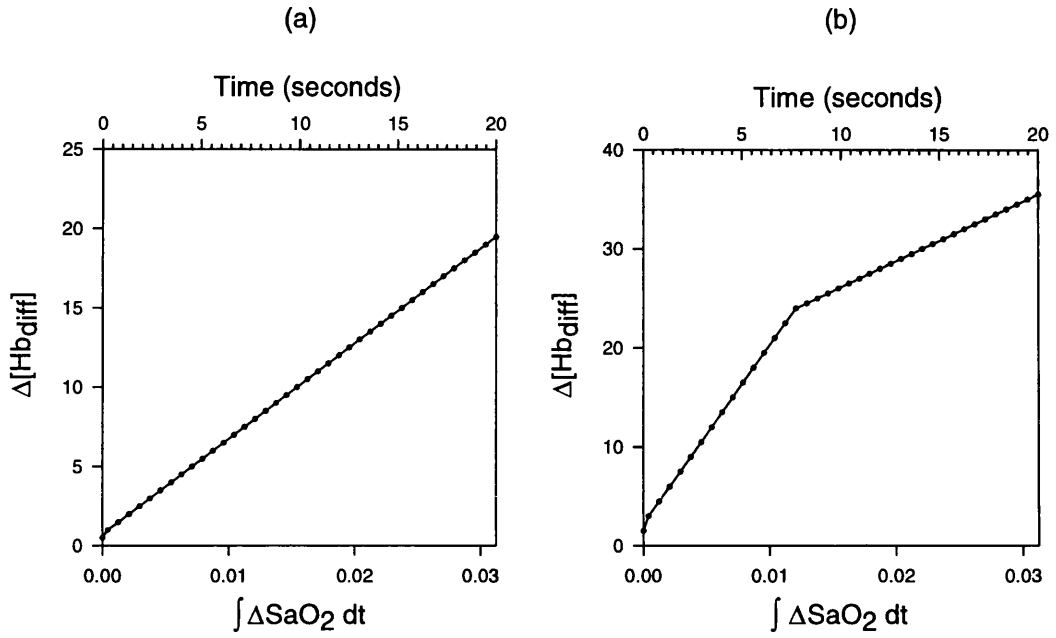

Figure 6.1 *The theorectical response of (a) a single and (b) a dual flow compartment. The data uses a simulated step in SaO_2 from 90 - 100%, with each point representing a 0.5s sample.*

first 8 seconds. Beyond this point the response is no longer linear and venous outflow begins. The identification of this exact point in the response function is therefore crucial in defining a set measurement period for the data described in Figure 4.5. The solution to the above analytical problem is therefore based around the measurement of the linear portion of the $[Hb_{diff}]$ response curve which is dependent upon the first (and fastest) vascular transit time (t_1). The point at which the response becomes non linear will be referred to in later sections as the first transit break point (τ_{bp}). It is the measurement of τ_{bp} which forms the basis of the described analysis.

6.3 Multiple Linear Regression Models

The following section describes the statistics involved in developing a multiple linear regression model. Given the number and diversity of the different schools of statistics, the terms and descriptions given here are those solely used by SPSS for Windows version 6.0 (SPSS Inc. Chicago, Ill.). Multiple linear regression models incorporate multiple independent

variables for the description of a single dependent variable. They are usually expressed in the form:

$$Y = B_0 + B_1X_1 + B_2X_2 + B_3X_3 + B_4X_4 + B_5X_5 + \ldots + B_iX_i \qquad \textbf{(6-1)}$$

where Y is the dependent variable and X_i is the value of the ith independent variable. The constant terms (B_i) are unknown parameters whose value scale the importance of each of the independent variables. When all independent variables are included in a multiple regression equation the statistics obtained are parallel to those obtained in regression with a single independent variable. These include adjusted R^2 which is the square of the multiple correlation coefficient. The following parameters are particularly important in describing the statistics of a multiple regression model;

6.3.1 Partial Regression Coefficients

The coefficients (B_i) are called partial regression coefficients since the value of each coefficient is influenced by each of the other independent variables in the equation. The values of a regression coefficient when it is the sole independent variable in the equation may differ significantly from its value when there are four other independent variables present in the equation.

6.3.2 Beta Coefficients

It is however erroneous to infer the importance of a particular variable simply from the value of its partial regression coefficient. Since the independent variables may originate from any source (e.g. height, weight, or age dependencies) the magnitude of the partial regression coefficients will depend directly upon the units in which the variables are measured (m, kg, or years respectively). Only if the independent variables are measured in exactly the same units does the magnitude of the partial regression coefficient indicate the relative importance of a particular variable.

Beta weights are therefore used to standardise these coefficients to allow a more direct comparison between them. The relationship between beta weights and partial regression coefficients is given as:

$$\beta_k = B_k \left(\frac{SD_k}{SD_Y}\right) \qquad \textbf{(6-2)}$$

where β_k, B_k and SD_k are the beta weight, partial regression coefficient and standard deviation for the kth independent variable respectively and SD_y is the standard deviation of the dependent variable.

6.3.3 Part and partial correlation coefficient

One of the best methods of assessing the relative importance or influence of a variable is to consider the increase in R^2 (ΔR^2) when a variable is entered into an equation that already contains the other independent variables. A large ΔR^2 demonstrates that the addition of a variable provides unique information about the total fit which is not available from the other independent variables which are already present. The signed square root of the increase in R^2 is called the part correlation coefficient. It should be remembered however that the increase in R^2 does not indicate what proportion of the unexplained variation this increase constitutes. The partial correlation coefficient is used to measure the proportional reduction in variation.

6.3.4 F-test

The most typical application of a multiple linear regression model is to determine the best fit to a set of data which may be described using a number of independent variables. In this instance some formula must be followed to dictate which of the independent variables contributes useful information to the fit. The most common procedure is to add the independent variables and assess their effect on the overall "goodness of fit" or R^2. It is true that R^2 always increases with the addition of added variables, however this does not mean that the equation with more variables provides a better fit to the data.

When adding a variable the most sensible approach is to assume the null hypothesis that the true population value for the change in R^2 is zero. This is referred to as the partial F-test where:

$$\Delta F = \frac{\Delta R^2 \ (N-p-1)}{q \ (1-R^2)} \qquad \textbf{(6-3)}$$

and N is the number of cases in the equation, p is the total number of independent variables and q is the number of independent variables entered at this step. The significance of ΔF can be obtained by considering the distribution of F with q and N-p-1 degrees of freedom. This F-test can also be thought of as a test of the hypothesis that when only the *i*th variable is added in a step, B_i is zero.

Various methods have been constructed to use the above statistics to provide a systematic approach to determining the best fitting routine. The most common of these methods are forward and backward elimination and stepwise regression.

6.3.5 Forward Elimination

In forward elimination the variable with the largest correlation with the dependent variable is first entered into the equation. The F-test for the hypothesis that the coefficient for the entered variable is zero is then performed. The F value calculated from this test is then compared with pre established criteria and is used to decide whether the variable should be included in the equation. In SPSS there are two ways of defining this criteria. The first is a straight forward minimum value of the F statistic that a variable must achieve in order to enter the equation. This is called the **F-to-enter (FIN)** value and is assigned a default value of 3.84. The second criterion is the significance associated with the F value. As described in section 6.3.4, the significance is itself dependent upon the number of degrees of freedom. A fixed F value may have different significance levels depending upon the number of variables already in the equation. The second criterion is called the **probability of F-to-enter (PIN)** and has a default value of 0.05. This means that a variable will only be entered into an equation if the significance of the F value is less than or equal to 0.05 (or another user specified value). In practice it is usually the PIN criteria which is used to determine whether a variable should remain in the equation. Once tested, if the first variable is included the forward selection continues and the statistics for the variables not in the equation are used to determine which variable will be selected next. The variable with the largest partial correlation (equivalent to the variable with the largest F value) is then selected and tested for inclusion into the equation. This process is repeated until there are no other variables that meet the entry criteria for the equation. If this occurs at the first variable the procedure is terminated with no variables in the equation.

6.3.6 Backward Elimination

This procedure is the reverse of forward elimination. Backward elimination starts with all the variables in the equation and then applies removal criteria to assess whether they should be removed from the equation. As with forward elimination there are two criteria. The first is the minimum F value a variable must have in order to remain in the equation (**F-to-remove, FOUT**). Variables with an F value less than FOUT are eligible for removal. The second criteria again depends upon the statistics of the F value in the form of the maximum **probability of F-to-remove (POUT)**. POUT is the favoured method and is usually assigned a value of 0.10.

A backward elimination model therefore begins with the selection of the variable with smallest partial correlation coefficient. If the POUT of this variable is greater than the default value the variable is removed from the equation. The equation is recalculated without this variable and the procedure is repeated until none of the variables satisfy the criteria for removal.

6.3.7 Stepwise Regression

As its name suggests stepwise regression is a combination of both backward and forward elimination. The first variable for inclusion in the equation is selected according to the criteria for forward elimination and is then tested according to the PIN significance. If it passes this test and remains, the second variable is selected under the same criteria. At this stage the first variable is re-examined to see whether it should be removed from the equation according to the removal criteria of backward elimination (POUT). This process continues and after each step variables already in the equation are examined for removal. To prevent the same variable being entered and removed repeatedly, PIN must be set at a value less than POUT (or FIN > FOUT). When no further variables can be either entered or removed from the equation the procedure terminates.

6.4 THE ANALYTICAL MODEL

As previously described, multiple linear regression models are most commonly used to determine the best fit to a data set from a collection of independent variables. In the case of stepwise regression a complete data set (set of cases) is presented for examination and through selection of different independent variables the equation which best describes that data (based on the pre established criteria) is determined. For example, data may have been collected to determine the relationship between the weight of a group of 100 subjects and their height, age and sex respectively. The stepwise model will test all 100 data points and provide an equation of the form given in equation 6.1 describing the best fit using those three given independent variables.

However the CBF problem presented in section 6.2 is slightly different. In this case the analysis must be used to determine the influence of adding successive data points (or cases) on the independent variables required to best describe the response function. The aim of this analysis is to detect the point (τ_{bp}) beyond which the fitting function is no longer a straight line.

Let us take the example given in Figure 6.1(a). For a single linear response y, the dependent variable is $\Delta[Hb_{diff}]$ and x, the independent variable is $\int\Delta SaO_2$. Since the response is linear, the function is described completely by the sole independent variable. Let us now consider the situation in Figure 6.1(b) where only the first portion of the response is linear, beyond this point it is clear that a polynomial fit would more closely fit the response function. $\Delta[Hb_{diff}]$ (y) remains the dependent variable but now several independent variables must be considered, namely x, x^2, x^3, x^4 x^5 etc. The number of independent variables which should be considered will obviously depend upon the function to be described and the total number of cases included in the analysis. Now imagine that stepwise regression is performed on the complete data set (m cases). An equation which best describes the function will be produced which will incorporate all or some of the polynomial terms. However if we now repeat the stepwise analysis but restrict it to the first n cases (where $n < \tau_{bp}$), only the x term will be used to describe this linear portion of the function. If the number of included cases is incremented by one before each stepwise regression analysis, it is possible to determine the exact data point at which a term, other than the linear x term, is selected for the equation which best describes the function. In this way stepwise regression analysis performed on an increasing number of data points can be used to identify the initial linear portion of the

response function and therefore τ_{bp}. It is this model which was thought most accurate for the measurement of the fast/first vascular transit time on the adult CBF data.

6.5 IMPLEMENTATION OF THE STEPWISE REGRESSION ANALYSIS

The practicalities of performing this type of analysis on a large data set must first be considered. It was decided that the software package SPSS for Windows provided the best tool for implementing the stepwise regression analysis. There were then three distinct stages to the implementation of the analytical model described in section 6.4 on the adult CBF data presented in section 4.2.6 and the sets of simulated data.

(i) Formatting data for importing into SPSS, i.e. assembling data sets incorporating y, x, x^2, etc.

(ii) Performing stepwise regression in SPSS on the above data set whilst incrementing the number of cases included in the analysis.

(iii) Extracting useful summary information from the SPSS "results" sheet in order to determine τ_{bp}.

The first and second stages required some labour intensive manipulation of the data in spreadsheets. Using previous analyses described in section 4.2.5 the appropriate sections of $\Delta[Hb_{diff}]$ (y) and $\int\Delta SaO_2$ (x) were extracted from each CBF measurement and the power terms (x^2, x^3, x^4, and x^5) were calculated. This data set was then imported into SPSS for the stepwise analysis. A simple program was written in SPSS to run the stepwise regression on the data set in a loop fashion. In the first loop, the first 4 data points of the set were used in the analysis, in the second loop the first 5 data points were used and so on until the analysis was performed on the whole 40 data points. Within each loop a full stepwise regression analysis was performed in which all of the independent variables (x, x^2, x^3, x^4, and x^5) were available for inclusion. Figure 6.2 shows an example of part of the SPSS output file following a stepwise regression analysis. All files of this type are given the extension ".lst". The file takes the form of a descriptive statistical summary rather than a set of tables containing the parameters of interest. For this reason an automated method of extracting the relevant information from this results list was essential and this formed stage three of the analysis routine.

```
* * * *  M U L T I P L E   R E G R E S S I O N  * * * *

Equation Number 1    Dependent Variable..  Y

Variable(s) Entered on Step Number

  4..   X2

Multiple R            .99985
R Square              .99969
Adjusted R Square     .99960
Standard Error        .15553

Analysis of Variance

                 DF        Sum of Squares      Mean Square
Regression        4           1020.81053        255.20263
Residual         13              .31447          .02419

F =   10549.93244       Signif F =  .0000

---------- Variables in the Equation ----------

Variable            B         SE B        Beta         T  Sig T

X          2232.862513  101.704880    1.270524    21.954  .0000
X2        -88471.18425 20216.38842    -.704664    -4.376  .0007
X4        1185637685.9 228880939.0    1.656936     5.180  .0002
X5        -67387654090 11692809087   -1.248931    -5.763  .0001
(Constant)    1.764354     .116350                15.164  .0000

---------- Variables not in the Equation ----------

Variable     Beta In  Partial  Min Toler        T  Sig T

X3           .789544  .093342  3.745E-06      .325  .7510


End Block Number   1   POUT =     .100 Limits reached.
```

Figure 6.2 *Extract from an SPSS output file after repeated stepwise regression of data shown in Figure 6.1(b). Stepwise selection continues until the PIN/POUT criteria are met ("End Block Number POUT = .100 Limits reached").*

6.5.1 Extraction of useful parameters from stepwise regression analysis

For each stepwise regression analysis the parameters shown in Figure 6.2 were calculated and included in the output file. It was decided that the most useful format for condensing this information was to transfer it into tabular format which could then be read into a spreadsheet package and used to generate graphs. C++ version 3.1 (Borland International, Inc., Scotts Valley, CA) was used to construct a program which searched the SPSS output (list) file line by line and extracted from it the relevant information. The source code for this program, named **extract.exe**, is given in full in Appendix B. In brief, the program performs the following functions;

1) A request is made for the user to enter the name of the SPSS output file to be summarised e.g. cbf01.lst.

2) An output file of the same name with extension ".txt" is created (i.e. cbf01.txt).

3) The program checks that the named ".lst" file exists.

4) A header is written to the text file. This contains the generic filename, date, PIN and POUT criteria used in the stepwise regression analysis and column headings for tabulated data.

5) The program then searches the SPSS output file for a "*" which marks the beginning of a set of stepwise analysis (as shown in Figure 6.2). A marker is assigned to this point in the file.

6) A search is made for the string "End Block Number" which marks the end of a set of stepwise regression analysis and when found a separate marker is assigned to this point in the file.

These search functions are therefore used to define the start and end points for the extract function to work within.

7) Using an extract function between these two markers the parameters multiple R, adjusted R^2, standard error, regression and residual points (used to calculate degrees of freedom), and F, are extracted and written to the output text file (cbf01.txt). These parameters must be present in each complete stepwise analysis for the program to continue.

8) The program then extracts the necessary information about the variables which are selected for the equation, including B, standard error in B, beta, T and sig T.

9) The same information is also extracted about the constant term in the equation.

The above search and extract routines (i.e. steps 5 to 9) are then repeated throughout the file so that for each completed set of stepwise regression analysis, information on all

variables included in the fit is written to the output file (cbf01.txt). The program is truncated when the end of file is reached. In this way the program **extract.exe** summarises the output files into a suitable format for spreadsheet analysis. The SPSS output file for subsequent sets of analysis on CBF data containing 40 points is approximately 100 kbytes in size. **extract.exe**

Table 6.i *A summary of the results of stepwise analysis on the single flow compartment shown in Figure 6.1(a), where n is the number of cases included in the analysis.*

R^2	n	ßx	ßx^2	ßx^3	ßx^4	ßx^5
1.0	1	1.0				
1.0	2	1.0				
1.0	3	1.0				
1.0	4	1.0				
1.0	5	1.0				
1.0	6	1.0				
1.0	7	1.0				
1.0	8	1.0				
1.0	9	1.0				
1.0	10	1.0				
1.0	11	1.0				
1.0	12	1.0				
1.0	13	1.0				
1.0	14	1.0				
1.0	15	1.0				
1.0	16	1.0				
1.0	17	1.0				
1.0	18	1.0				
1.0	19	1.0				
"	"	"				
1.0	38	1.0				
1.0	39	1.0				
1.0	40	1.0				

summarises this to a text file of typical size 20 kbytes.

The format of the extracted file (cbf01.txt) is designed to allow the salient features of the incremental stepwise regression to be clearly seen, i.e. for each data set the independent variables which are used in the "best fit" equation.

6.6 TESTING THE MODEL WITH SIMULATED DATA

As with any analytical model it is important to define the limits of its applicability to the given problem. The following section will describe how the above model was tested using computer generated simulated data. This should also provide a more concise explanation of the different stages of the analysis and the use of the extracted data.

Let us return again to the example CBF data given in Figure 6.1 and use this as a starting block. Figure 6.1(a) is an example of a data set of 40 points where the dependent variable, y, has a purely linear relationship with the independent variable, x. From this data, a set of additional independent variables x^2, x^3, x^4 and x^5 can be computed. Using the total of five independent variables, the data can be tested using the stepwise regression analysis to determine the exact initial portion of the data where a purely straight line relation is appropriate (i.e. where only the x term is used to describe the best fit). The data is passed through the stepwise regression analysis loop program and the results of this analysis are then summarised using the search and extract program (**extract.exe**). Table 6.i shows a condensed summary of the resulting text file. It can be seen that the statistics demonstrate a perfect straight line fit throughout with $R^2 = 1$. As each extra point is added into the analysis the model re-examines all available independent variables but accepts only the x term. As expected none of the other variables are included into the equation at any point (i.e. $ß_{x2} = B_{x2} = ß_{x3} = B_{x3} = ß_{x4} = B_{x4} = ß_{x5} = B_{x5} = 0$). These results may be represented graphically by the plot shown in Figure 6.3 where the number of points (abscissa) is plotted against the unsigned magnitude of the beta weight for each independent variable (ordinate). This type of plot will be referred to as the *beta results graph* and is a useful visual summary of the results of the stepwise regression. τ_{bp} can be clearly identified on this graph as the point where either $ß_{x2}$, $ß_{x3}$, $ß_{x4}$ or $ß_{x5}$ has a non zero value. In this example, the τ_{bp} is not reached because a second flow compartment is not present. Although this result is self evident, given the data set used, it is a useful example of the way in which the results of the stepwise regression can be displayed.

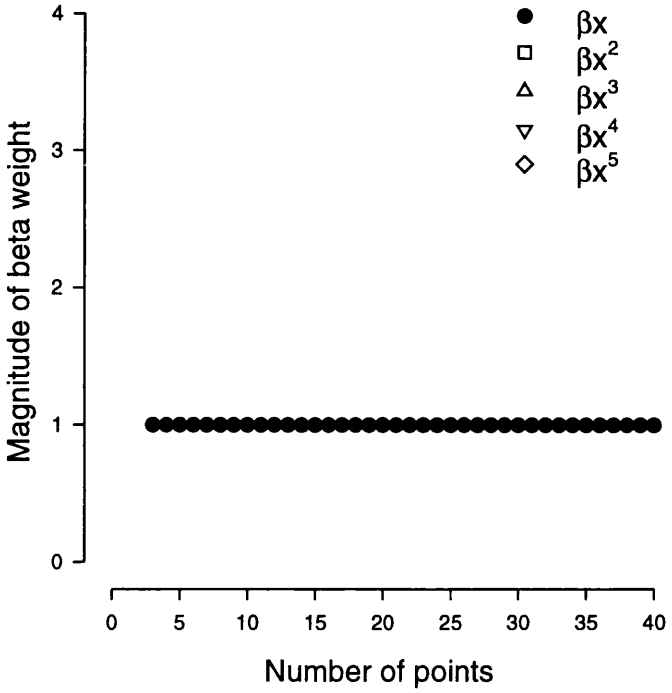

Figure 6.3 *Beta results graph for the data shown in Figure 6.1(a). Since the data can be described as a purely linear function, $\beta x^2 = \beta x^3 = \beta x^4 = \beta x^5 = 0$ for all cases.*

Moving on to a more interesting example, Table 6.ii shows the summarised results following identical analysis performed on the data shown in Figure 6.1(b). In this case the data clearly does not demonstrate a solely straight line dependence. Visual inspection alone determines that beyond the 16th point the response is better described by a curve, i.e. τ_{bp} = 17. This is shown in the beta results graph (Figure 6.4) as the introduction of the x^5 term when the 17th point is included in the analysis ($ß_{x2} = B_{x2} = ß_{x3} = B_{x3} = ß_{x4} = B_{x4} = 0$, $ß_{x5} = B_{x5} = 0.05$). Up until this point the function could be described as a purely linear one, however after the 16th point extra variables were required to more accurately describe it. Since each point represents a 0.5 second data sample it could therefore be concluded in this simulated data set, that the mean CBF value should be calculated using the first 8 seconds of the response, i.e. the period where the response function is a straight line.

Table 6.ii *A summary of the results of the stepwise analysis on the dual flow data shown in Figure 6.1(b).*

R^2	n	ßx	$ßx^2$	$ßx^3$	$ßx^4$	$ßx^5$
1.0	1	1.00				
1.0	2	1.00				
1.0	3	1.00				
1.0	4	1.00				
1.0	5	1.00				
1.0	6	1.00				
1.0	7	1.00				
1.0	8	1.00				
1.0	9	1.00				
1.0	10	1.00				
1.0	11	1.00				
1.0	12	1.00				
1.0	13	1.00				
1.0	14	1.00				
1.0	15	1.00				
1.0	16	1.00				
1.0	17	1.04				0.05
1.0	18	1.27	0.70		1.66	1.25
1.0	19	1.25	0.57			
...	...	...	...	...	...	...
1.0	38	1.87		1.63		0.84
1.0	39	2.29	1.65	1.69		0.33
1.0	40	2.32	1.69	1.74		0.35

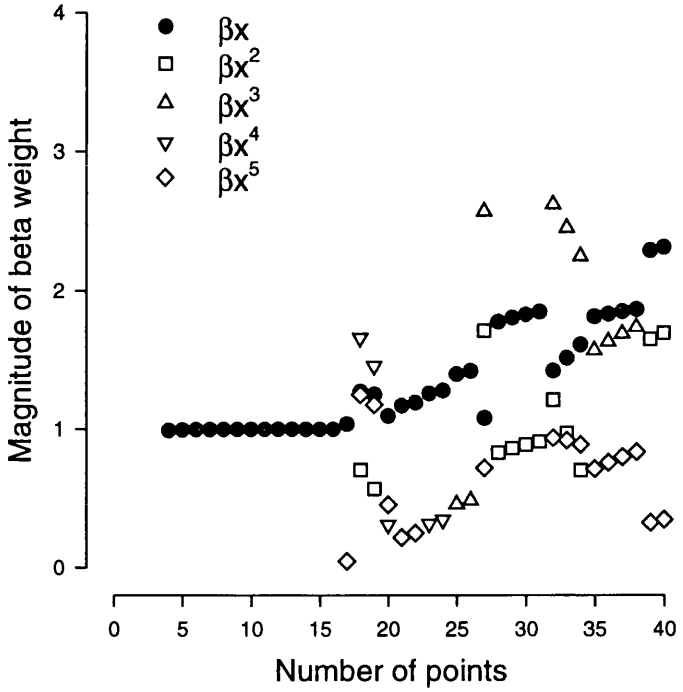

Figure 6.4 *Beta results graph for dual flow compartment data (Figure 6.1(b)). Beyond the 16th point independent variables other than x are brought into the fit.*

6.6.1 Establishing useful simulated data sets

All the simulated data was based around the assumption of two flow compartments as described in Figure 6.1(b). Let us consider here, in more detail, the basic components of a dual flow system and how they can be described mathematically. These descriptions can then be used to construct a useful set of simulated data with which to test the analytical method.

A dual flow system is the combination of two flow compartments each with a defined flow and transit time. The first flow compartment, shown in Figure 6.5(a), has a transit time t_1 and generates the following relationship between ($\Delta[Hb_{diff}]$), y and ($\int\Delta SaO_2$), x:

$$\begin{aligned} y_1 &= m_1 x \quad \text{for } x \leq t_1 \\ y_1 &= c_1 \quad \text{for } x > t_1 \end{aligned} \tag{6-4}$$

Note that t_1 is the point at which the tracer starts to leave the field of view, i.e. τ_{bp}.

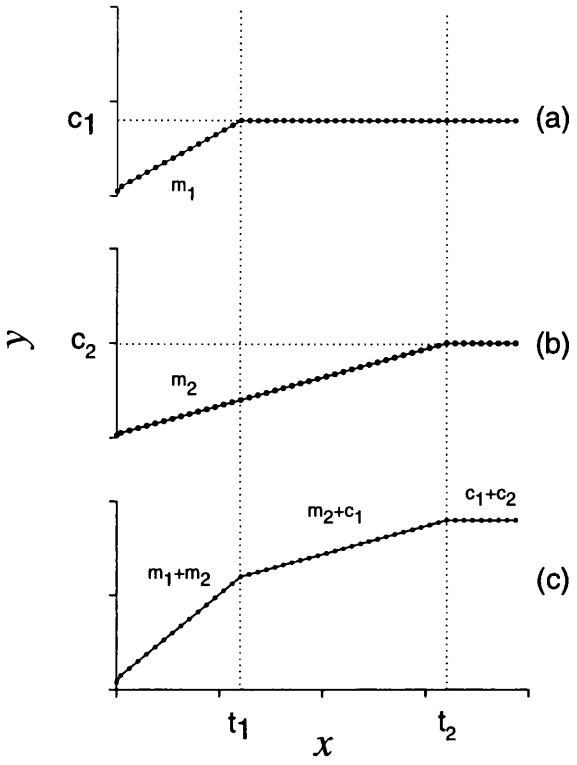

Figure 6.5 *Construction of simulated data using (a) a slow flow compartment and (b) a faster flow compartment. The resulting dual flow model (c), allows both the ratio of the flow rates and transit times to be varied.*

The second flow compartment, shown in Figure 6.5(b), with a transit time of t_2, is described by the equation:

$$\begin{aligned} y_2 &= m_2 x \quad for \quad x \leq t_2 \\ y_2 &= c_2 \quad for \quad x > t_2 \end{aligned} \tag{6-5}$$

where $m_1 > m_2$ and $t_2 > t_1$.

When these two compartments are combined the resulting dual flow compartment, shown in Figure 6.5(c), can be described by the equation:

$$\begin{aligned} y &= (m_1 + m_2)x \quad for \; x \leq t_1 \\ y &= m_2 x + c_1 \quad for \; t_1 < x \leq t_2 \\ y &= c_1 + c_2 \quad for \; x > t_2 \end{aligned} \tag{6-6}$$

The simulated data sets were therefore designed to answer the following questions;

(i) how does the model behave for variations in the fastest transit time, i.e. t_1?

(ii) how does the model behave for variations in the ratio between the response of the first and second compartment i.e. $m_2/(m_1+m_2)$?

(iii) how does the addition of noise on these data sets affect the use of the model?

These questions will be dealt with in turn in the following sections.

6.6.2 Variation in t_1

In the simulated data sets 40 points were used to model 0.5 second sampling of data over a 20 second period. Data sets were prepared in which $m_2/(m_1+m_2)$ was fixed at 0.5 and the value of t_1 was varied from 2.5s to 10s in increments of 0.5s (i.e. from the 5th to the 20th point in steps of 1). The $m_2/(m_1+m_2)$ ratio of 0.5 was used to approximately reproduce (simulate) the experimentally observed ratio of grey (fast) to white (slow) matter flow rates in the adult cerebral circulation[1]. The lower limit of t_1 was fixed at 2.5s (the 5th point) since the model uses up to a fifth order polynomial fit. In all cases the five independent variables x, x^2, x^3, x^4 and x^5 were available for selection.

The break point was successfully detected (i.e. τ_{bp} correctly defined the end of the linear portion of the response) for all values of t_1 except, when $t_1 = 2.5$s. For $3 < t_1 < 4.5$ the first term introduced into the equation was the x^2 term and when $5 < t_1 < 10$ it was the x^5 term which was selected.

6.6.3 Variation in $m_2/(m_1+m_2)$

In this simulated data set t_1 was fixed at a value of 8s and the ratio between the rate of rise of the first and second compartments, $m_2/(m_1+m_2)$, was varied. A range of $m_2/(m_1+m_2)$ from 0.1 to 0.9 was used. The model successfully identified the break point in all cases. For $0.10 < m_2/(m_1+m_2) < 0.33$ the x^2 term was the first higher order term brought into the equation and when $0.33 < m_2/(m_1+m_2) < 0.90$ the x^5 term was introduced.

6.6.4 Adding noise to the simulated data sets

Although the above data provides evidence that the incremental stepwise analysis is a good analytical model for detecting τ_{bp} with perfect data, the use of the method where data is subject to both instrument and physiological noise must be considered.

Quantification of the level of instrument noise can be approached from both a theoretical and experimental point of view. The previously described simulated data sets have been designed to approximate the $\Delta[Hb_{diff}]$ vs $\int\Delta SaO_2$ response curve. Calculation of the contribution of instrumentation noise levels on this data is not trivial since it will depend upon several factors. The NIR spectrophotometer noise will itself depend upon the light levels in the form of (Poissonian) photon noise (and therefore interoptode spacing) and the choice of algorithm. Since an oximeter with minimal signal averaging is used for CBF measurements the level and nature of noise on the SaO_2 signal is also somewhat unpredictable. For the case of these simulated data sets it was decided to calculate the expected NIRS instrument noise from known typical light levels and use this as a best case estimate.

6.6.4.1 *Estimation of noise level of $[Hb_{diff}]$ measurements with NIRO 500*

These calculations were based upon $[Hb_{diff}]$ data collected with the NIRO 500 described in section 3.3.3. An estimate of the typical standard deviation (SD) on $[Hb_{diff}]$ measurements was thought to provide the most appropriate level of noise to apply to the simulated data. These measurements were made on a stable resin phantom with absorption and scattering characteristics close to that of tissue[2]. As previously described, the NIRO 500 actually measures optical density (OD) changes and uses an algorithm (in the form of a matrix calculation) to convert this data into changes in concentration of [Hb], $[HbO_2]$ and CtOx. The calculation of typical noise levels on the $[Hb_{diff}]$ data can be split into two stages, (i) the measurement of noise levels on the OD data in the form of the standard deviation (SD) and (ii) the propagated error arising from the matrix transform. Optical density (OD) data were collected on the phantom at light levels similar to those obtained during adult cerebral studies. The SD on a seven minute section of OD data was calculated at a single wavelength (849nm) as 0.0020 OD. The matrix used to convert OD data into chromophore concentration data for the four wavelength system has the form:

	λ_1	λ_2	λ_3	λ_4
Hb	$\alpha 1_{Hb}$	$\alpha 2_{Hb}$	$\alpha 3_{Hb}$	$\alpha 4_{Hb}$
HbO_2	$\alpha 1_{HbO2}$	$\alpha 2_{HbO2}$	$\alpha 3_{HbO2}$	$\alpha 4_{HbO2}$
CtOx	$\alpha 1_{CtOx}$	$\alpha 2_{CtOx}$	$\alpha 3_{CtOx}$	$\alpha 4_{CtOx}$

where λ_n are the measurement wavelengths and αn_x is the specific extinction coefficient factor for the x chromophore at the nth wavelength.

The error multiplier of OD noise arising from the algorithm can be considered as the mathematical error from the matrix calculation. Since $[Hb_{diff}]$ is purely the difference between [Hb] and $[HbO_2]$, the error multiplier on $[Hb_{diff}]$ ($\delta[Hb_{diff}]'$) is the square root of the linear sum of the squares for [Hb] and $[HbO_2]$ at each wavelength[3]:

$$(\delta[Hb_{diff}])'^2 = (\alpha 1_{HbO_2} - \alpha 1_{Hb})^2 + (\alpha 2_{HbO_2} - \alpha 2_{Hb})^2 + (\alpha 3_{HbO_2} - \alpha 3_{Hb})^2 + (\alpha 4_{HbO_2} - \alpha 4_{Hb})^2 \quad \textbf{(6-7)}$$

Inserting the relevant coefficients for the NIRO 500 used in the above study gives $\delta[Hb_{diff}]'$ a value of 3.26. The total error on the $[Hb_{diff}]$ signal ($\delta[Hb_{diff}]$) is then just simply the product of δOD and $\delta([Hb_{diff}]')$, equivalent in this case to 6.5 μmolar.cm.

This figure can be compared to the experimentally observed SD level on the calculated $[Hb_{diff}]$ signal. For the same seven minute data section $\delta[Hb_{diff}]$ was estimated at 5.1 μmolar.cm. The small discrepancy between the two methods is probably due to the fact that the former method assumes the same δOD value at all four wavelengths. An SD value of 5.2 μmolar.cm was thought to represent a reasonable estimate for the noise on a given $[Hb_{diff}]$ signal. In order to scale this figure to the arbitrary levels of the simulated data sets, it was easier to represent this SD as a percentage of the total $\Delta[Hb_{diff}]$ being measured. Further analysis of the CBF data collected on the ten adult volunteers (section 4.2.6) demonstrated that the mean ($\pm$SD) $\Delta[Hb_{diff}]$ recorded over 40 points during a CBF measurement was 210 $\pm$ 60 μmolar.cm. From these calculations, it was estimated that the simulated data sets should have an SD noise level equivalent to at least 2.5% of the total change in the dependent variable.

6.6.5 Variation in noise levels

Gaussian noise at the level estimated above was then applied, using a random number generator, to five sets of simulated data where t_1 and $m_2/(m_1+m_2)$ were fixed at 8s and 0.66 respectively. Using the same t_1 and $m_2/(m_1+m_2)$ criteria, five data sets were generated where the noise was increased to a level equivalent to 3.3% and 5% of the total change in the dependent variable. Examples from each of these data sets are shown in Figure 6.6.

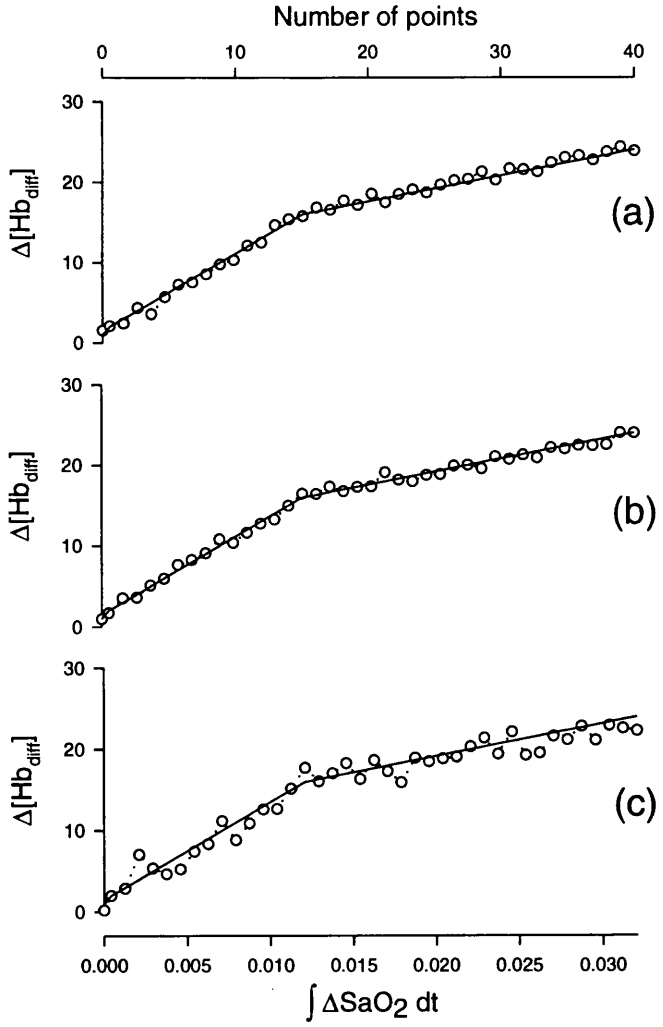

Figure 6.6 *Examples of addition of Gaussian noise (hollow circles) to simulated data. In each plot the noise level is the equivalent of an SD of (a) 2.5%, (b) 3.3% and (c) 5% of the total* $\Delta[Hb_{diff}]$.

The incremental stepwise regression analysis model was tested on each data set. It was hypothesised that the model was less likely to successfully detect the τ_{bp} in data with a higher degree of noise. Based on this hypothesis the stepwise regression analysis was repeated for each of the data sets using different **PIN** and **POUT** criteria. **PIN** was varied between 0.001 and 0.1. A summary of the results is given in Table 6.iii. When examining these results it should be remembered that when t_1 is 8s, τ_{bp} should be 17, indicating that the response is linear up until the 16th point. As expected the hypothesis was confirmed, i.e. that the success of the model was dependent upon the degree of noise on the signal. As **PIN** is decreased it becomes increasingly difficult for a second variable to be introduced into the equation, thus the τ_{bp} appears to be much later than it actually is.

Table 6.iii *Results of stepwise analysis on data sets with different levels of noise analysed using three PIN criteria. The actual t_1 for each set was 8s, equivalent to τ_{bp} = 17.*

PIN	τ_{bp} SD = 2.5%	τ_{bp} SD = 3.3%	τ_{bp} SD = 5%
0.001	20.0 ± 0.6	21.0 ± 0.9	24.6 ± 1.0
0.05	17.8 ± 1.6	17.0 ± 2.7	21.6 ± 0.8
0.10	16.4 ± 3.3	16.4 ± 3.5	20.6 ± 1.0

6.7 RESULTS FROM STEPWISE REGRESSION ANALYSIS ON ADULT DATA

The described regression model was developed to improve the analysis routine used to calculate CBF on clinical data. The method was therefore used to reanalyse the CBF data collected on the ten adult volunteers presented in Chapter Four. The following section will describe the results of that analysis and the possible advantages of employing such a technique for improving the estimation of CBF and also in providing another useful physiological parameter for consideration in the assessment of cerebral haemodynamics.

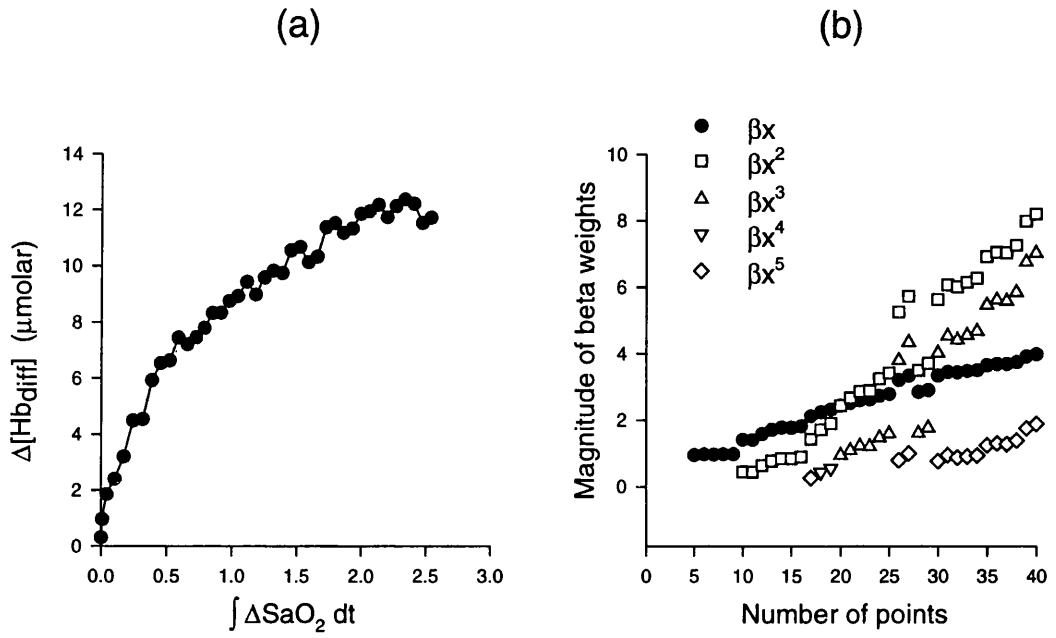

Figure 6.7 *(a) The $\Delta[Hb_{diff}]$ vs $\int\Delta SaO_2$ response curve from an adult volunteer and (b) the resulting beta results graph. In this subject τ_{bp} = 11, equivalent to a first transit time of 5s.*

The $\Delta[Hb_{diff}]$ vs $\int\Delta SaO_2$ curves for each of the ten subjects was analysed according to the protocol described in section 6.5. For the stepwise regression, values of PIN and POUT were set at 0.05 and 0.10 respectively given the noise level on the data. Figure 6.7 shows (a) an example $\Delta[Hb_{diff}]$ vs $\int\Delta SaO_2$ response curve for a single subject with (b) the corresponding beta results graph. The mean (± SD) τ_{bp} for all subjects was 11.0 ± 2.1, equivalent to a first detected transit time, t_1, of 5.0 ± 1.0 second. The inter subject coefficient of variation was 20% and the intra subject coefficient of variation ranged from 4 to 25%.

As shown in section 4.2.6, the period over which CBF is measured has a significant effect on the calculated value. Since the aim of this analysis was to improve the estimation of the valid CBF measurement period, the CBF data from each subject was reanalysed using the appropriate τ_{bp} for each measurement, e.g. if the τ_{bp} was calculated to be 11 points, CBF was recalculated for that measurement (using equation 4.13) over the first 5 seconds. Incorporating the results of the stepwise analysis method in this way the mean (± SD) CBF for the whole group was 15.9 ± 3.9 $ml.100g^{-1}.min^{-1}$ with an inter subject coefficient of variation of 24%. The mean intra subject coefficient of variation was also 24%.

6.8 INTERPRETATION OF RESULTS

The introduction of this chapter identified three criteria which should be met by a data analysis technique developed for the measurement of CBF. An interpretation of the results presented in this chapter should therefore include an assessment of how successful the described technique was in fulfilling these objectives.

6.8.1 Accuracy and reproducibility in providing a mean CBF value

The analytical model described in this chapter forms the preliminary stages of a more automated and objective approach to the manipulation of NIRS CBF data. Many of the methods described in the introductory chapter of this thesis use a tracer technique either in the form of wash-in or wash-out curves and in many cases the convolution of several effects must be considered. The stepwise regression analysis is an attempt to separate out at least one of the important parameters from the $\Delta[Hb_{diff}]$ vs $\int\Delta SaO_2$ response curve, i.e. the first (fastest) transit time.

The τ_{bp} calculated on the adult data suggests that the first detected transit time is approximately 5 seconds. This is in line with other transit time estimates using PET and ^{133}Xenon[1]. The reliable detection of this transit time may itself be a useful physiological parameter. As described in Chapter One, CBF, CBV and transit time are all intimately linked. A transit time of 5 seconds is usually associated with a CBF of 50 - 60 $ml.100g^{-1}.min^{-1}$. It is encouraging therefore, that since the measurement of τ_{bp} is dependent solely on the time course of the response, rather than its exact magnitude, it bypasses all the problems of extracerebral tissue contribution which have been shown to hamper the exact quantification of CBF. It provides further proof that the CBF method is indeed valid but resulting values must be scaled to take into account the non cerebral tissue DPF effect. The transit time measurements may provide a reliable and reproducible measurement of haemodynamics.

The recalculated CBF values failed to demonstrate a dramatic improvement in either inter or intra subject variation. It may be supposed therefore that a coefficient of variation of 20% is the best that can be hoped for given the hardware limitations of sampling rate and the crude artefact rejection employed in beat to beat oximetry. This analysis may have served to demonstrate that the majority of variation in CBF measurements is not due to variable transit time as may have been presupposed, but is in fact due to other instrument (or physiological)

factors. In fact, although this coefficient of variation may sound high, it must be put in context with that of other techniques. Data on intra and inter subject variation for PET CBF measurements (the usual gold standard technique) is surprisingly scarce. Long term reproducibility studies have shown variability of up to ±20% [4] and ±26% [5]. PET measurements made on a group of 30 normal adults within a tight age band demonstrated an inter subject coefficient of variation of 17%[6].

6.8.2 Accommodation of different noise levels on data

It has been shown here that the described stepwise regression analysis is appropriate if the level of noise on a signal is taken into account. The results suggest that the model will work with moderate degrees of noise but may be improved by "tuning" the **PIN** and **POUT** criteria to the level of noise on the signal. It may indeed be practical to incorporate within the analysis process a function to estimate the level of noise on the signal. This could be done by considering the light levels and geometry of the particular measurement. Once the noise level has been assessed, the acceptance or rejection criteria for stepwise analysis (i.e. **PIN** and **POUT**) could be set accordingly.

The question of the additional physiological noise present on the signal could form the basis of an entire thesis in its own right and has not been included in this model. It has been shown in Chapter Five that there may be some very obvious sources of oscillations of haemodynamic signals (i.e. respiratory or cardiac linked), however the origins and effects of the dynamics of the microcirculation (particularly in the brain) are phenomenon which are complex and not well understood. The origin and effects of instrument noise are more easily described and accounted for. The data presented in section 6.6.4.1 suggests that attention must be paid to optimising the light levels employed in NIRS studies. $\delta[Hb_{diff}]$ is directly dependent upon the photon noise (i.e. the number of photons reaching the detector) and therefore the thickness of tissue illuminated. The limits of the model with regard to noise levels have been demonstrated and it is fair to say that even more complex mathematical routines would still have great difficulty in defining subtle features from data with a low signal to noise ratio. One additional point which may be important is the way in which pulse oximeters output the SaO_2 data and in particular the output step size of the instruments. Many oximeters only output data in discrete 0.5% steps, which for a typical SaO_2 flow swing ($\approx$ 5%) means only 10 possible data values, i.e. the x ($\int\Delta SaO_2$) axis is not strictly a continuous parameter. These points must

be considered in the further design of instrumentation, particularly in the systems used to deliver and retrieve light from the tissue surface.

The particular model described here (using 5 independent variables) is restricted to detecting a τ_{bp} which occurs at least after the fifth point of the curve, i.e. a transit time of at least 2.5 seconds. These findings again point towards an inherent limitation in the hardware used to collect such data. In order to reliably detect dynamic features in the sub 2-3 second range an increase in sampling rate is essential. For example, a 100 ms sampling interval would provide 20 points within the first two seconds. A compromise is obviously necessary in order to balance the minimum noise criteria described above with the maximum sampling rate criteria described here.

6.8.3 Automated use of the program in real time at the bedside

The design of this analysis technique is such that the user needs only to define the "take off point" of both the SaO_2 and $[Hb_{diff}]$ signals during a CBF measurement. Beyond this the routines described for formatting of data, running the stepwise regression, extracting the τ_{bp} and calculating mean CBF could quite feasibly be combined into a single program. One could envisage that automated calculation of mean CBF at the bedside could take only a few seconds. In order to maintain quality control within the measurements, other parameters such as changes in $[Hb_{sum}]$, $PaCO_2$ and MAP would also be need to be included within this analysis.

6.9 REFERENCES

1. Leenders K.L., Perani D., Lammertsma A.A., Heathers J.D., Buckingham P., Healy M.J.R., Gibbs J.M., Wise R.J.S., Hatazawa J., Herold S., Beaney R.P., Brooks D.J., Spinks T., Rhodes C., Frackowiak R.S.J., Jones T. (1990) Cerebral blood flow, blood volume and oxygen utilisation. Normal values and effect of age. *Brain* 113;27-47
2. Firbank M. (1994) The design, calibration and usage of a solid scattering and absorbing phantom for near infra red spectroscopy. *Ph.D., University of London.*
3. Cope M. (1991) The development of a near infrared spectroscopy system and its application for non invasive monitoring of cerebral blood and tissue oxygenation in

the newborn infant. *Ph.D., University College London.*

4. Lenzi G.L., Frackowiak R.S.J., Jones T. (1982) Cerebral oxygen metabolsim and blood flow in human cerebral ischemic infarction. *J. Cereb. Blood Flow & Metab.* 2;321-335

5. Frackowiak R.S., Lenzi G.L., Jones T., Heather J.D. (1980) Quantitative measurement of regional cerebral blood flow and oxygen metabolism in man using ^{15}O and positron emission tomography: theory, procedure, and normal values. *J Comput. Assist. Tomogr.* 4;727-736

6. Madsen P.L., Holm S., Lassen N.A. (1993) A critical appraisal of the gold standard; global levels of CBF, CMR_{O2}, and CMR_{glu} determined with the Kety-Schmidt technique. In "*Quantification of Brain Function, Tracer Kinetics and Image Analysis in Brain PET*", eds Uemura K., Lassen N.A., Jones T., Kanno I., Elsevier Science Publishers B.V., .

CHAPTER 7

SUMMARY, CONCLUSIONS AND FURTHER WORK

7.1 SUMMARY

Since a full discussion of the results presented in this thesis are given at the end of each of the appropriate sections, the purpose of this final chapter is to summarise the important conclusions of the project as a whole and to suggest further work.

The aim of the work in this thesis was to investigate the measurement of adult cerebral haemodynamics using the technique of near infrared spectroscopy. As a background to this work, the clinical importance of CBF and CBV measurements in the adult, together with the current techniques used for their measurement, have been discussed. The theoretical principles of light interaction with tissue and their application to spectroscopy measurements in the NIR have been detailed. Descriptions of spectroscopic instrumentation currently in use have been given, including details of a commonly used clinical monitor, the pulse oximeter. The physiological principles behind the measurement of CBF, CBV and $SmcO_2$ using NIRS have then been outlined with particular emphasis on the application of these techniques to measurements in the adult. A full description has been given of sets of measurements performed on healthy adult volunteers for the measurement of CBF, CBV and $SmcO_2$ using NIRS. The further investigation of respiratory linked oscillations in cerebral haemodynamics is also detailed. Finally, the development and testing of a novel data analysis method for the calculation of CBF has been described.

7.2 CONCLUSIONS

The measurements of CBF, CBV and $SmcO_2$ described in this thesis are the first measurements of their kind to be made in adults using NIRS. The conclusions from each will be considered in turn, with comments about the new CBF analysis technique included in section 7.2.1;

7.2.1 CBF measurements

It is clear that NIRS can be used to measure CBF in adults and that the technique is more sensitive than initially anticipated in resolving the distribution of flow rates in the cerebral circulation. However the limitations imposed by instrumentation must be appreciated. It appears that current spectroscopy systems are not capable of sampling rapidly enough to fully define the initial high flow compartment which may have a very short transit time. The importance of accurate, reliable and rapid data collection from the pulse oximeter has been confirmed. It appears that the physiological assumptions inherent in the technique are valid within the defined limits, i.e. for small changes in SaO_2 within the physiological range. The loss of tracer via diffusion is negligible and the effects on the cerebral circulation due to changes in SaO_2 are within acceptable limits. The contribution of extracerebral tissue to the measurement of CBF and in particular its effect on the absolute values obtained, clearly require further investigation.

The stepwise regression analysis appears to be a useful method of standardising the CBF calculation and reducing the subjective influence of the user. It has also provided information about the likely transit time within the detected flow measurements, which it is hoped will in itself prove to be a useful clinical parameter in the investigation of cerebral haemodynamics.

Looking ahead, it may be possible to apply a similar analysis method to fully describe the later compartments in the flow model. It has been suggested in this thesis that the lower flow in the extracerebral circulation (i.e. bone, scalp), contributes a slow component to the measured $\Delta[Hb_{diff}]$ vs $\int\Delta SaO_2$ response, perhaps up to a minute after the $[Hb_{diff}]$ take off point. Transforming the model to detect multi compartmental flow rates (rather than just a dual compartmental flow) would depend upon, among other factors, the noise on the signals and the limitations this would place on resolving more than two flow rates. The question of

establishing a comprehensive multi-compartmental model which would also take into account the distribution of tracer arrival times would form a substantial project, but may rely upon some experimental data on the slurring of the input $\Delta[HbO_2]$ function between the lungs and the brain (sees section 7.3.1.1).

7.2.2 CBV measurements

NIRS provides a simple non invasive technique for the measurement of CBV. This in itself is important given that there are currently no other CBV techniques which can be used at the bedside. As anticipated, CBV measurement is less complicated than that of CBF since it does not require such high temporal resolution. The problems of extracerebral tissue contribution, especially to the pathlength, are still relevant and undoubtedly have an effect on the absolute quantification. Using the changes in CBV as a trend measurement may itself prove to be a useful clinical tool in adult intensive care. For example, in those patients where ICP is routinely monitored a parallel measure of changes in CBV may provide important information about the status of their cerebral autoregulation. This may be enhanced by making a series of absolute CBV measurements at the beginning of a study to calibrate the changes in CBV so that they can be expressed as a percentage of the total volume.

7.2.3 $SmcO_2$ measurement

Whilst the measurement of peripheral arterial oxygen saturation (SaO_2) provides useful information about the delivery of oxygen to the brain, a measure of the actual level of cerebral oxygen consumption and uptake is a more useful guide for the direction of therapies. Measurements of jugular bulb venous saturation are currently being used to assess consumption, but are prone to movement and calibration artefact. The measurement of $SmcO_2$ may therefore be a useful clinical parameter in the management of patients with compromised cerebral haemodynamics. The fact that this parameter may be measured from spontaneous changes in cerebral haemodynamics is itself important and, together with the measurements made at different levels of IEP, demonstrates the advantage of NIRS as a technique which can provide a near continuous monitor of cerebral haemodynamics.

7.3 FURTHER WORK

The studies described in this report demonstrate that measurements of the above cerebral haemodynamic parameters are possible using NIRS in adults. As with many projects of this kind, the answer to one set of questions raises others and identifies many new avenues of research. Several further questions about the application of NIRS to the field of adult neurology remain unanswered, including;

i) How can the contribution of extracerebral tissue be quantified?

ii) How can these measurements be validated against other known techniques?

iii) Is it possible to further adapt instrumentation to measure other clinically useful parameters such as the response of CBV and CBF to changes in $PaCO_2$?

These questions have already influenced the direction of further projects, some of which are now described.

7.3.1 Extracerebral tissue contribution

7.3.1.1 *Experimental Studies*

A study is already underway to determine the contribution of extracerebral tissue by making NIRS measurements of CBF and CBV on exposed dura during neurosurgical procedures. These data will make it possible to directly compare measurements of CBF and CBV with and without skull and scalp tissues in the field of view and hence further our understanding of the contribution of extracerebral tissue to these absolute measurements.

The new IMOS system described in section 3.4.2 has now been developed for clinical use. One use of this system has been the measurement of DPF in the heads of 100 adult volunteers. As with the existing time of flight data, these measurements define the total optical pathlength in the scalp, skull and cerebral tissue combined. The next step therefore is to measure DPF directly on the dura and since the IMOS system is now "semi-portable" it may be possible to make these direct cerebral measurements on a group of patients in the near future.

As described in section 4.2.7.2, the effects of extracerebral tissue are twofold, the first

due to their vascular content, and the second their contribution to total optical pathlength. Using the new methods of measuring optical pathlength in tissue described in section 3.4, it may be possible to define more clearly the actual optical pathlength of the cerebral tissue. When DP is measured using the time of flight or IMOS system, the mean path of light is measured through all the tissues between the source and detector. In the water peak measurements (section 3.4.3), pathlength is measured only in those tissues contributing to the absorption peak due to water. Heterogeneous tissues such as the adult head may therefore give rise to significant differences between the DP estimates obtained using the time and phase resolved methods and the method using the strength of the water absorption peak. These differences will depend upon the distribution of water throughout the tissues and the magnitude of the partial differential pathlengths (PDP) in the various regions. Studies are planned to compare DP measured simultaneously using the time resolved method and the water peak method in a group of adult volunteers as a function of optode spacing and to attempt to define the relative PDP in adult scalp, skull and brain tissue.

As seen in section 4.2, during the measurement of CBF a single response function is measured in the brain due to the change in $[Hb_{diff}]$. The data in Chapter Six suggests that useful information may be gained from the deconvolution of this single function to determine the contribution to the slurring of the input function due to the distribution of arrival times of tracer or the distribution of transit times through the brain. To assist in this analysis it may be possible to use another technique to investigate more thoroughly the time course of the $[HbO_2]$ tracer through the cerebral circulation. As described in section 1.4.7, deoxyhaemoglobin is paramagnetic and changes in its concentration can be detected using NMR. It may therefore be possible to perform NIR measurements simultaneously with NMR imaging of the brain. In this way the input function, $\Delta[HbO_2]$, can be viewed by both techniques simultaneously. NMR can be used to chart the arrival of the tracer in the different tissues in the NIRS field of view and to provide response functions for each of these tissues. It may then be possible to calculate the contribution from each tissue required to reconstruct the total convolved function seen by NIRS alone. It may also be possible to measure the exact arrival time and mean transit time of the tissue of interest and compare these values with those of τ_{tp} given in section 6.7.

7.3.1.2 *Theoretical Studies*

There is much work in progress in developing mathematical models (both finite element and Monte Carlo) of the light distribution in the adult head using detailed anatomical maps and assumed values for the optical characteristics of different tissues such as white and grey matter, cerebrospinal fluid, skull and skin. As with any mathematical model, the results are highly dependent upon the tissue parameters used, in this case μ_a and μ_s'. Once accurate values for these parameters have been obtained for all tissues in the light path, this modelling should be able to predict the likely depth of penetration of NIR light in the adult head and hence indicate the effect of extracerebral tissue on NIRS measurements. In this way the future of adult cerebral NIRS studies may depend upon a combination of experimental and theoretical studies.

7.3.2 Validation Studies

If a measurement technique is to be validated, it is necessary to consider the most appropriate gold standard. As discussed in Chapter One, there are several CBF measurement techniques which each have their own advantages. Validation studies of CBV and CBF are planned in which NIRS measurements will be compared with PET in the neonate, Xenon clearance in anaesthetised adults and microspheres in the anaesthetised dog. It is hoped that the PET measurements may provide information about the regions of interest which best correlate with the NIRS CBF and CBV measurements. The Xenon clearance technique will allow a comparison of CBF measurements in adult humans as part of a clinical study. The microspheres technique is to be used in an animal model, to again determine the likely contribution of intra and extracerebral tissue to the NIRS CBF measurements.

7.3.3 Instrumentation and CO_2 Responsivity Measurements

As detailed in Chapter One, the response of the cerebral circulation to changes in PaO_2 and $PaCO_2$ may provide useful clinical information. It is possible that the techniques described in this thesis may be used to provide information about the response of CBV and CBF to changes in PaO_2 and $PaCO_2$ in adults. As previously described, the measurement of CBF and

CBV requires careful manipulation of FiO_2 which in this case was achieved by manually controlling the flow meters of an anaesthetic trolley. If, for example, changes in $FiCO_2$ as well as FiO_2 need to be controlled, these manipulations may be difficult to reproduce manually, particularly for repeated measurements. The recent design of an automated gas blender will allow more complicated manoeuvres to be performed repeatedly and accurately in the planned physiological measurements. The automated blender could be used to change or hold $FiCO_2$ constant whilst performing the necessary manipulations in FiO_2 to measure CBF and CBV. Studies of this kind are planned on neonatal piglets and on adult human volunteers.

7.4 Concluding Remarks

Since its first clinical application some two decades ago, NIRS has contributed widely to the assessment of cerebral oxygenation and metabolism. Its non invasive nature has allowed the technique to be utilised in an intensive care environment where more traditional modalities are impractical. It should be remembered however that NIRS is still in its infancy and the limits of its applicability and usefulness have yet to be fully defined. This thesis has described the potential of the technique in the investigation of adult cerebral haemodynamics. Validation of the absolute parameters (CBF and CBV) still depends upon further experimental and theoretical studies to determine the exact contribution of extracerebral tissues, as well as the development of more sophisticated analysis routines in order to extract the maximum amount of information from the available data. Although the spatial resolution of NIRS will never match that of PET or MRI, the high temporal resolution is still to some extent an untapped potential and one that may well reveal exciting new aspects of the cerebral circulation which have previously gone undetected.

The ultimate goal in tissue spectroscopy remains absolute quantification of the concentration of oxygen dependent chromophores. The way in which such information will in turn be interpreted clinically must also be approached. Recent technological developments are bringing this goal nearer, but must be guided by concrete clinical questions if the potential of NIRS is to be fully realised.

APPENDIX A

CALCULATION OF PROPORTION OF TRACER LOST TO TISSUE DIFFUSION DURING CBF MEASUREMENT

At an SaO_2 of 100% the concentration of oxygen in the arterial blood can be calculated from knowledge of haemoglobin concentration ([tHb]), the O_2 carrying capacity of haemoglobin and the molecular weight of haemoglobin (MW_{Hb}) (neglecting the contribution of dissolved oxygen in the plasma):

For a normal adult [tHb] = 15 $g.100ml^{-1}$

= 0.15 $g.ml^{-1}$

MW_{Hb} = 64500

1 mol Hb = 4 mol O_2

$\therefore$ Concentration of O_2 in blood = (0.15 x 4)/64500

= 9.3 $\mu mol.ml^{-1}$

$\therefore$ O_2 delivery to the brain = CBF x 9.3 $\mu mol.100g^{-1}.min^{-1}$

Normal adult CBF = 50 $ml.100g^{-1}.min^{-1}$

$\therefore$ O_2 delivery to the brain = 50 x 9.3 $\mu mol.100g^{-1}.min^{-1}$

= 465 $\mu mol.100g^{-1}.min^{-1}$

The concentration of O_2 in tissue can be derived from the tissue PO_2 and the solubility of O_2 in tissue:

Solubility of O_2 in H_20 @ 37°C = $2.32.10^{-4}$ $l.kg^{-1}.kPa^{-1}$

Brain tissue density [1] = 1.06 $g.ml^{-1}$

$\therefore$ Concentration of O_2 in tissue @ 37°C = $2.32.10^{-5}$ $l.100g^{-1}.kPa^{-1}$

1 mol O_2 = 22.4 l O_2

$\therefore$ Concentration of O_2 in tissue $= 2.32.10^{-5} / 22.4$

$= 1.04\ \mu mol.100g^{-1}.kPa^{-1}$

Mean brain tissue PO_2 = 4 kPa [2]

$\therefore$ Concentration of O_2 in tissue $= 1.04 \times 4$

$= 4.2\ \mu mol.100g^{-1}$

For a step change in SaO_2 from 90 - 95%, capillary oxygen haemoglobin saturation will change from approximately 60 - 65%[3]. Assuming the normal adult dissociation curve this is equivalent to an increase in capillary PO_2 from 4.1 - 4.5 kPa, i.e. a 10% change in capillary PO_2. It can be assumed that within the physiological range, tissue O_2 concentration will also change by this amount.

10% increase in tissue O_2 concentration = $0.4\ \mu mol.100g^{-1}$

If this diffusion takes place over a capillary transit time of 2 seconds[4], the offloading rate of O_2 from capillary to tissue in this instance is:

$$0.4 / (2/60) = 12\ \mu mol.100g^{-1}.min^{-1}$$

$\therefore$ Loss of O_2 to tissue / O_2 delivery to brain = 12 / 465 = 0.025 = 2.5%

REFERENCES

1. Woodard H.Q. and White D.R. (1986) The composition of body tissues. *Br. J. Radiol.* 59;1209-1219
2. Lubbers D.W. (1968) The oxygen pressure field of the brain and its significance for the normal and critical oxygen supply to the brain. In "*Oxygen Transport in Blood and Tissue*", eds Lubbers D.W., Luft U.C., Tews E., Wilzeb E., George Thieme Verlag, Stuttgart.
3. Tauschek D., Hoper J., Gaab M.R., Kessler M. (1992) Monitoring of cortical intracapillary hemoglobin oxygenation in patients during brain surgery - first results. *Adv. Exp. Med. & Biol.* 317;737-741
4. Hudetz A.G. (1992) Computer simulation of erthrocyte transit in cerebrocortical capillary network. *Adv. Exp. Med. & Biol.* 317;659-670

APPENDIX B

SOURCE CODE FOR C PROGRAM (EXTRACT.EXE)

The following program was used to summarise, in a tabular form, the output file from the stepwise regression analysis used to estimate τ_{bp}.

```
#include   <stdio.h>
#include   <string.h>
#include <stdlib.h>

#define                FALSE   (0)
#define                TRUE    (1)
#define                EXFAIL  (-2)

FILE            *infile, *outfile;
char             inname[20], outname[20], gename[20];

/* Sub routines: */
int              WaitYN(void);
long             Search(FILE * fp, int index, long searchfrom);
long             Extract(FILE * fp, int index, long extractfrom);
long             Gotoend(FILE * fp, long endmark);
int              Writeheader(FILE * fp);
int              i;


int
main(int argc, char **argv)
{
        int              flag = FALSE;
        long             marker = 0;

        while (flag == FALSE) {
                if (argc == 2) {
                        strcpy(gename, argv[1]);
                        argc = 0;
                } else {
                        printf("Please enter the text filename without extension:");
                        scanf("%8s", &gename[0]);
                }

                printf("\nThe filename you have chosen is %s \n", gename);
                printf("\nThe data extracted from this file will be saved");
                printf("\nin a file called %s.txt\n", gename);

                printf("\nDo you wish to continue?");

                flag = WaitYN();

                /* Create output file and name it input name.txt */

                strcpy(outname, gename);
                strcat(outname, ".txt");
                outfile = fopen(outname, "w");

                if (outfile == NULL) {
                        printf("Cannot create output file.\n");
                        goto ABORT;
                }
                /* Convert into *.lst file and check this file exists */

                sprintf(inname, "%s.lst", gename);
                infile = fopen(inname, "r");

                if (infile != NULL) {

                        Writeheader(infile);

                        while ((marker = Search(infile, i, marker)) != EOF) {
                                marker = Extract(infile, i, marker);
```

```
                                marker = Gotoend(infile, marker);
                                if (marker == EXFAIL) {
                                        /* Abort here ... */
                                        printf("There is a problem with the data in this
file\n");
                                        fclose(infile);
                                        fclose(outfile);
                                        remove(outname);
                                        goto ABORT;
                                }
                        }


                        /* File has been sucessfully parsed */
                        fclose(infile);

                } else {
                        printf("The file you have chosen (%s) does not exist.\n", inname);
                        printf("the output file (%s.txt) will be removed\n", gename);
                        fclose(outfile);
                        remove(outname);
                        goto ABORT;
                }
        }
        fclose(outfile);
        return (0);

ABORT:                          /* Crash message */
        printf("An error has occurred\n");
        return (1);

}

int
WaitYN(void)
{
        char            a[5];
        scanf("%1s", &a[0]);
        if ((a[0] == 'y') || (a[0] == 'Y')) {
                return TRUE;
        } else {
                return FALSE;
        }

}

long
Search(FILE * fp, int index, long searchfrom)
{
        /*
         * Searches SPSS output file for result of stepwise regression and
         * returns the result to an output file
         */

        int             FLAG_marker;
        float           limnum, pin, pout;
        long            starmark;
        char            line[300];
        char           *temp;
        char            pcon[100], limit[100], method[100];

        FLAG_marker = FALSE;

        fseek(fp, searchfrom, SEEK_SET);
        printf("The value of search from is %d\n", searchfrom);

        while ((FLAG_marker == FALSE) && (fgets(line, 299, fp) != 0)) {


                if ((temp = strstr(line, "*")) != NULL) {
                        starmark = ftell(fp);
                        printf("The location is: %d\n", starmark);
                }
                if ((temp = strstr(line, "End")) != NULL) {
                        sscanf(line, "End Block Number   1   %s =      %s Limits reached.\n",
pcon, limit);
                        limnum = atof(limit);
                        printf("string = %s float = %f\n", limit, limnum);
                        fseek(fp, starmark, SEEK_SET);
                        printf("The value of starmark is %d\n", starmark);
                        FLAG_marker = TRUE;
                }
        }
```

```
        if (FLAG_marker == FALSE) {
                return EOF;
        } else {
                return starmark;
        }


}

/* Subroutine for extracting data from page before END Block */

long
Extract(FILE * fp, int index, long extractfrom)
{
        int             i, nvars_found, nvars_needed;
        char            line[300];
        float           mulr, rsq, se, f;
        float           bx[6], sebx[6], betax[6], tx[6], sigtx[6];
        float           ubetax[6];
        float           conb, conseb, cont;
        int             FLAG_marker;
        long            errmark;
        int             reg, res, df, np;

        char           *temp, string[50];
        char            tempstr[50];
        char            bxs[50], sebxs[50], betaxs[50], txs[50], sigtxs[50];
        char            conbs[50], consebs[50], conts[50];


        for (i = 1; i <= 5; i++) {
                bx[i] = sebx[i] = betax[i] = tx[i] = sigtx[i] = ubetax[i] = 0.0;
        }
        /* ****************************************** */
        /* MUST SET THESE IF MORE VARIABLES ARE ENTERED */
        nvars_needed = 6;
        nvars_found = 0;

        fseek(fp, extractfrom, SEEK_SET);
        printf("The value of extractfrom is %d\n", extractfrom);

        FLAG_marker = FALSE;

        while ((fgets(line, 299, fp) != 0) && (FLAG_marker == FALSE)) {


                if ((temp = strstr(line, "Multiple R")) != NULL) {
                        sscanf(line, "Multiple R %s", &tempstr);
                        mulr = atof(tempstr);
                        printf("Multiple R value is %f \n", mulr);
                        nvars_found += 1;
                }
                if ((temp = strstr(line, "Adjusted R Square")) != NULL) {
                        sscanf(line, "Adjusted R Square %s", &tempstr);
                        rsq = atof(tempstr);
                        printf("Adjusted R Square value is %f \n", rsq);
                        nvars_found += 1;
                }
                if ((temp = strstr(line, "Standard Error")) != NULL) {
                        sscanf(line, "Standard Error %s", &tempstr);
                        se = atof(tempstr);
                        printf("Standard Error value is %f \n", se);
                        nvars_found += 1;
                }
                if ((temp = strstr(line, "Regression")) != NULL) {
                        sscanf(line, "Regression %s", &tempstr);
                        reg = atof(tempstr);
                        printf("Regression value is %d \n", reg);
                        nvars_found += 1;
                }
                if ((temp = strstr(line, "Residual")) != NULL) {
                        sscanf(line, "Residual %s", &tempstr);
                        res = atof(tempstr);
                        printf("Residual value is %d \n", res);
                        df = reg + res;
                        printf("Degrees of Freedom is %d\n", df);
                        nvars_found += 1;
                        np = df + 1;

                }
                if ((temp = strstr(line, "F =")) != NULL) {
                        sscanf(line, "F = %f", &f);
                        printf("F value is %f \n", f);
```

```
                        nvars_found += 1;
                }
                /*
                 * All the obligatory variables have been scanned, now looking for the
                 * coefficients for X
                 */

                for (i = 1; i <= 5; i++) {
                        /* Create the search string */

                        if (i > 1) {
                                sprintf(string, "X%d", i);
                        } else {
                                strcpy(string, "X ");
                        }

                        if ((temp = strstr(line, string)) == line) {
                                sscanf(&line[3], "%s %s %s %s %s", bxs, sebxs, betaxs, txs,
sigtxs);

                                bx[i] = atof(bxs);
                                sebx[i] = atof(sebxs);
                                betax[i] = atof(betaxs);
                                tx[i] = atof(txs);
                                sigtx[i] = atof(sigtxs);

                                if (betax[i] < 0) {
                                        ubetax[i] = (betax[i]) * (-1);
                                } else {
                                        ubetax[i] = betax[i];
                                }

                        }
                }
                if ((temp = strstr(line, "(Constant)")) != NULL) {
                        sscanf(line, "(Constant) %s %s %s", conbs, consebs, conts);
                        conb = atof(conbs);
                        conseb = atof(consebs);
                        cont = atof(conts);
                        FLAG_marker = TRUE;
                }
        }

        /* Print the results of each scan to the output file */

        fprintf(outfile, "\n%8.4f %8.4f %8.4f %4d %4d %10.2f %6d %6d", mulr, rsq, se, reg,
res, f, df, np);
        fprintf(outfile, "%12.4f %12.4f %12.4f", conb, conseb, cont);

        for (i = 1; i <= 5; i++) {
                printf("Values for X%d are %f %f %f %f \n", i, bx[i], sebx[i], betax[i],
tx[i]);

                fprintf(outfile, "%20.2f %20.2f %12.4f %12.3f %12.5f", bx[i], sebx[i],
betax[i], tx[i], sigtx[i]);
                fprintf(outfile, "%12.4f", ubetax[i]);
        }

        if (nvars_found != nvars_needed) {
                errmark = ftell(fp);
                printf("The value of errmark is %d\n", errmark);
                return EXFAIL;
        } else {
                return ftell(fp);
        }
}
long
Gotoend(FILE * fp, long endmark)
{
        /*
         * Sets cursor position to the beginning of the line after "End"
         * string
         */

        long            pageend;
        char            line[300];
        char           *temp;
        int             FLAG_marker;

        FLAG_marker = FALSE;

        while ((fgets(line, 299, fp) != 0) && (FLAG_marker == FALSE)) {

                if ((temp = strstr(line, "End")) != NULL) {
                        pageend = ftell(fp);
```

```
                        FLAG_marker = TRUE;
                }
        }
        if (FLAG_marker == FALSE) {
                return EOF;
        } else {
                return pageend;
        }
}

int
Writeheader(FILE * fp)
{

        float           pin, pout;

        char           *temp;
        char            line[300], method[50];
        char            pins[50], pouts[50];


        fprintf(outfile, "Extracted Data from %s.lst using programme SPSS.EXE\n", gename);

        while ((fgets(line, 299, fp) != 0) && (strstr(line, "End") == NULL)) {
                if ((temp = strstr(line, "Block")) != NULL) {
                        sscanf(line, "Block Number 1. Method:%s Criteria PIN %s POUT %s\n",
method, pins, pouts);
                        pin = atof(pins);
                        pout = atof(pouts);
                        fprintf(outfile, "Method: %s\n", method);
                        fprintf(outfile, "PIN Criteria = %4.2f\n", pin);
                        fprintf(outfile, "POUT Criteria = %4.2f\n", pout);
                }
        }
        fprintf(outfile, "\n\n\n");
        fprintf(outfile, "%8s %8s %8s %4s %4s %10s %6s %6s", "MULR", "ADJR2", "SE", "REG",
"RES", "F", "DOF", "NUM_P");
        fprintf(outfile, "%12s %12s %12s", "CONST_B", "CONST_SEB", "CONST_T");
        fprintf(outfile, "%20s %20s %12s %12s %12s %12s", "B_x", "SEB_x", "Beta_x", "T_x",
"SigT_x", "MagBeta_x");
        fprintf(outfile, "%20s %20s %12s %12s %12s %12s", "B_x2", "SEB_x2", "Beta_x2", "T_x2",
"SigT_x2", "MagBeta_x2");
        fprintf(outfile, "%20s %20s %12s %12s %12s %12s", "B_x3", "SEB_x3", "Beta_x3", "T_x3",
"SigT_x3", "MagBeta_x3");
        fprintf(outfile, "%20s %20s %12s %12s %12s %12s", "B_x4", "SEB_x4", "Beta_x4", "T_x4",
"SigT_x4", "MagBeta_x4");
        fprintf(outfile, "%20s %20s %12s %12s %12s %12s\n", "B_x5", "SEB_x5", "Beta_x5",
"T_x5", "SigT_x5", "MagBeta_x5");

}
```